Improved Dynamics in Hybrid Particle-Field Molecular-Dynamics Simulations of Polymers

Verbesserte Dynamik in hybriden Teilchen-Feld-Molekulardynamik-Simulationen von Polymeren

Vom Fachbereich Chemie der Technischen Universität Darmstadt zur Erlangung des Grades Doctor rerum naturalium (Dr. rer. nat.)

Genehmigte Dissertation von M.Sc Zhenghao Wu
Tag der Einreichung: 14.09.2021, Tag der Prüfung: 25.10.2021

1. Gutachten: Prof. Dr. Florian Müller-Plathe
2. Gutachten: Prof. Dr. Nico van der Vegt
Darmstadt 2021

TECHNISCHE UNIVERSITÄT DARMSTADT

Eduard-Zintl-Institut für Anorganische und Physikalische Chemie

Improved Dynamics in Hybrid Particle-Field Molecular-Dynamics Simulations of Polymers
Verbesserte Dynamik in hybriden Teilchen-Feld-Molekulardynamik-Simulationen von Polymeren

Genehmigte Dissertation von M.Sc Zhenghao Wu

1. Gutachten: Prof. Dr. Florian Müller-Plathe
2. Gutachten: Prof. Dr. Nico van der Vegt

Tag der Einreichung: 14.09.2021
Tag der Prüfung: 25.10.2021

Darmstadt 2021

Erklärungen laut Promotionsordnung

§8 Abs. 1 lit. c PromO

Ich versichere hiermit, dass die elektronische Version meiner Dissertation mit der schriftlichen Version übereinstimmt.

§8 Abs. 1 lit. d PromO

Ich versichere hiermit, dass zu einem vorherigen Zeitpunkt noch keine Promotion versucht wurde. In diesem Fall sind nähere Angaben über Zeitpunkt, Hochschule, Dissertationsthema und Ergebnis dieses Versuchs mitzuteilen.

§9 Abs. 1 PromO

Ich versichere hiermit, dass die vorliegende Dissertation selbstständig und nur unter Verwendung der angegebenen Quellen verfasst wurde.

§9 Abs. 2 PromO

Die Arbeit hat bisher noch nicht zu Prüfungszwecken gedient.

Darmstadt, 14.09.2021

Z. Wu

This doctoral dissertation is conducted under the supervision of Prof. Dr. Florian Müller-Plathe of Eduard-Zintl-Institut für Anorganische und Physikalische Chemie at Technische Universität Darmstadt. This work is a part of the Sonderforschungsbereiche und Transregio 146, titled “Multiscale Simulation Methods for Soft Matter Systems” funded by the Deutsche Forschungsgemeinschaft. This is a cumulative dissertation consisting of the following 4 research articles:

- Wu, Z.; Kalogirou, A.; De Nicola, A.; Milano, G.; Müller-Plathe, F. Atomistic Hybrid Particle-field Molecular Dynamics Combined with: Restoring Entangled Dynamics to Simulations of Polymer Melts. J. Comput. Chem. 2021, 42 (1), 6–18.
- Wu, Z.; Milano, G.; Müller-Plathe, F. Combination of Hybrid Particle-Field Molecular Dynamics and Slip-Springs for the Efficient Simulation of Coarse-Grained Polymer Models: Static and Dynamic Properties of Polystyrene Melts. J. Chem. Theory Comput. 2021, 17 (1), 474-487
- Wu, Z.; Alberti, S. A. N.; Schneider, J.; Müller-Plathe, F. Knotting Behaviour of Polymer Chains in the Melt State for Soft-Core Models with and without Slip-Springs. J. Phys.: Condens. Matter 2021, 33, 244001.
- Wu, Z.; Müller-Plathe, F. Slip-Spring Hybrid Particle-Field Molecular Dynamics for Coarse-Graining Branched Polymer Melts: Polystyrene Melts as an Example. Submitted to Macromolecules.

Acknowledgement

First of all, I would like to deeply thank my thesis advisor (Doktorvater) — Prof. Dr. Florian Müller-Plathe for his guidance and support throughout my doctoral studies at Darmstadt. Similar to "Doktorvaterïn German, there is an old proverb in China: One day as my teacher, for the rest of my life I would regard him like my father. I could not imagine how I would have developed personally and in research without multi-dimensional interactions with him.

I would like to thank my collaborators and colleagues: Prof. Giuseppe Milano, Prof. Ralf Riedel, Prof. Friederike Schmid, Prof. Antonio De Nicola, Prof. Hossein Eslami, Prof. Nico van der Vegt, Andreas Kalogirou, Ying Zhan, Wei Li, Dr. Bing Li, Dr. Vikram Reddy Ardham, Dr. Yunfeng Mao, Prof. Saurav Prasad, Prof. Hari Krishna Chilukoti, Dr. Shubhadip Das, Gustavo G. Rondina, Hongyang Huang, Dr. Eunsang Lee, Dr. Hans-Jürgen Bär, Dr. Kenkoh Endoh, Dr. Swaminath Bharadwaj, Marvin Bernhardt and Viktor Klippenstein. I have learned a tremendous amount of knowledge about different disciplines from them. Special thanks to Jurek Schneider, Tianhang Zhou, Tobias Materzok, Yash Jain, Simon Alberti, my officemate Melissa Meinel and my roommate Maohua Zhang for their company during my PhD journey. The winters in Germany were not that grey because of them. I would also like to thank our wonderful group secretary, Frau Dana Voss, for her help with personal and group administrations, e.g., my settling in Darmstadt and organizing group all events.

Finally, I would like to express my everlasting gratitude to my father, Qinghua Wu, and my mother, Xiaoying Ling. Without their support, I would not have been able to complete this thesis. This thesis is dedicated to my family.

Zusammenfassung

Im letzten halben Jahrhundert haben sich die Simulationsverfahren in der Chemie erheblich weiterentwickelt, mit dem Ziel, ein umfassendes Verständnis der Struktur-Eigenschafts-Beziehungen von Polymeren zu erlangen und quantitative Vorhersagen über das strukturelle, dynamische und rheologische Verhalten von Polymermaterialien zu treffen. Molekulardynamische Simulationen mit Modellen, die auf atomarer Ebene aufgelöst sind, liefern die genauesten Ergebnisse unter ihnen. Leider erfordern die damit verbundenen räumlichen und zeitlichen Dimensionen Rechenleistungen, die in realistischem Maßstab heute unerreichbar sind. Solche Hürden können durch die Verwendung grobkörniger Modelle, die nur einige wenige relevante Freiheitsgrade beibehalten und die anderen auf eine gemittelte Weise behandeln, gemildert werden. Dieses Verfahren ermöglicht groß angelegte Simulationen, schränkt aber die Fähigkeit ein, chemische Details zu beschreiben. Daher ist eine effiziente systematische Grobkörnigkeit, die eine direkte Simulation des mesoskaligen Verhaltens von Polymermaterialien mit detaillierter Chemie ermöglicht, nach wie vor eine äußerst anspruchsvolle Aufgabe.

In dieser Dissertation stellen wir eine neuartige Berechnungstechnik für die Simulation von Polymeren vor, indem wir eine hybride Teilchenfeld-Molekulardynamik Methode (hPF-MD) und das multi-chain slip-spring Modell miteinander kombinieren, nämlich den hybriden Partikelfeld-Molekulardynamik Ansatz mit slip-springs (SS-hPF). Bei der ursprünglichen hPF-MD Methode werden die nicht gebundenen Wechselwirkungen zwischen den Teilchen durch das Dichte-Funktionsfeld Potential berechnet. Dieses Potential ist effektiv ein Soft-Core Potential, was bei der Modellierung von Polymerschmelzen oder konzentrierten Polymerlösungen zu Kettenüberkreuzungen führt. Folglich fehlen in diesen Systemen die Kettenverschränkung und die damit verbundenen dynamischen Mechanismen, z. B. Kettenreptation. Die zweite Komponente, das multi-chain slip-spring Modell, trägt zur Verbesserung der Dynamik in ursprünglichen hPF-MD Simulationen von Polymeren bei. Die so genannten slip-springs sind temporäre Bindungen zwischen Polymerketten, die die topologischen Einschränkungen zwischen Polymerketten künstlich nachahmen. Als Proof-of-Concept Beispiele entwickeln und validieren wir SS-hPF Simulationen linearer Polymere anhand eines atomistischen Modells von Polyethylenschmelzen und eines systematischen grobkörnigen Modells von Polystyrolschmelzen. Darüber hinaus verallgemeinern wir den SS-hPF-Simulationsansatz, um verzweigte Polymere simulieren zu können. Darüber hinaus untersuchen wir die Eigenschaften, die wahrscheinlich durch die lokale Molekülpackung beeinflusst werden, wie z. B. die Selbstverflechtungen oder Knoten in Polymerschmelzen, die durch Soft-Core Modelle simuliert werden. Schließlich sind wir davon überzeugt, dass unsere Arbeit einen effizienten und praktischen Ansatz zur Erstellung chemiespezifischer grobkörniger Modelle für Polymere bietet.

Abstract

Over the past half century, molecular dynamics simulation techniques have advanced considerably, aiming to provide a comprehensive understanding of the structure-property relationships of polymers and to make quantitative predictions of the structural, dynamical and rheological behaviors of polymeric materials. Specifically, molecular dynamics simulations with atomic-level resolution models provide, in principle, the most accurate results among them. Unfortunately, the associated spatial and temporal dimensions involved in these polymer modelings will require computational costs that are unaffordable on a routine basis today. Such hurdles can be mitigated by using coarse-grained models that retain only a few relevant degrees of freedom and treat the others in an averaged manner. This procedure allows for large-scale simulations, but limits the ability to describe chemical variations. Therefore, efficient systematic coarse-graining, which allows direct simulation of the mesoscale behavior of polymeric materials with detailed chemistry, remains an extremely challenging task.

In this dissertation, we introduce a novel computational technique for simulations of polymers by combining the hybrid particle-field molecular-dynamics (hPF-MD) simulation method and the multi-chain slip-spring model, namely, slip-spring hybrid particle-field molecular-dynamics approach (SS-hPF). In the original hPF-MD, the non-bonded interactions between particles are computed through the density-functional-field potential. This potential is effectively soft-core, resulting in chain-crossing events in modeling polymer melts or concentrated polymer solutions. Consequently, chain entanglement and associated dynamical mechanisms, e.g., chain reptation and arm retraction, are absent in these systems. The second component, the multi-chain slip-spring model, thus enters to improve the dynamics in original hPF-MD simulations of polymers. The so-called slip springs are transient bonds between polymer chains that artificially mimic the topological constraints between polymer chains. As proof-of-concept examples, we develop and validate SS-hPF simulations of linear polymers using an atomistic model of polyethylene melts and a systematic coarse-grained model of polystyrene melts. Moreover, we generalize the SS-hPF simulation approach to be able to simulate branched polymers, since the presence of a small fraction of chain branching can significantly modify the dynamical and rheological behaviors in polymeric materials. In addition, we study the properties that are likely to be affected by local molecular packing, such as the self-entanglements or knots in polymer melts simulated by soft-core models with and without slip-springs. Finally, we believe our work provides an efficient and practical approach to establish chemistry-specific coarse-grained models for polymers.

Inhaltsverzeichnis

1 Introduction **1**
- 1.1 Background . . . 1
- 1.2 Challenges and Objectives . . . 4
- 1.3 Structure of the Thesis . . . 5

2 Methods **7**
- 2.1 Hybrid Particle-Field Molecular-Dynamics Simulations . . . 7
  - 2.1.1 Theory . . . 7
  - 2.1.2 Interaction Energy . . . 8
  - 2.1.3 Computational Details . . . 8
- 2.2 Multi-Chain Slip-Spring Models . . . 9
  - 2.2.1 Initialization . . . 9
  - 2.2.2 Movement . . . 10
  - 2.2.3 Destruction/Creation . . . 10
- 2.3 Hybrid Molecular-Dynamics/Monte-Carlo Simulations . . . 10

3 Results **13**
- 3.1 Atomistic Hybrid Particle-Field Molecular Dynamics Combined with Slip-Springs: Restoring Entangled Dynamics to Simulations of Polymer Melts . . . 13
- 3.2 Combination of Hybrid Particle-Field Molecular Dynamics and Slip-Springs for the Efficient Simulation of CG Polymer Models: Static and Dynamic Properties of Polystyrene Melts . . . 33
- 3.3 Slip-Spring Hybrid Particle-Field Molecular Dynamics for Coarse-Graining Branched Polymer Melts: Polystyrene Melts as an Example . . . 52
- 3.4 Knotting Behaviour of Polymer Chains in the Melt State for Soft-Core Models with and without Slip-Springs . . . 99

4 Conclusion and Outlook **113**

1 Introduction

1.1 Background

Multiscale modelling techniques (Figure 1.1) have become an irreplaceable tool in material science over the past few decades[1–5]. The characteristics and properties of materials are commonly controlled by their structures and processings on multiple spatial-temporal scales, ranging from sub-atom ($<$ Angstrom) to grain ($>$ microns) or larger, and from femtosecond to seconds or longer. This phenomenon is more typical in soft-matter systems such as polymers. For instance, a polymer is composed of repeating units, so-called monomers, that are connected to each other by covalent bonds, and a single monomer is constituted by a group of atoms. Therefore, the structure of a polymer at least has three levels: atomic, monomeric and molecular levels. Yet (even in the foreseeable future), a unified simulation model has not been found to cover all of these scales simultaneously with a "good-enough" accuracy.

At the most microscopic scale concerned in material science, a widely-used simulation method is the *ab initio* quantum chemistry[6–8]. It provides a reliable route to model systems containing tens, or even hundreds of atoms via numerically solving the electronic Schrödinger equation, given the positions of atomic nuclei, and the total number of electrons in the system to obtain useful information such as electronic energy, electron density, and other system properties. The last three decades have witnessed the great progress in the development of the *ab initio* approach in both methodology (e.g. accurate density-functionals) and software (e.g., Gaussian[9] and VASP[10]), which results in an extensive application of *ab initio* simulations[11–13]. However, it is still computationally expensive to solve the many-electron Schrödinger equations for systems beyond thousands of atoms sampling over nanoseconds. In consequence, even a simple homopolymer melt system with low-molecular-weight chains becomes intractable.

To deal with larger systems containing thousands of atoms such as the one aforementioned, it is more appropriate to use all-atom (AA) models empirically parameterized from reference models with a higher accuracy such as *ab initio* models. In these models, electronic interactions of atoms are approximated by simple potential functions, a set of which is commonly named as "force-field" in molecular-dynamics (MD) simulation community. Even though an AA force-field simplifies degrees of freedom of a target system by an order of a magnitude, it is sufficient to, e.g., predict glass transition temperature of several commodity polymers[14] and identify antibody binding sites in viruses[15].

The soft materials are ubiquitous in our daily life including examples of rubber, plastics, woods, as well as foams, gels, oil, etc. Most of these materials are made of large complex molecules, e.g., a single molecule easily composed of as many as thousands or even millions of atoms. To simulate such a large system over hundred nanoseconds or longer, the MD simulation with AA models is not sufficient any more within the current computational power. At the larger scale, coarser models are required, which ideally retain a few degrees of freedom of interest, and average out others, which are assumed to be unnecessary, to save the computational expense. A typical example of this type of coarse-grained (CG) models is the popular Kremer-Grest bead-spring models for polymers[16]. Specifically, these CG models are built in a top-down way, and they do not capture chemical details of a specific polymer. In order to predict material

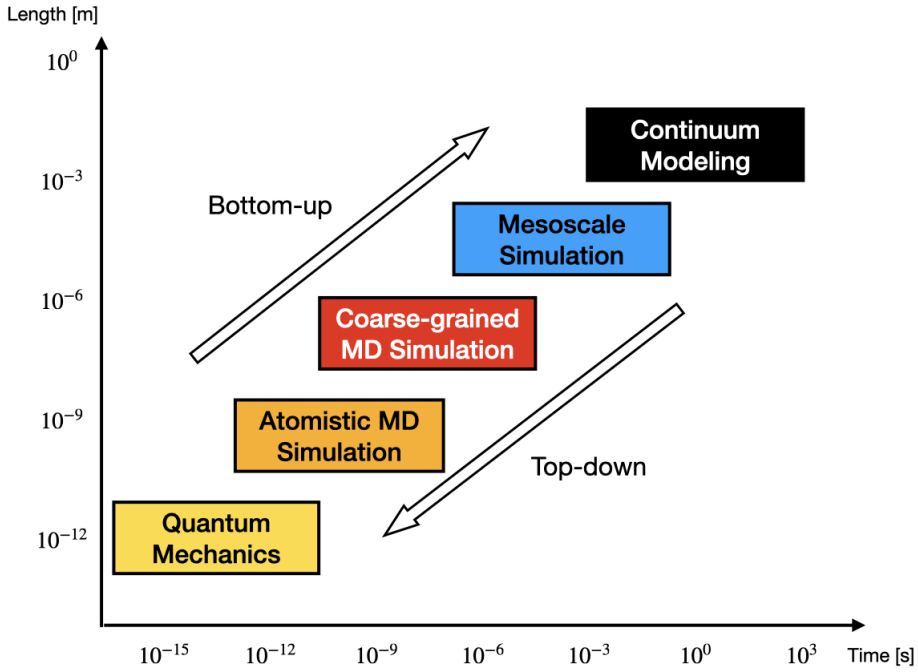

Abbildung 1.1: Simulation methods for associated length and time scales.

properties quantitatively, the development of systematic coarse-graining is thus of great significance, which aims to construct higher-level CG models from lower-level AA models in a systematic manner. If needed, additional information from, e.g., experimental results, can be added to make quantitative predictions. Along the history of systematic coarse-graining, various methods have been proposed including the Iterative Boltzmann Inversion[17], Force-Matching[18], Conditional Reversible Work[19] and others. Recently, machine learning techniques have emerged as an alternative approach to construct the effective interaction energy between CG beads[20, 21]. These data-driven methods have shown their advantages to address several key problems in classical coarse-graining such as accuracy[22, 23] and transferability[24]. The resulting CG models using these methods are commonly at the monomer level to retain necessary chemical details.

One step further continuing along the path of coarse-graining is to lump more atoms together into a single CG bead. Most of these highly coarse-grained models are designed to preserve the structural or thermodynamical consistency with reference fine-grained models or experimental measurements. A primary example can be referred to the Dissipative Particle Dynamics (DPD)[25]. DPD simulations are conventionally considered as mesoscopic models with a DPD bead roughly representing several monomers, although the exact relation between them and real chemistry is often unlcear. Another example is the soft sphere models[26, 27], which model the entire polymer chain as a single CG bead. In general, the effective interaction between CG beads are largely softened due to increasingly coarse-graining. These soft-core models are usually used to study morphological behaviors such as the self-assembly of block copolymers[28, 29].

Another route to make simulations at larger spatial-temporal scales possible is to use computationally efficient potential functions. For example, inspired by self-consistent field theory for polymers, the intermolecular interactions are decoupled into molecules interacting with an external potential field dependent

on local densities in the single-chain-in-mean-field (SCMF) approach[30]. This density-functional-field interactions requires no mutual information between neighboring molecules, making it possible to realize intensive parallelization on modern computing clusters. The system coordinates are sampled by Monte Carlo moves. The SCMF method has been successfully applied to simulate the morphologies of battery electrolytes at the engineering scale[31]. Another example is the hybrid particle-field molecular dynamics (hPF-MD) method developed by Milano and coworkers[32]. Similar to SCMF, a particle-mesh formulation is also employed to construct the external potential dependent on the local densities for the non-bonded interactions between particles. In contrast, the equation of motion in hPF-MD simulations is integrated via molecular dynamics rather than Monte-Carlo used in SCMF. The versatility of hPF-MD methods is demonstrated by a wide range applications includeing biomolecular lipids[33], vesicles[34], peptides[35] as well as polyelectrolytes[36], polymer melts[32] and nanocomposites[37, 38], all facilitating bridging the gap between atomistic and mesoscopic scales. It is noted that the density-functional-field potential described here is effectively soft since it is still finite even for overlapping particles.

As the interaction energy between particles turns effectively soft, bond-crossing events start taking place in all soft-core models mentioned above, leading to unphysical chain interpenetration. Consequently, the entangled dynamics, a significant dynamical mechanism in high-molecular-weight polymers induced by chain uncrossability, is not reproduced using such soft-core models. In the past two decades, various approaches attempting to resolve this issue in these highly coarse-grained models have been proposed. For instance, Padding and Briels reintroduced the chain uncrossability condition into a highly coarse-grained polyethylene model with 20 CH_2 units mapped onto 1 CG bead using their Twentanglement algorithm[39]. This algorithm tracks all bond-bond distances and slows down their relative motions when they are close together to prevent bond-crossing events. The resulting mesoscopic polyethylene model was shown to successfully reproduce the scaling behavior of diffusion coefficients and viscosities compared with the reptation theory and experimental observations. Following the idea of monitoring bond-bond distances, similar approaches such as the Soft Segmental Repulsive potential[40], which basically introduces additional soft repulsive forces between bonds, have also been shown to massively decrease the bond-crossing events and postulate reasonable dynamical behaviors of entangled polymer melts. Although the chain uncrossability can be well restored, these methods usually suffer from bad computational efficiency due to the requirement to calculate bond-bond distances (pairwise) at each instant of simulation time.

The topological constraints between polymer chains can also be reincorporated into high-level coarse-grained models using so-called slip-links or slip-springs. The concept of slip-links was first proposed by Doi and Edwards as an alternative of the tube model to understand the topological constraints in polymer melts and elastomers in the late 1970s[41, 42]. Instead of a mean-field treatment in the tube model[43], the polymer chain is considered to reptate through a series of fixed rings in the slip-link model of Doi and Edwards. Later, several versions of slip-link models at different levels of coarse-graining were proposed by Schieber and coworkers[44–47]. Their models also consider slip-links as immobile rings fixed on the background, but introduced additional important mechanisms such as constraint release for slip-links. Predictions of both linear and non-linear rheologies can be made for various polymeric systems using their models. Additionally, Masubuchi *et al.* developed a three dimensional premitive chain network (PCN) model with chain uncrossability modelled by slip-links[48]. Different with previous slip-link models, slip-links in PCN models are fluctuating with each connecting two chain strands. In 2005, Likhtman developed the first slip-spring model, in which the links are described as phantom chains represented by springs instead of links affinely fixed in space[49]. Inspired by the single-chain slip-spring model of Likhtman, multiple versions of multi-chain slip-spring models have been developed by different groups[50–53]. The multi-chain feature makes it possible for slip-spring models to simulate a broader range of systems such as the polymer interface. However, these methods that easily predict dynamics and rheology of polymers usually lack a rigorous

molecular foundations. Recently, a multi-scale strategy that brings detailed MD models to mesoscopic slip-spring based Brownian dynamics simulations was proposed[54, 55]. The combination of the slip-spring model with systematic highly coarse-grained polymer models (e.g., 52 CH_2 units mapped onto 1 CG bead) offers a potential to model entangled polymers with reasonable molecular information in spatial-temporal scales close to experiments[55]. More recently, the hierarchical simulation strategies are also employed to link AA-MD to mesoscale slip-spring and slip-link simulations for bottom-up predictions of polymer dynamics[56, 57].

1.2 Challenges and Objectives

The scope of this thesis is the development of new hPF-MD methods and models that are capable of predicting accurate dynamics of polymeric systems with detailed molecular information encoded to reach large spatial-temporal scales. Specifically, the thesis aims to extend and validate the predictive power of the hPF-MD approach combined with slip-springs for dynamical properties of test systems including linear and branched polymer melts at both atomistic and CG levels over a wide range of molecular weights.

It is generally considered as a challenging work in the simulation community to model dynamics of polymers, especially those with high molecular weight, over a long enough simulated time to characterize relevant properties simultaneously using realistic models. The hPF-MD method, which utilizes density-functional-fields to describe the polymer non-bonded interactions, is expected to bridge the atomistic and mesoscopic scales. Although it has shown multiple advantages, e.g., computational efficiency, to predict structural properties of extensive polymer systems[36, 38, 58], there was very few rigorous work (as far as I know, only one[59]) making use of the hPF-MD method to study dynamical problems prior this work. A major issue is the feature of soft-core density-functional-field interactions to allow bond-crossings, leading to the loss of dynamical mechanisms such as entangled dynamics, which in turn is significant for high-molecular-weight polymer melts or concentrated polymer solutions. At this point, we introduce the second ingredient, namely, the multi-chain slip-spring model. The slip-springs are transient bonds between polymer chains, artificially mimicking the topological constraints induced by excluded-volume interactions[50, 52]. In order to combine these two simulation models, special methodology and software are needed. Therefore, the first objective of this thesis is to develop:

- Efficient algorithms and codes to combine the hPF-MD and multi-chain slip-spring models.

Next, the effectiveness and robustness of the new simulation method has to be validated against theoretical predictions and available experimental properties. Additionally, its computational performance also needs to be evaluated by comparing with the reference simulation methods which are standard AA-MD or CG-MD simulations in this work. With these in mind, one of the main objectives is to develop and validate:

- Slip-spring hPF-MD simulations of linear polymer melts using both atomistic and systematic CG models as proof-of-concept examples

In commercial products of polymeric materials, it was found that the presence of a small portion of chain branchings distinctly modifies their dynamical and rheological behavior, e.g., showing a higher zero-shear viscosity η_0 than in linear counterparts with the same molecular weight. Essentially, the topology of chains significantly alters dynamical and rheological properties of polymer melts. Accordingly, it is of great fundamental and practical importance to generalize:

- The slip-spring hPF-MD method for simulations of branched polymers.

The soft-core models are sufficient for reproducing structural properties and thermodynamic properties of hard-core models in most cases. However, the properties probably impacted by the local molecular packing such as the self-entanglements or knottings in polymer melts simulated by these models are still unclear. Therefore, an additional focus of this thesis is to examine:

- Knotting behaviors of polymer melts in soft-core models with and without topological constraints — slip-springs

1.3 Structure of the Thesis

The thesis consists of 4 chapters. Chapter 1 conveys backgrounds and motivations of this thesis. Chapter 2 provides an introduction to the techniques involved in this thesis. Chapter 3 presents research output of this thesis including three peer-reviewed papers (Section 3.1, 3.2 and 3.4) and one under-reviewed manuscript (Section 3.3). Eventually, Chapter 4 concludes the main achievements of this thesis and offers my future perspective relevant to this thesis.

2 Methods

In this chapter, we introduce the methods associated with the work of this thesis. Certainly, the main method employed in this work is molecular dynamics including the potential functions, thermostats, integrators, and the related parallelization schemes. However, the novelty of the thesis is the hPF-MD formalism of the density-functional-field description of non-bonded interactions and its combination with slip-springs to recover the entangled dynamics of polymers. Therefore, we mainly introduce these two components here: hPF-MD and slip-spring models. For interested readers, two excellent books are recommended for a thorough understanding of foundations in molecular dynamics simulations[60, 61].

2.1 Hybrid Particle-Field Molecular-Dynamics Simulations

2.1.1 Theory

The central concept of hPF method is the separation of the total Hamiltonian of a system into two parts:

$$H = \sum_{i=1}^{M} H_0(\{R, \dot{R}\}_i) + W([\{\phi\}]) \tag{2.1}$$

where the first term is the summation of $H_0(\{R, \dot{R}\}_i)$, which denotes single-molecule intramolecular bonded interactions such as bond, angle and dihedral interactions as a function of particle positions R and velocities $\dot{R}$ explicitly, over M molecules in a system; The intermolecular interactions are included in the second term $W([\{\phi\}])$, which depends on a collection of local particle densities $\{\phi\} = \{\phi_1, \phi_2, ..., \phi_N\}$, where N is the number of particle species. The density-functional-field external potential acting on a particle of species K can then be obtained by taking the derivative of $W([\{\phi\}])$ respect to the local particle density:

$$V_K(r) = \frac{\partial W([\{\phi\}])}{\partial \phi_K(r)} \tag{2.2}$$

It yields the corresponding force acting on a particle i of species K:

$$F_i = -\nabla V_K(r_i) \tag{2.3}$$

With molecular properties expressed as above, the system is sampled with the molecular dynamics equation of motion in hPF-MD simulations.

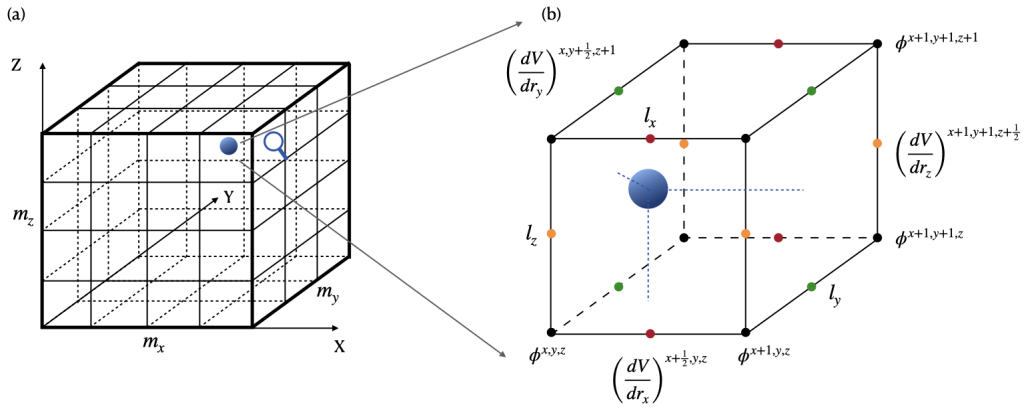

Abbildung 2.1: (a) Schematic figure of the partitioning of simulation box into $m_x \times m_y \times m_z$ cell; (b) Schematic figure of a particle in a unit cell.

2.1.2 Interaction Energy

In the standard hPF-MD simulations, the interaction energy is described by the following functional inspired by the Flory-Huggins polymer theory:

$$W[\phi] = \frac{1}{\phi_0}\left[\sum_{K<L}\chi_{K,L}\phi_K(R)\phi_L(R) + \frac{1}{2\kappa}\left(\sum_L \phi_L(R) - \phi_0\right)^2\right] \tag{2.4}$$

In this expression, the first term is the interaction energy between densities, where $\chi_{K,L}$ is the mean field coupling term between particle species K and L, analogous to the Flory-Huggins parameter χ. The second term physically represents the incompressibility condition for liquids, essentially providing an excluded-volume interactions, where κ is the compressibility factor which governs the local fluctuations of the density. The constant parameter ϕ_0 denotes the average number density of the whole system. The corresponding external potential $V_K(R)$ for a particle of species of K at position R, is given by:

$$V_K(R) = \frac{1}{\phi_0}\left[\sum_L \chi_{K,L}\phi_L(R) + \frac{1}{\kappa}\left(\sum_L \phi_L(R) - \phi_0\right)\right] \tag{2.5}$$

2.1.3 Computational Details

With the underlying theory of the hPF-MD method introduced, let us take a look at the computational techniques of the hPF-MD simulations. The most important one is the computation of the external potential field from the local densities. In order to calculate the local particle densities, a particle-mesh approach is employed. Firstly, the three dimensional simulation box is partitioned into $m_x \times m_y \times m_z$ cells as shown in Figure 2.1 (a). The cell size is $l_x = L_x/m_x$, $l_y = L_y/m_y$, and $l_z = L_z/m_z$ with $L_{x,y,z}$ is the edge length of the simulation box. Then, the particles are distributed onto the cells through the cloud-in-cell algorithm. Specifically, a particle is split onto the vertices of a cell according to the weight function:

$$W(\bar{x},\bar{y},\bar{z}) = \varrho(\bar{x})\cdot\varrho(\bar{y})\cdot\varrho(\bar{z}) \tag{2.6}$$

where $\varrho(\bar{x}) = 1 - \bar{x}$ and $\bar{x} = x/l_x - \mathrm{floor}(x/l_x)$ are the normalized distance between a particle and a vertex as seen in Figure 2.1 (b). The overall density field $\{\phi\}$ is then obtained via summing contributions from all particles. Hence, the density-functional-field potential energy at the vertices can be calculated. The next step is to calculate forces. It requires the computation of gradients of the density-functional-field potential energy at the vertex position r_i. In the current version of hPF-MD method, this gradient is calculated approximately using the finite-difference between neighboring vertices (Figure 2.1 (b)):

$$\left(\frac{dV_K}{dr_x}\right)^{x+\frac{1}{2},y,z} \approx \frac{1}{l_x}(V_K^{x+1,y,z} - V_K^{x,y,z}) \tag{2.7}$$

where the superscripts x,y and z denote the cell index along xyz directions, respectively; r_x denotes the coordinate of a vertex along x axis. As shown in Equation 2.4, the force can be calculated directly from the gradient of external potential fields obtained above. Finally, we linear interpolate potential energies and forces acting on the particles (which are anywhere in the cell and not necessarily on the vertices) from the values on the vertices of cells using the same weights as for distributing the particles (Equation 2.6).

2.2 Multi-Chain Slip-Spring Models

This section introduces the multi-chain slip-spring models employed in a series of studies presented in **Chapter 3**. Generally, the multi-chain slip-spring model is a phenomenological model, which aims to mimic the effects of topological constraints, e.g., entanglements, between polymer chains using explicit two body interactions. A simple schematic form of slip-springs is illustrated in Figure 2.2. Bead-spring chains are depicted by grey beads connected with light grey springs which represent elastic bonds. Slip-springs are shown as dark springs. They are bonds connecting two beads of two different chains. They act in the same way as topological constraints between chains. Although the slip-spring models implemented in atomistic and CG models are actually different in some technical details, they share the same theoretical idea in most aspects. Specifically, the slip-spring model in this thesis is mainly constituted by 3 components: initialization, movement and destruction/creation. A series of attempts to move slip-springs or to destroy it and create it somewhere else is performed between blocks of MD steps during which the particles are moved. Therefore, the particle positions are fixed, when the slip-springs are reassigned, and the slip-springs are a fixed part of the Hamiltonian in any MD block.

2.2.1 Initialization

To initialize a slip-spring simulation, we first need to build the initial configuration of slip-springs at the beginning of a simulation. In this work, slip-spring are randomly created in the system for pairs of particles that are allowed to hold slip-springs following a simple distance criterion. For instance, in a system of CG polystyrene (PS) melts with a monomer mapped by a a single CG bead, the distance criterion is $l_{ss} < 0.9 \times d_T$, where l_{ss} and d_T are the length of a slip-spring and the tube diameter of PS melts (≈ 7.5), respectively. We note that the distance criteria maybe chosen differently depending on unit models and coarse-graining degrees.

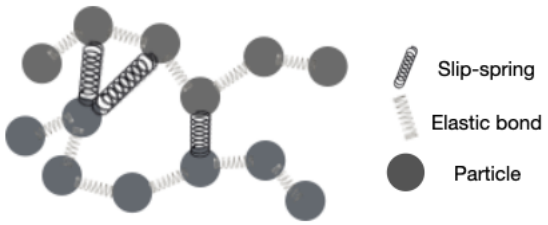

Abbildung 2.2: Schematic figure for slip-springs between bead-spring polymer chains. Polymer beads are represented by the dark grey beads. Dark and light grey springs represent the slip-springs and elastic bonds between polymer beads, respectively.

2.2.2 Movement

Slip-springs are allowed to slide along polymer chains. The movement of slip-springs is governed by a Monte-Carlo algorithms, for whose details readers are referred to the **Method** section of respective studies in **Chapter 3**. The mechanisms for a slip-spring attempting to move along a polymer chain are shown in Figure 2.3. For this slip-spring, one of its two attachments will be chosen. Then, the chosen slip-spring attachment can move either left or right by one step with equal possibility. The step size for a slip-spring move is essentially associated with the overall mobility of slip-springs. In both atomistic polyethylene and CG polystyrene models, a step size equal to one monomer is chosen.

2.2.3 Destruction/Creation

When one of attachments of a slip-spring sits at a chain end, there is a chance for this slip-spring to be destroyed. In the equilibrium state, the average number of entanglements in a polymer melt is constant. Correspondingly, the number of slip-springs also remains unchanged through the simulation for simplicity. Therefore, whenever an existing slip-spring is destroyed, a new slip-spring will be created randomly in the system with one attachment forced to locate at a chain end as seen in Figure 2.4. This attachment is then paired with the other one attached randomly on a bead in its nearest region. The combined destruction/creation move is also subjected to a Monte-Carlo criterion.

2.3 Hybrid Molecular-Dynamics/Monte-Carlo Simulations

In this section, we briefly introduce the algorithm that combines the hPF-MD and slip-spring MC. A simple flow chart is shown in Figure 2.5. At the beginning of the simulation, the particle coordinates and slip-spring configurations are initialized. Then, the particle coordinates and slip-spring configurations are sampled alternating using hPF-MD and Monte-Carlo, respectively. Specifically, the particle coordinates are frozen and the Monte-Carlo moves of slip-springs enters every so many hPF-MD simulation steps Δt_{MC}, where Δt_{MC} is an input parameter of the slip-spring model. The number of MD steps between slip-spring MC blocks is typically 100-500 steps. Finally, the whole simulation is stopped after the target hPF-MD simulation steps t_{MD}. Similar hybrid MD/MC simulation schemes can also be found in reactive molecular dynamics algorithms[62] and other slip-spring models[52, 53, 55].

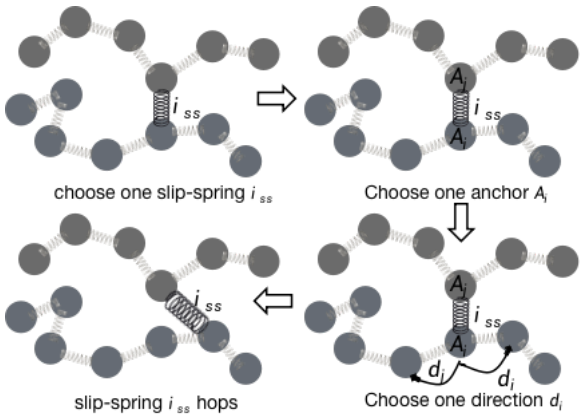

Abbildung 2.3: Schematic figures to describe the movement of a slip-spring.

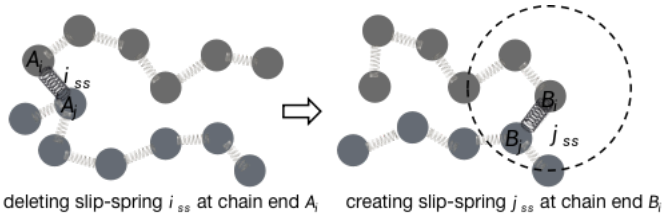

Abbildung 2.4: Schematic figures to describe the destruction/creation process of a slip-spring.

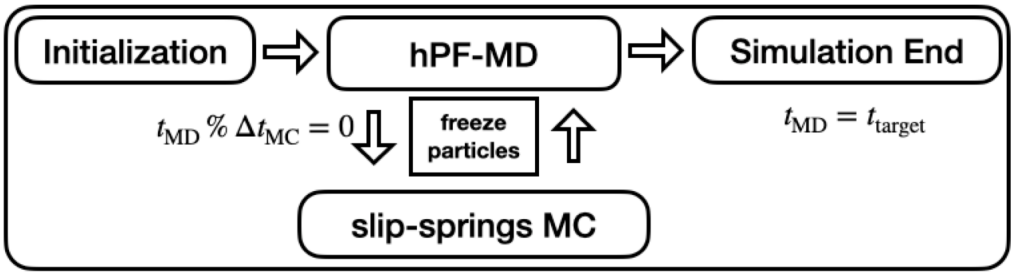

Abbildung 2.5: A simple Flow chart describes the system evolution of a slip-spring hPF-MD simulation. t_{MD} is the hPF-MD simulation step; Δt_{MC} is an input parameter that determines the frequency to update the slip-spring configurations and t_{target} is the target simulation step.

3 Results

3.1 Atomistic Hybrid Particle-Field Molecular Dynamics Combined with Slip-Springs: Restoring Entangled Dynamics to Simulations of Polymer Melts

Received: 23 June 2020 | Revised: 7 September 2020 | Accepted: 11 September 2020

DOI: 10.1002/jcc.26428

FULL PAPER

Journal of COMPUTATIONAL CHEMISTRY WILEY

Atomistic hybrid particle-field molecular dynamics combined with slip-springs: Restoring entangled dynamics to simulations of polymer melts

Zhenghao Wu[1] | Andreas Kalogirou[1] | Antonio De Nicola[2] | Giuseppe Milano[2] | Florian Müller-Plathe[1]

[1]Eduard-Zintl-Institut für Anorganische und Physikalische Chemie, Technische Universität Darmstadt, Darmstadt, Germany

[2]Department of Organic Materials Science, Yamagata University, Yamagata-ken, Japan

Correspondence
Florian Müller-Plathe, Eduard-Zintl-Institut für Anorganische und Physikalische Chemie, Technische Universität Darmstadt, Alarich-Weiss-Str. 8, 64287 Darmstadt, Germany.
Email: f.mueller-plathe@theo.chemie.tu-darmstadt.de

Funding information
Deutsche Forschungsgemeinschaft, Grant/Award Number: SFB-TRR 146

Abstract

In hybrid particle-field (hPF) simulations (*J. Chem. Phys.*, **2009** *130*, 214106), the entangled dynamics of polymer melts is lost due to chain crossability. Chains cross, because the field-treatment of the *nonbonded* interactions makes them effectively soft-core. We introduce a multi-chain slip-spring model (*J. Chem. Phys.*, **2013** *138*, 104907) into the hPF scheme to mimic the topological constraints of entanglements. The structure of the polymer chains is consistent with that of regular molecular dynamics simulations and is not affected by the introduction of slip-springs. Although slight deviations are seen at short times, dynamical properties such as mean-square displacements and reorientational relaxation times are in good agreement with traditional molecular dynamics simulations and theoretical predictions at long times.

KEYWORDS

atomistic, dynamics, entangled polymer, hybrid particle-field simulation, slip-spring

1 | INTRODUCTION

Atomistic molecular dynamics (MD) calculations provide, in principle, all the information desired for soft-matter systems: structure, thermodynamics, and dynamics. In many practical applications, however, they are too computationally expensive to allow the treatment of large enough systems for long enough times. This has led to numerous efforts to derive coarse-grained (CG) models, which are simplified by aggregating a varying number of atoms into single superatoms. The different coarse-graining procedures ensure that the CG models still reproduce some aspects of the studied systems.[1] In this contribution, we follow a different route to make MD calculations faster. First, we maintain the description of the *bonded* interactions at the desired level, which can be itself by CG or, as in this paper, atomistic. Second, the *nonbonded* interactions are approximated by the interactions of atoms with a potential field, which is, in turn, determined from the atomic density. This so-called hybrid particle-field molecular dynamics (hPF-MD) method was introduced by Milano and Kawakatsu a decade ago.[2] It borrows several implementation tricks from the self-consistent-field (SCF) theory.[3,4]

In hPF-MD, the nonbonded forces acting on a particle are expressed as function of the derivatives of local density gradients. This reformulation enables much more efficient simulations than standard MD as the evaluation of *nonbonded* pair forces is replaced by building particle-to-mesh density fields and computing the density field potentials. Both steps are of first order in the number of particles. The hPF-MD model has been demonstrated to be effective to investigate homopolymers and block copolymers at both CG[2] and atomistic resolutions.[5,6] More recently, the hPF-MD model was

[Correction added on 09 September 2020, after first online publication: Projekt Deal funding statement has been added.]

validated in describing the conformational and dynamical properties of biological systems such as lipid bilayers[7–9] and biosurfactants.[10,11] After the integration of electrostatics,[12,13] the hPF-MD method was further successfully applied in charged systems particularly of polyelectrolytes, charged amphiphiles[14] and polypeptides.[15]

The hPF-MD method has, therefore, been around for a decade, and its capabilities and shortcomings are well-known. We will discuss them in this contribution only, as far as needed for our redevelopment, and otherwise refer the reader to the existing literature.[2,5,7,8,15] For various types of soft matter, the structural properties in are usually well reproduced hPF-MD, with the exception of very small-scale structures, such as the short-range part of a radial distribution function. The soft interactions of the density-functional-field, however, eliminate the mechanisms, which are necessary for the correct dynamics. For example, polymer chains are able to interpenetrate mutually due to the absence of excluded-volume interactions, as the *nonbonded* atom-atom interaction is effectively soft-core. This allows fast equilibration of polymer melts also for long chains, but precludes entanglements and reptation dynamics, rendering all dynamic properties, from diffusion to rheology, artificial, and qualitatively wrong.

The problem of incorrect chain crossability also arises in very CG polymer models, since from a certain degree of coarse-graining onward, interactions necessarily become soft-core.[1] To recover the chain entanglements in simulations with such soft *nonbonded* interactions, several attempts have been reported. Padding and Briels proposed an algorithm called TWENTANGLEMENT to detect and prevent chain-crossing events by including an additional interbond interactions in mesoscopic simulations of polymer melts.[16,17] Similar attempts are also made by Pan and Manke to reduce the frequency of artificial chain segment crossing events in dissipative particle dynamics (DPD) simulation via introducing a segmental repulsive potential.[18] Alternative methods have been developed to represent the uncrossability (entanglements) in molecular simulations. Schieber and coworkers demonstrated successive versions of discrete slip-link models for predicting the rheology of entangled polymer liquids and gels, where the chain is CG to the entanglement level and the dynamics of chains is split into chain sliding and constraint release.[19,20] Due to the failure of the standard tube model in describing the experimental neutron spin-echo measurements, Likhtman introduced a new single-chain dynamic slip-link model (slip-spring hereafter) to describe the experimental results for neutron spin echo, linear viscoelasticity, and diffusion of monodisperse polymer melts.[21] Along with the development of these single-chain models, several multi-chain models have been proposed. Shanbhag et al. presented a dual slip-link model for studying the relaxation of entangled star polymers with chain-end fluctuations and constraint release, which explained deviations observed in dielectric and stress relaxation experimental data. Later, Masubuchi et al. proposed a primitive chain network,[22] in which the chains are dispersed in the space and connected by slip-links to form a network. This model is able to reproduce the linear and nonlinear viscoelasticitic properties of entangled polymer melts. However, it is not rigorous in terms of thermodynamical properties because the free-energy description of the model has not been found. Inspired by the single-chain slip-spring model of Likhtman, Masubuchi and coworkers performed a series of multi-chain simulations where the entanglements are replaced by slip-springs instead of the excluded-volume interaction[23–26] with an accurate description of the free energy in the system. Chappa et al.[27] and Langeloth et al.[28] in parallel proposed models incorporating the slip-springs with DPD simulations. The mean-square displacements (MSDs) of beads from their models are demonstrated in favorable agreement with the tube model predictions.[27–29] Later, Ramírez-Hernández et al. reported a theoretically informed entangled polymer simulation approach. In their approach, the topological effects that arise from the noncrossability of molecules are introduced through effective fluctuating interactions, mediated by slip-springs, between neighboring pairs of polymer chains.[30] Recently, Theodorou and coworkers[31] developed a mesoscopic particle-field Brownian dynamics methodology for simulating polymeric materials in realistic time scales. In their approach, the CG beads consist of several Kuhn segments, and the entanglement effect is introduced by the slip-springs, similar to the previous work in this field.

Thus, multi-chain slip-springs have been shown in multiple circumstances to re-introduce the effect of entanglements into the dynamics of polymer chains for particle models too CG. This is where the second technique of our approach, namely slip-springs, comes in. We adopt our own slip-spring model, which has already been used successfully with DPD.[28,29] Slip-springs are virtual harmonic bonds between monomers of two different polymer chains. These virtual bonds are not connecting segments of chains statically and permanently but they can move along the chains following a Monte-Carlo governed hopping dynamics. This naturally restricts lateral chain motion and facilitates the longitudinal one. The use of slip-springs with dissipative-particle dynamics is another proven technology, with its range of applicability well established.[28,29,32] We will, therefore, not review its features in detail, but only to the extent needed for the combination with hPF-MD.

In this paper, we report, for the first time, a combination of hPF-MD with slip-springs, and we validate the performance of the combination of the two components. Those, we regard as established methods with their advantages and disadvantages well documented in the literature. In particular, we first check whether the addition of slip-springs changes any static structural properties of the hPF-MD method, or whether they can be combined safely. This is mainly done by comparing these results for hPF-MD simulation with and without slip-springs. Second, we study the capability of slip-springs to restore entangled dynamics to hPF-MD. To this end, we compare slip-spring hPF-MD calculations with both hPF-MD (no slip-springs) and reference traditional atomistic MD simulations, as far as we are able to afford them. An atomistic model of polyethylene (PE) is chosen as an example to examine the effectiveness of slip-springs in reproducing the entangled dynamics in hPF-MD simulations. Our slip-spring hPF-MD model demonstrates good reproduction of polymer structures compared to the reference MD simulations. Additionally, the topological entanglements as analyzed by the Z1 method[33–35] are consistent

with those from MD simulations and the number of entanglements (kinks) per chain is in qualitative agreement with the chain-length dependent number of slip-springs in the long-chain region. Entangled behavior in translational and reorientational dynamics are characterized by MSDs, bond and end-to-end vector reorientational autocorrelation functions in multiple ways. The time scaling behavior clearly shows that reptation motion can be restored, whereas slight accelerations are found in the short-time regime in both translational and orientational dynamics. This serves to demonstrate that the new slip-spring hPF-MD combination is an alternative to traditional atomistic MD for the study of structural and dynamical properties of polymer systems, as it is much faster. Its well-controlled approximations maintain enough agreement with the reference calculation to be a useful tool.

2 | METHODOLOGY

2.1 | Model

In our model, the dynamics of the polymer system is divided into two parts: (1) Newtonian motion of atoms and (2) hopping movement of slip-springs. The Newtonian motions are governed by three types of forces: (a) bonded, (b) density-functional, and (c) slip-spring potentials. The *bonded* potentials such as bond, angle, and dihedral potentials are exactly the same as used in standard atomistic MD simulations, see below. The *nonbonded* interactions are calculated using the density-functional potential field of the hPF-MD model. For a system of different types of particles, the total interaction energy in the density field is

$$W[\rho(r)] = \frac{1}{\rho_0}\int dr \left(\frac{k_B T}{2} \sum_{i,j} \chi_{i,j} \rho_i(r) \rho_j(r) + \frac{1}{2\kappa} \left(\sum_i \rho_i(r) - \rho_0 \right)^2 \right) \quad (1)$$

where the Flory-Huggins parameter $\chi_{i,j}$ represents the strength of the mean field interaction between particles of type i and j, ρ_0 is the average number density of the system, ρ_i and ρ_j are the number densities of particles of type i and j in the density field, respectively, and κ is the compressibility factor for the system. The density-functional potential acting on individual particles is obtained from the functional derivative of the total field interaction energy with respect to the local density which is given by:

$$U_i^{\text{field}}(r) = \frac{\delta W[\rho(r)]}{\delta \rho_i(r)} = \frac{1}{\rho_0} \left(k_B T \sum_j \chi_{i,j}(r) \rho_j(r) + \frac{1}{\kappa} \left(\sum_i \rho_i(r) - \rho_0 \right) \right) \quad (2)$$

Between lattice points, the potential is numerically interpolated, so that the *nonbonded* force acting on an atom at any point in this space can be calculated. More details about the density-functional potential and its implementation can be found in former publications.[2,5,10–12,14,15]

A constant number of slip-springs is introduced to mimic the binary contacts of topological constraints between entangled strands, replacing chain noncrossability in hPF-MD simulations. As discussed in ref. [36], monomers of a Rouse chain are confined to a tube-like region by an effective harmonic potential formed by the neighboring chains. In this spirit, a harmonic bonding potential is employed for slip-springs in this work:

$$U_{\text{ssp}}(r) = \frac{1}{2} K_{\text{ssp}} (r - r_{0,\text{ssp}})^2 \quad (3)$$

where r is the distance between two connected atoms, K_{ssp} is the slip-spring force constant and $r_{0,\text{ssp}}$ is the equilibrium distance of the slip-spring.

Initially, one end of each slip-spring is connected randomly to an atom. The other connected atom is chosen nearby under the distance criterion $\frac{1}{2} r_{0,\text{ssp}} < r < 2 r_{0,\text{ssp}}$. Slip-springs are allowed to exist as interchain or intrachain, representing entanglements between different chains and self-entanglements, respectively. The movements of these interchain and intrachain slip-springs are controlled in the same way by a Metropolis Monte-Carlo scheme. The locations of slip-springs on atoms are frozen during the Newtonian motion of atoms, and they are mobile only in the intervening Monte-Carlo phases. In a single Monte-Carlo step, each slip-spring attempts to move by one monomer to the left or to the right along the backbone of either polymer chains with an equal probability. The move is accepted with probability $p = min\left(1, e^{-\Delta U_{\text{ssp}}/k_B T}\right)$, where ΔU_{ssp} is the difference of the slip-spring energy between the trial and the old configuration. For simplicity, the movements of slip-springs are completely independent of each other, which means they can pass through one another and one atom can host multiple slip-springs. This implementation is different to some recently developed slip-spring models which apply an excluded volume repulsion between slip-springs.[30,37] It is, however, still not clear whether the excluded volume interaction of slip-springs makes a qualitative difference on the dynamics of polymer melts.[23,27,28,30] In the rare event that two ends of a slip-spring are connected to the same monomer, this slip-spring is destroyed and recreated randomly elsewhere in the system to avoid the formation of entanglement knots. The influence of this annihilation behavior of slip-springs on the dynamics is negligible due to the extremely rare occurrence of this event. To model the disentanglement at chain ends and the constraint release mechanisms, we also introduced a relocation Monte-Carlo move: If one end of a slip-spring reaches the end of the polymer chain, it may be destroyed and recreated at another randomly chosen chain end in the system. The relocation move is accepted with probability $p = \min\left(1, e^{-\Delta U_{\text{ssp}}/k_B T}\right)$, where ΔU_{ssp} is the difference of the slip-spring energy between the new trial slip-spring and the old one. Under this formalism, the lateral chain motion is strongly restricted by the interchain slip-springs, while the longitudinal motion of the chain along the contour remains allowed.[28,29]

The time evolution of the simulation uses alternating MD and MC blocks. The atom positions are propagated by integrating the equation

of motion under NVT conditions over n_{MD} timesteps using a verlocity-Verlet[38] algorithm and a Nosé-Hoover[39] thermostat. Between MD intervals, the configurations of slip-springs are renewed via n_{MC} Monte-Carlo trial moves described above. At the end of an MC block, the Hamiltonian for the subsequent MD has thus been altered. The simulation ends when the total simulation time (MD steps) is reached.

2.2 | Simulations details

We employ the same united-atom model of PE[40] for performing reference MD simulations (denoted as MD in the following), hPF-MD simulations without slip-spring (hPF-MD), and slip-spring hPF-MD simulations. There are several advantages to choose this polymer model as our example. First, this study investigates structural and dynamical properties of PE melts with chain length N (number of carbons in the backbone) ranging from C_{150} to C_{2600} covering weakly to strongly entangled regimes. As a reference, the experimental entanglement length of PE melts is around N = 85.[41] The study of entangled PE requires long simulation times to show the features of entangled dynamics. The choice of united-atom model of PE reduces the computing expense. Moreover, united atom models of PE have been used in a large body of literature investigating its structures, dynamics and rheology properties, and their relation to experiment.[41–46] The force field of the united-atom model of PE is shown in Table 1. The atoms have no partial charges.

In the particle-field part, the lattice constant of the density grid is chosen as 2 Å which is close to the skeletal bond length 1.53 Å and the updating interval of density field is set to be 1 MD timestep to guarantee enough chemical details captured. At a melt density of ~0.77 g/cm^3, a grid cell contains, on average, ~0.29 united atoms. As this contribution is focused on the interplay of hPF-MD and slip-springs, we use this rather fine grid to rule out approximation errors due to the numerics of the grid treatment, we deliberately forgo, for the moment, the possibility of coarser grids, which would effectively CG the *nonbonded* interactions and would further speed up the calculations.[47] The Flory-Huggins parameter χ is 0 for homogeneous polymer melts. The incompressibility factor $1/\kappa$ is chosen as 5 kJ/mol which is similar with previous studies.[5,48] For a better description of the structural behavior of PE melts in hPF-MD simulations, we utilize an additional intramolecular Leonard-Jones potential for 1–5 interactions (Table 1), similar to that used in Monte-Carlo simulations of single polymer chain in melt states,[49,50] whereas carbon atoms separated by more than four bonds only interact by the *nonbonded* interactions as modeled by the field.

In our slip-spring formalism, the confinement of a polymer chain to its tube is governed by a set of slip-spring parameters: n_{MD} and n_{MC}, K_{ssp} and $r_{0,ssp}$, and N_{ssp}. Generally, the mobility of slip-springs is determined by n_{MD} and n_{MC}, and the effect in our model is similar to the findings in the slip-spring-DPD simulation of entangled polymer melts.[28,29] We choose n_{MD} = 500 time steps and n_{MC}/n_{MD} = 1 after testing several combinations of n_{MD} and n_{MC}. Recent MD simulations suggested that the distance of binary contacts in polymer entanglements is between $\frac{1}{2}\sigma$ and 2σ, where σ is the monomer diameter.[51] We use a similar equilibrium distance for the slip-springs $r_{0,ssp}$ = 5.28 Å, which is the distance of the first peak of the inter-monomer radial distribution function. The collective localizing strength of the slip-springs should be strong enough to confine the polymer chains, but any single one should not be too strong, thus K_{ssp} is chosen to be 300 kJ/mol$\approx\frac{1}{5}K_b$. Hence, the number of slip-springs N_{ssp} per chain is the only variable remaining in our formalism. It is determined from the reference MD simulations. Specifically, we first conduct slip-spring hPF-MD simulations with varying number of slip-springs in the system. The number of slip-springs is then determined when the target property (MSDs in this work) of the slip-spring hPF-MD simulations matches that of the reference MD simulations. The resulting number of slip-springs per chain is found to be dependent on the polymer chain length in a linear relation (see details in Figure S2). The relation between N_{ssp} and the related topological entanglement statistics is discussed below.

All PE melts studied in this work are summarized in Table 2. The initial configurations of all systems except PE (C_{2600}) are taken from the reference MD simulations after the density of the systems has been converged. In the case of PE (C_{2600}), we take the density of PE (C_{1300}) and equilibrate the system by a hPF-MD simulation following

TABLE 1 United-atom force field for polyethylene[40,46]

Force field	Analytical form	Parameters
Bond	$U_{bond}(r) = \frac{1}{2}K_b(r-r_b)^2$	K_b = 1,463 kJ/Mol, r_0 = 1.53 Å
Angle	$U_{angle}(\theta) = \frac{1}{2}K_\theta(\theta-\theta_0)^2$	K_θ = 250.8 kJ/Mol/rad^2, θ_0 = 109.5°
Dihedral	$U_{dihedral}(\phi) = \sum_{i=0}^{3} C_i(\cos\phi)^i$	C_0 = 7.26, C_1 = −18.77, C_2 = 3.24, C_3 = 29.21 (kJ/Mol)
Pair	$U_{LJ}(r) = 4\epsilon\left[\left(\frac{\sigma}{r}\right)^{12} - \left(\frac{\sigma}{r}\right)^{6}\right]$, $r < r_C$	σ = 4.01 Å, ϵ = 0.47 kJ/Mol, r_C = 10 Å

TABLE 2 Systems of polyethylene melts studied

N	M	N_{ssp}	d (Å)
150	60	9.7	64.7
200	60	11.6	71.1
250	48	13.4	70.8
300	40	15.3	70.8
350	35	17.1	71.2
520	53	23.5	93.3
1,300	25	52.5	97.6
2,600	25	100.8	97.6

Abbreviations: N, number of carbon atoms; M, number of chains in the melts; Nssp, number of slip-springs per chain; d, size of the simulation box.

the equilibration procedure introduced in ref. [19]. The MD time step δt is 1 femtosecond for all simulations. All simulations are performed in the NVT-ensemble at a temperature of 450 K, to ensure that the polymer is in the melt state and that neither crystallization nor vitrification occurs, using GPU-Accelerated Large-Scale Molecular Simulation Toolkit (GALAMOST)[52] integrated with the in-house code of the slip-spring model.

3 | RESULTS AND DISCUSSION

3.1 | Structural properties

3.1.1 | Statistics of polymer chains

First, we compute the mean square distance $\langle R^2(s)\rangle$ between monomers separated by a number of bonds s along the backbone of polymer chains, as shown in Figure 1. Systems of the longest polymers (C_{2600}) in hPF-MD simulations with and without slip-springs reach the same characteristic distance $\left\langle R(s)^2\right\rangle/s \approx l_0^2 C_\infty = 17.47 \pm 0.22$ Å^2, where l_0 is the skeletal bond length (1.53 Å) and $C_\infty = 7.46 \pm 0.09$ is the characteristic ratio for the polymer with a given chemistry and temperature. As a reference, the PE characteristic ratio from experiments is $C_\infty^{exp} = 7.5 \pm 1.7$(423 K).[53] The good overlap of the results from the hPF-MD simulations with and without slip-springs indicates that the conformations of the linear chain and the correlation between monomers are, as expected, not affected by the introduction of slip-springs. Compared to the MD results (C_{350}), an excellent reproduction can be seen for small and large numbers of bonds ($s < 50$ and $s > 200$) and a slight deviation (less than 5%) for intermediate number of bonds s which is due to the too weak short-range correlation provided by soft potential of density fields. It is, thus, a feature introduced by the hPF-MD approximation itself and not by the addition of slip-springs.

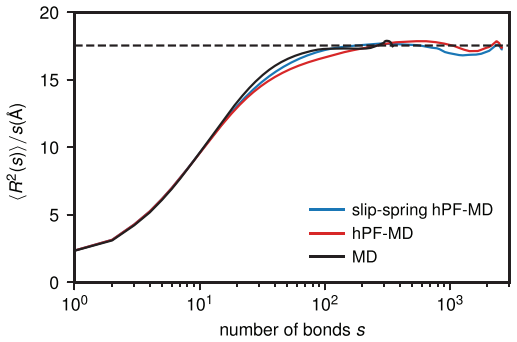

FIGURE 1 Normalized mean square distance between monomers of one chain as function of number of bonds s between them along the backbone for hPF-MD (red, PE-C_{2600}), slip-spring hPF-MD (blue, PE-C_{2600}), and MD (black, PE-C_{350}) simulations. The dashed line is the plateau value from the MD simulation [Color figure can be viewed at wileyonlinelibrary.com]

The probability distributions of the end-to-end distances $P(R_{ete})$, with C_{150} and C_{350} as examples, are shown in Figure 2. The coincidence of the probabilities at all length scales shows the good agreement of our model with the reference MD simulations on the structures. In theory, the mean-square radius of gyration (R_g^2) and the mean-square end-to-end distance (R_{ete}^2) of linear Gaussian polymer chains in the melt are linearly related to the chain length or molar mass, which is believed to be still valid in strongly entangled polymers. Figure 3 shows R_g^2 and R_{ete}^2 for different chain lengths of hPF-MD with and without slip-springs as well as reference MD simulations in a double-logarithmic scale. From the fits in Figure 3, we extract scaling exponents for R_g^2 and R_{ete}^2, which are 1.01 and 1.01, respectively, numerically equal to 1. This is in excellent agreement with the

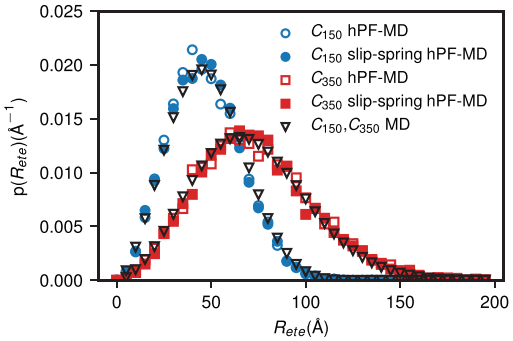

FIGURE 2 Distribution of end-to-end distance for polyethylene C_{150}(circles) and C_{350}(squares) in melts. Results from our hPF-MD (hollow), slip-spring hPF-MD (filled), and MD (black) simulations are compared [Color figure can be viewed at wileyonlinelibrary.com]

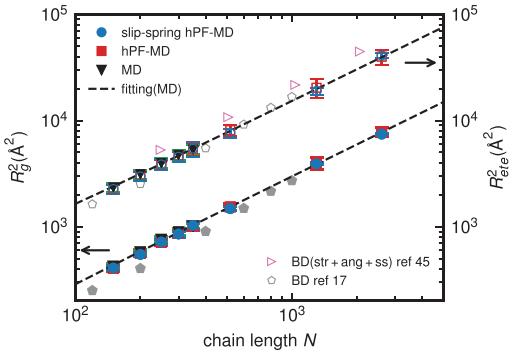

FIGURE 3 Dependence of radius gyration R_g^2 (filled, left axis) and end-to-end distance R_{ete}^2 (hollow, right axis) on the chain length N. Results from hPF-MD(red), slip-spring hPF-MD(blue), and MD(black) simulations are compared. These results are compared with the Brownian dynamics simulations of long polyethylene chain (pink triangles[45] and gray pentagons[17]). Dashed lines are the power law fits for the MD results [Color figure can be viewed at wileyonlinelibrary.com]

theoretical predictions. Furthermore, R_g^2 and R_{ete}^2 are separated by a factor of 6.01 for long PE chains, which is very close to the value of 6 predicted for Gaussian chains. The MD values of both the radius of gyration and end-to-end distance of short chains (C_{150}, C_{350}) are reproduced very well by the hPF-MD simulations with and without slip-springs. For long PE chains (C_{520}, C_{1300}, C_{2600}), the configurations of PE chains still follow the scaling law which is extrapolated from our MD results. The good reproduction of both R_g and R_{ete} compared with reference MD simulations shows the validity of our slip-spring hPF-MD simulations for structural properties, which is consistent or even better than the original hPF-MD model.[5,48] The configurations of polymer chains do not change with the introduction of slip-springs. This further confirms that slip-springs do not alter the equilibrium properties the polymers. It is worth noting that the impact of slip-springs on the statistics of polymer chains may depend on the incompressibility condition (κ in Eq. (2)) of our system. Specifically, if the compressibility factor κ is large, which means that the system is compressed more easily, the additional interactions of the slip-springs may in principle cause contraction of the polymer chains. With the current combination of parameters, though, this is evidently not the case.

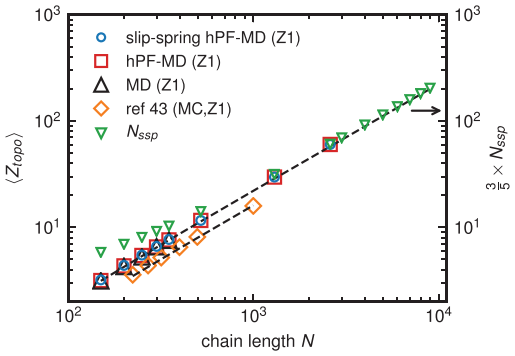

FIGURE 4 Dependence of the average number of topological entanglements per chain $\langle Z_{topo} \rangle$ (left axis) on the chain length N. $\langle Z_{topo} \rangle$ from our hPF-MD(red), slip-spring hPF-MD (blue), and MD (black) as well as other simulation results (orange)[43] are compared. Number of slip-springs per chain N_{ssp} (right axis, green) is compared with $\langle Z_{topo} \rangle$. Dashed lines are the linear fit of $\langle Z_{topo} \rangle$ of our MD results with slope ~0.02 [Color figure can be viewed at wileyonlinelibrary.com]

3.1.2 | Topological entanglement analysis

The phenomenological tube model assumes that a long polymer chain is confined to a tube-like region and it is only allowed one-dimensional reptational motion along it.[54,55] Numerous studies have tried to find a microscopic definition of topological confinements or entanglements.[35,51,56–58] One can analyze the topological entanglements by means of contour-length minimization or chain-shrinking for the polymer chains via CReTA[57] and Z1[33–35] algorithms. In brief, these algorithms construct primitive paths (PP) by fixing the chain ends in space and minimizing their contour-lengths without allowing chains to cross each other. This means that the excluded volume effect is preserved to avoid chain-crossings. The statistics of the topological constraints such as the entanglement length N_e is believed to be closely related to dynamical analysis and rheological measurements according to the tube model.[56] Results calculated on the same configuration using CReTA and Z1 are found almost identical. As the Z1 algorithm converges faster and is more efficient for large systems,[35] we choose it in this work to further investigate structural differences between MD and hPF-MD simulations in terms of topological entanglements and the configurational effect of slip-springs in hPF-MD simulations. It is worth noting that the statistics of topological entanglements obtained from Z1 code in hPF-MD simulations with and without slip-springs is calculated only from single, static configurations, without recourse to entangled dynamics. In theory, polymer chains could cross each other in pure hPF-MD simulations, if we fixed the chain ends and minimized the chain length, and the final contour length would simply be the end-to-end distance. In the Z1 *analysis*, we impose chain uncrossability, even if in the parent hPF-MD simulation the chains were allowed to cross. In systems with the slip-spring hPF-MD model, the slip-springs are interpreted as topological entanglements which are identical to "kinks" in Z1 code. Here, the contour length can be calculated by summing up the distances between chain-ends and segments connected by slip-springs.

The number of entanglements (kinks) per chain $\langle Z_{topo} \rangle$ and the slip-springs per chain N_{ssp} are plotted as a function of N in Figure 4. Both $\langle Z_{topo} \rangle$ and N_{ssp} are proportional to the polymer chain length in general. The overall good agreements between MD and hPF-MD simulations are observed by the overlap between symbols of $\langle Z_{topo} \rangle$. These observations indicate that hPF-MD simulations with soft *non-bonded* interactions can generate configurations of entangled melt similar to the standard MD with hard-core interactions. Furthermore, the introduction of slip-spring does not affect the statistics of topological entanglements at all. Moreover, comparing to Monte-Carlo simulations of PE melts by Kröger et al.,[43] who used a united-atom model at 450 K, our simulation results are seen in good qualitative agreement with theirs, although slightly larger. If the N_{ssp} are multiplied by 0.6 (Figure 4, right axis), they coincide with the topological entanglements $\langle Z_{topo} \rangle$ in well-entangled PE melts. Thus, for long enough chains, each slip-spring is comparable to 1.67 topological entanglements (kinks) in the Z1 analysis, while in short chains (C < 1,000), each slip-spring is comparable to fewer topological entanglements.

The entanglement length N_e is defined through:

$$N_e = (N-1)\frac{\langle R_{ete}^2 \rangle}{\langle L_{pp} \rangle^2} \quad (4)$$

where the bracket indicates the ensemble average and L_{pp} represents the primitive path length. This definition of N_e is denoted as classical

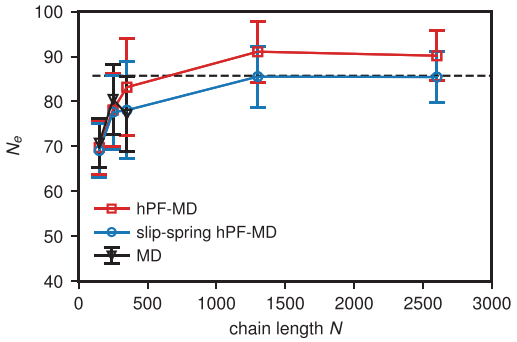

FIGURE 5 Dependence of entanglement length N_e computed by the Z1 code on the chain length N. Results of N_e from hPF-MD (red), slip-spring hPF-MD (blue) and MD (black) are compared. The dashed line is the entanglement length for polyethylene melts from the experiment[59] [Color figure can be viewed at wileyonlinelibrary.com]

S-coil in the Z1 code.[34,43] In Figure 5, the entanglement length N_e from the Z1 analysis shows asymptotic behavior in all simulations. It increases with the chain length and reaches a plateau for long chains. Good agreement is observed between MD and hPF-MD results, indicating the good reproduction of the topological entanglement, even though the excluded volume is imposed only postsimulation at the analysis stage (Z1 algorithm). For comparison, the entanglement length N_e of long enough polymer chains from the hPF-MD simulations with (N_e = 85.7 ± 5.9) and without slip-springs (N_e = 90.2 ± 6.2) is found to be close to the experimental entanglement length N_e = 85.7, the value of which was calculated from the plateau modulus of ultrahigh-molecular-weight PE in the melt state at temperature T = 463 K.[41,59] It is notable here that the entanglement length computed by the Z1 code is not initially aimed to be quantitatively comparable to the experimental measurements due to the different methods (definitions) used for its determinations, although the molecular weight dependence of N_e was estimated in prior experimental studies.[60,61] The slip-spring hPF-MD entanglement length appears to be systematically shorter than the pure hPF-MD values for the three longest chains by about 10%, thereby being in closer agreement with the experiment. It is at present not clear whether this fact is coincidental or whether the introduction of slip-springs preconfigures the melt conformations to have more topological entanglements.

3.2 | Translational dynamics

The diffusive motion of entangled polymers has been well investigated by both experiments and molecular simulations.[42,62–66] In well-entangled polymer melts of very long chains, the MSD of the central monomers $g_1^{\mathrm{mid}}(t)$ should show five distinct regimes corresponding to the different underlying relaxation mechanisms, which are postulated by the tube model. The corresponding scaling behaviors are

$$g_1^{\mathrm{mid}}(t) \approx \begin{cases} C_0 t^2, & t < \tau_b \\ C_1 t^{1/2}, & \tau_b < t < \tau_e \\ C_2 t^{1/4}, & \tau_e < t < \tau_R \\ C_3 \dfrac{t^{1/2}}{N^{1/2}}, & \tau_R < t < \tau_d \\ C_4 \dfrac{t}{N^2}, & \tau_d < t \end{cases} \quad (5)$$

where C_0, C_1, C_2, C_3, and C_4 are phenomenological parameters. One can then determine the characteristic times: ballistic time τ_b, entanglement time τ_e, Rouse time τ_R, and terminal (disentanglement) time τ_d by the intersections between the power-law fits of different regimes.

PE united-atom models of C_{150}–C_{350} are simulated by all methods and longer chains (C_{520}–C_{2600}) are only simulated by hPF-MD simulations with and without slip-springs. Within the time scale simulated, good agreement with the theoretical predictions (Equation 5) is clearly seen (Figure 6) for the MD simulation data and excellent reproduction of the entangled dynamics is found for the slip-spring hPF-MD model. The characteristic time from free Rouse motion to constrained Rouse motion τ_e is shifted due to the low monomeric friction from the soft-core particle-field potentials in the hPF-MD model.

Figure 6 generally shows three different representations of the MSD of the central monomers of the polymer chain. The choice of central monomers excludes the effect of chain ends, which gives better agreements when comparing with the tube model.[66,67] Note that no phenomenological or emprical shifting has been performed on the curves in Figure 6. In Figure 6a, the normal MSDs from our MD and hPF-MD simulations span around 10 orders of time which makes it difficult to see clear characteristic behaviors and differences between them. Figure 6b,c shows the same data but rescaled with $t^{0.5}$ and $t^{0.25}$ which reduces the range of the vertical axis to around 6 orders and exposes the differences among them, allowing clearer comparisons with the scaling predictions of the tube model. In theory, the free Rouse motion ($\tau_b < t < \tau_e$) is seen as plateau in the representation of g_1^{mid} rescaled with $t^{0.5}$ (Figure 6b) and the constrained Rouse motion (entangled dynamics, $\tau_e < t < \tau_R$) is seen as a deep depression. In Figure 6c,d where g_1^{mid} is rescaled by $t^{0.25}$, the constrained Rouse motion is observed as a horizontal plateau. In the following, we mainly focus on the rescaled representations of the MSD.

The monomer MSDs of PE with different chain lengths follow a universal behavior in the ballistic regime ($t < \tau_b$). Above τ_b, theoretically, the polymer segments conduct free Rouse motion ($\tau_b < t < \tau_e$). Our MD and pure hPF-MD results reproduce this behavior (Figure 6b), but the latter is significantly faster. The acceleration seen in pure hPF-MD simulations is not surprising because the friction is reduced due to the softness of the particle-field potential, consistent with previous hPF-MD studies.[5,48] Polymer segments begin to feel confinements from the neighboring chains at τ_e, which is 2 ns for MD simulations, entering the constrained Rouse regime ($\tau_e < t < \tau_R$). Due to the absence of entanglements, τ_e does not exist in pure hPF-MD simulations. As seen in Figure 6c, no depression can be found, indicating that only free Rouse motions exist there. For slip-spring hPF-MD, in contrast, no long and stable plateau is seen in Figure 6b, which

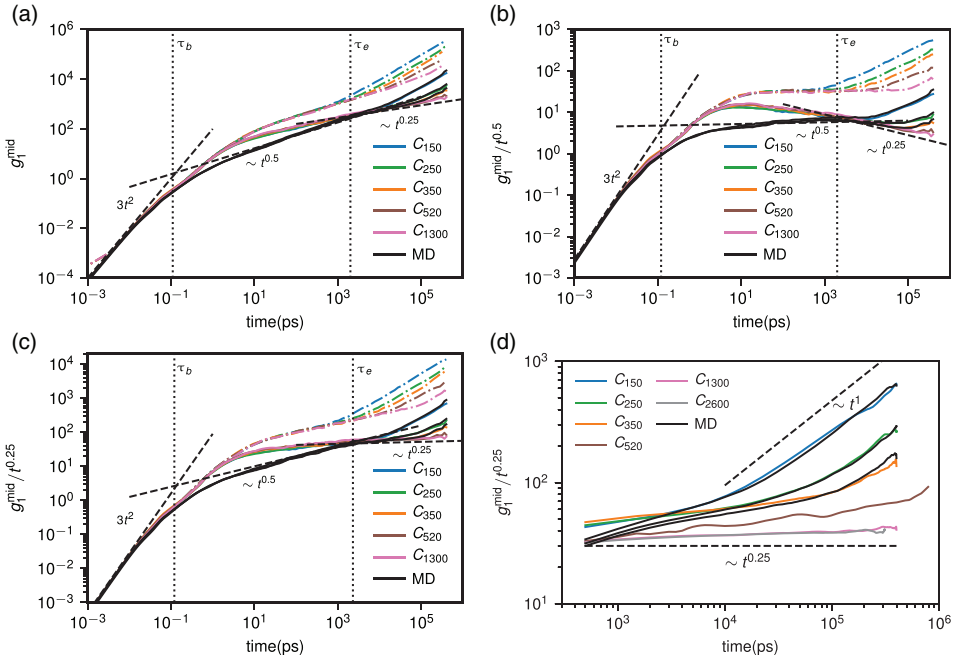

FIGURE 6 Mean square displacements of central monomers from hPF-MD (dot dashed lines), slip-spring hPF-MD (solid lines), and MD (black solid lines) simulations, (a) raw data, (b) rescaled by $t^{0.5}$ power law, (c) rescaled by $t^{0.25}$ power law, and (d) zoom on the reptation regime. The dashed lines are regimes postulated by the tube model for ballistic ($t < \tau_b$), free Rouse motion ($\tau_b < t < \tau_e$) and constrained Rouse motion ($\tau_e < t < \tau_R$) regimes. The vertical dotted lines are borders between two regimes, which are the characteristic time for polyethylene melts [Color figure can be viewed at wileyonlinelibrary.com]

means that free Rouse motion is barely taking place and the constrained Rouse regime begins early. These well-developed constrained Rouse motions are evident as the horizontal plateau in Figure 6c. The coincidence of the curves of $g_1^{mid}/t^{0.25}$ in Figure 6d demonstrates the good agreement of MSDs beyond $\tau_e \approx 2$ ns between the reference MD and the slip-spring hPF-MD simulations. This is a strong indication of the effectiveness of the slip-spring model to restore entangled dynamics to pure hPF-MD simulations. At the same time, the stable plateaus in this representation exhibit the expected $t^{0.25}$ scaling behavior for long polymer chains. In contrast, the acceleration of hPF-MD with respect to the reference MD simulations at short times ($\tau_b < t < \tau_e$) is still observed after introducing slip-springs, suggesting that the slip-springs impose constraints on the dynamics at the length and time scales of the entire polymer chain, rather than alter the local segmental dynamics. It should be noted here that the apparent coincidence of segmental MSDs between the classic MD and the slip-spring hPF-MD simulations are only statistical at long times in the time range which is computationally accessible for mildly entangled polymers ($N_C < C_{520}$) in this work.

The entanglement effects can also be identified through the ratios of MSDs of the end and center of a chain g_1^{end}/g_1^{mid} (Figure 7). For an ideal well entangled linear Gaussian chain, the diffusion of the end and central monomers is similar below the ballistic time τ_b, since it is only affected by the background friction. In this stage $g_1^{end}/g_1^{mid} = 1$. Upon entering the free Rouse regime ($\tau_b < t < \tau_e$), the diffusion of the

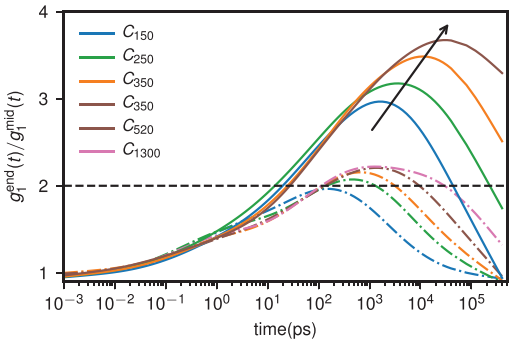

FIGURE 7 Ratios of the monomer mean square displacements of chain end and center, g_1^{end}/g_1^{mid} from hPF-MD (dot dashed lines) and slip-spring hPF-MD (solid lines) simulations. The dashed line refers to the Rouse model prediction of $g_1^{end}/g_1^{mid} = 2$ at the intermediate time regime [Color figure can be viewed at wileyonlinelibrary.com]

monomers is not only influenced by the background friction, but also by the bond connectivity of the chain. Chain end monomers are only connected to one piece of the chain, resulting in less restriction than for the central monomers of the chain. Thus, during this period, the g_1^{end}/g_1^{mid} curve increases with time and is expected to reach the Rouse model value of 2 at $t = \tau_e$ in principle. Above $t = \tau_e$, the motion of the central monomers starts to feel the topological confinements from the neighboring chains, while the chain ends are still free to move to take part in the tube renewal. The g_1^{end}/g_1^{mid} curve keeps increasing and, at $t = \tau_R$, it is predicted according to the tube model to reach a maximum value. After that, the entire chain starts to move coherently and fully diffuses around the terminal time τ_d. In this regime, the g_1^{end}/g_1^{mid} curve decays back to 1. For the result in Figure 7, we take 10 monomers from chain center and the outermost 5 monomers at each chain end as our samples. The curves have been smoothed by a spline interpolation for better visualization. The hPF-MD simulations with and without slip-springs share the same qualitative trend. Particularly, at $t < 10$ ps, the g_1^{end}/g_1^{mid} curves are well overlapped. However, the maximum values of pure hPF-MD simulations do not increase much with the chain length, they seem to reach their maxima around $t \approx 2$ ns with $g_1^{end}/g_1^{mid} \approx 2.1$. For slip-spring hPF-MD simulations, the g_1^{end}/g_1^{mid} curves increase faster and reach their maxima later than for pure hPF-MD simulations. These obvious differences after introducing slip-springs confirm the ability of the slip-springs to better confine the motion of the chain centers. Moreover, the maximum value of g_1^{end}/g_1^{mid} slip-spring hPF-MD increases with the chain length, consistent with the previous Monte-Carlo and MD simulations and the theoretical predictions for entangled polymers.[62,67,68]

We also extract the maxima of the peaks in Figure 7 and plot them together with the theoretical predictions of the tube model as function of $\langle Z_{topo} \rangle^{-\frac{1}{2}}$, as seen in Figure 8. The number of entanglements per chain $\langle Z_{topo} \rangle$ used in this plot is the one computed by the Z1 code (see above). A value of $\max(g_1^{end}/g_1^{mid}) = 4\sqrt{2}$ is predicted theoretically from the Evans-Edwards model for polymers with infinite entanglements Z_∞.[68] In the pure hPF-MD simulations, the maximum values of the g_1^{end}/g_1^{mid} remain close to the Rouse prediction of 2 and for all $\langle Z_{topo} \rangle$. This means that only the Rouse behavior is found and entanglement effects are absent in the pure hPF-MD model for all chain lengths. By introducing slip-springs into the hPF-MD model, in contrast, the maxima clearly increase with $\langle Z_{topo} \rangle$, qualitatively consistent with the theoretical predictions of the tube model. This shows once more the capability of slip-springs to mimic the topological constraints in the hPF-MD model. There are, however, discrepancies between the tube model predictions and the slip-spring hPF-MD, which are probably owed to the different descriptions of the polymer model. An ideal Gaussian chain is assumed in the tube model, while in our simulations, an atomistic model with stronger chain rigidity is adopted.

The diffusion coefficients have also been estimated[69,70] from linear regime of the MSD curve ($t > t_d$). According to the Rouse and tube model, the diffusion coefficient D of a linear entangled polymer melt system follows the scaling behavior given by:

$$D \sim \begin{cases} N^{-1}, & N < N_e \\ N^{-2}, & N > N_e \end{cases} \tag{6}$$

Figure 9 plots chain-length dependent diffusion coefficients. The diffusion coefficients from the pure hPF-MD simulations (red squares) scale approximately with N^{-1}, which shows no signature of reptation and is consistent with the chain-crossings allowed by the soft density-field interactions. In contrast, for the hPF-MD simulations with slip-springs, D scales with $N^{-2.03}$ for $N > N_e$, indicating the recovery of

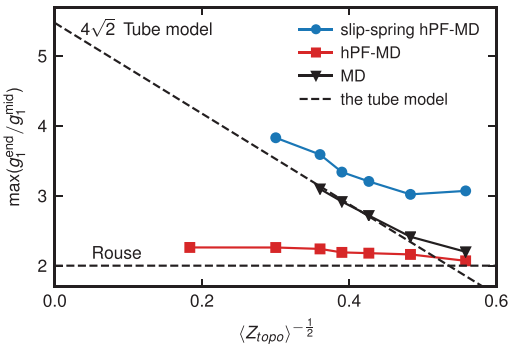

FIGURE 8 Dependence of maximum of the ratio g_1^{end}/g_1^{mid} from hPF-MD (red), slip-spring hPF-MD (blue), and MD (black) simulations on $\langle Z_{topo} \rangle^{-\frac{1}{2}}$. The dashed line is the theoretical prediction of Rouse model and the tube model [Color figure can be viewed at wileyonlinelibrary.com]

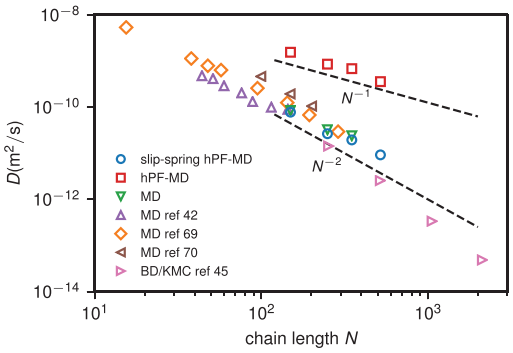

FIGURE 9 Scaling behavior of the diffusion coefficients with respect to the chain length. For hPF-MD simulations (red squares), $D_{hPF} \sim N^{-1}$; For slip-spring hPF-MD simulations (blue circle), the diffusion coefficients scale with N^{-2}; The results are compared with our MD simulations (green inverted triangle) and other MD simulations of polyethylene melts (purple triangles,[69] orange diamonds,[42] brown triangles,[70] and pink triangles[71]). The dashed lines are guide lines to the eye [Color figure can be viewed at wileyonlinelibrary.com]

entangled dynamics. We also note that D from the slip-spring hPF-MD simulations is very close to the atomistic MD calculations of us and others quantitatively, the deviations of which may be attributed to the low statistics at long times needed for calculating the diffusion coefficients.

3.3 | Orientational dynamics

Polymer dynamics can also be measured in terms of orientational autocorrelation functions of various intrachain vectors. In well entangled polymers, the decay of the segmental orientational autocorrelation functions is significantly slowed by the entanglements. These retardations in orientational dynamics have been observed in NMR and dielectric spectroscopy[72–77] and molecular simulations.[67,78] In MD simulations, the normalized orientational auto-correlation functions are calculated as:

$$\mathrm{ACF}(t) = \left\langle \vec{u}(t)\cdot\vec{u}(0) \right\rangle \tag{7}$$

where $\vec{u}(t) = \vec{l}(t)/\left|\vec{l}(t)\right|$ is the segmental unit vector with $\left|\vec{l}(t)\right|$ being the segment length at time t and the bracket denotes the ensemble average. The shortest $\vec{l}(t)$ is the backbone bond vector, which samples the local segmental dynamics. The longest is the end-to-end vector, which is only fully relaxed at the disentanglement time τ_d in entangled polymers. The relaxation time of the end-to-end vector τ_{ete} is the longest single-chain relaxation time in entangled polymer melts. In the Doi-Edwards tube model, τ_{ete} is predicted to be proportional to the third power of the chain length of entangled polymers N, while in experiments this characteristic exponent is measured as $N^{3.4}$. The deviation is interpreted by the other two underlying relaxation mechanisms: contour length fluctuation and constraint release which accelerate the disentanglement process and have been widely discussed.[55,79–82] Since in our slip-spring model, the implementation naturally includes these two relaxation mechanisms besides reptation, the molecular weight dependence of τ_{ete} is expected to approach the experimental value.

Figure 10 exhibits the next-neighbor bond orientational auto-correlation function for various chain lengths in MD, hPF-MD and slip-spring hPF-MD simulations. The results are averaged over 50 bond vectors in the central part of the chain. Generally, the developments of the ACF function are similar to the translational diffusion characteristics, which can be distinguished with several characteristic times (τ_b, τ_e...). As seen in the figure, the curves coincide in the ballistic regime ($t < \tau_b$), afterward they are separated and show different decay rates. The hPF-MD simulations with and without slip-springs share the same behavior up to $t \approx 10$ ps, which is consistent with findings in the MSDs, indicating that slip-springs do not alter the short-time segmental-orientation behavior either. After this time, the hPF-MD simulations with and without slip-springs deviate and the deviation increases with time. Discrepancies between MD and both hPF-MD simulations starts above the ballistic time $\tau_b \approx 0.5$ ps. Above $\tau_e^{MD} \approx 2$ns, the ACF of slip-spring hPF-MD coincides again with that from MD simulations within the fluctuation of the data. Overall, the transition around the characteristic times ($\tau_b \approx 0.5$ ps, $\tau_e^{hPF} \tilde{1}0$ps and $\tau_e^{MD} \approx 2$ns) is consistent with that of the MSDs g_1 shown above. This consistency implies that our slip-spring model influences translational and orientational segmental dynamics in the same way.

The other limit of single-chain relaxation time is that of the end-to-end vector, τ_{ete}, which can be estimated from the autocorrelation function of the end-to-end unit vector $\mathrm{ACF}_{ete}(t)$. The autocorrelation

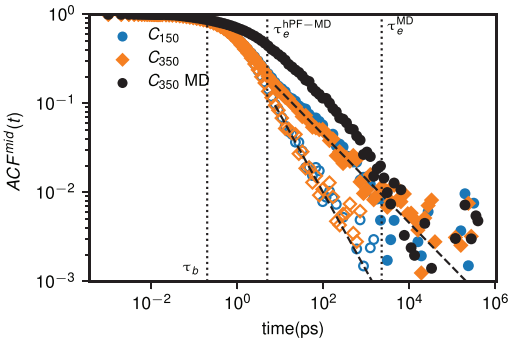

FIGURE 10 Bond orientational autocorrelation function averaged over the 50 bond vectors in the central chain from hPF-MD (hollow), slip-spring hPF-MD (filled), and MD (black) simulations of PE-C_{150} and PE-C_{350}. Dashed lines are the exponential fitting for hPF simulations with and without slip-springs [Color figure can be viewed at wileyonlinelibrary.com]

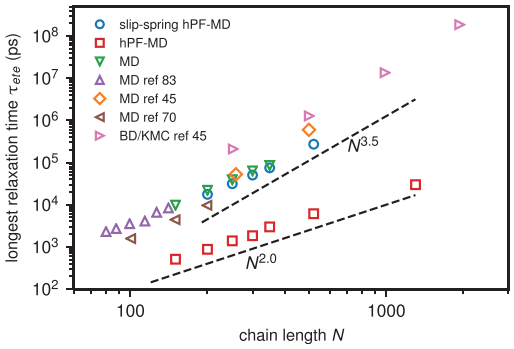

FIGURE 11 Results of relaxation time of end-to-end vector τ_{ete} as function of the chain length N from hPF-MD (red), slip-spring hPF-MD (blue), and MD (black) simulations. These results are compared with other molecular dynamics simulations (purple triangle,[83] orange diamond,[45] brown triangle[70]), and equation of state Brownian dynamics simulation (pink triangle[45]). The dashed lines are a guide to the eye which are power law scaling ($\tau_{ete} \sim M^{3.5}$) of entangled dynamics observed in experiments and scaling ($\tau_{ete} \sim M^{2.0}$) of unentangled Rouse behavior [Color figure can be viewed at wileyonlinelibrary.com]

function is expected to show exponential decay at long times when $ACF_{ete}(t)$ is smaller than a certain value (i.e., $1/e$). An exponential fit to this regime

$$ACF(t) = \exp\left[-\left(\frac{t}{\tau_{ete}}\right)\right] \quad (8)$$

yields τ_{ete} as a fit parameter. As discussed above, the Rouse model predicts $\tau_{ete} \sim N^2$ in unentangled polymer melts. The dependence of the relaxation time of end-to-end vectors τ_{ete} on the chain length of entangled PE chain from MD, hPF-MD simulations with and without slip-springs is shown in Figure 11. For the hPF-MD simulations, τ_{ete} is found to follow the Rouse prediction $\tau_{ete} \sim N^2$ for all chain lengths examined. With addition of the slip-springs, the chain reorientational mobility also slows down and its scales roughly as $\tau_{ete} \sim N^{3.5}$ in the limit of long chains, once more indicating the recovery of the reptation motions by the introduction of slip-springs. In passing, we note that the relaxation of the end-to-end vector is related to the stress relaxation in polymer melts.[78,82,84,85] Since slip-spring hPF-MD reproduces the relaxation behavior of fully atomistic MD, it should offer a way to obtain, in principle, rheological properties of polymer melts. This is an interesting prospect, not yet pursued in this contribution, for obtaining rheological properties from hPF-MD. The traditional MD route via the Green-Kubo relation $G(t) = V\langle\sigma_{\alpha\beta}(t)\sigma_{\alpha\beta}(0)\rangle/k_BT$ from the stress fluctuation in equilibrium melts, does not work in hPD-MD since a rigorous presciption for calculating the stress tensor components $\sigma_{\alpha\beta}(t)$ for the particle-field terms has not (yet) been worked out.

4 | CONCLUSIONS

This work shows that the combination of multi-chain slip-springs with hybrid particle-field-MD (hPF-MD) simulations reproduces most aspects of entangled dynamics in polymer melts at atomistic resolution. The hybrid particle-field simulation is known for its computational efficiency compared to classic MD simulations. The combination with slip-springs inevitably requires additional computations. The calculation of slip-spring forces is in fact adds a small number of terms to the bond forces, and is thus cheap. The most demanding part is the neighbor search in relocation step. However, it takes place only infrequently through the whole simulation. As a consequence, the speed of the hybrid particle-field simulation with slip-springs reaches around 75% of the unmodified hPF-MD simulations for systems composed of up to 5×10^5 particles in the current serial implementation of slip-spring Monte-Carlo movements. The slip-springs successfully replace the topological constraints and efficiently offset the chain crossings inherent in hPF-MD models. Static polymer properties are reproduced well by hPF-MD simulations with and without slip-springs such as the chain conformations and primitive path statistics. Correct static structure calculations are not necessarily found in other single-chain or multi-chain slip-spring models.[23,86] In addition, the detailed comparisons of the equilibrium structural properties between hPF-MD with and without slip-springs indicate that the introduction of slip-springs alters neither the chain statistics nor the topological entanglements, even though no additional correction potential is utilized. This suggests that, at least for polymer melts, the interactions from the density-field are sufficient to sustain the polymer configurations, similar as for the DPD model reported earlier.[28,29] This is an advantage of our slip-spring hPF-MD model over some other slip-spring models.[23,27]

The unmodified hPF-MD ignores chain noncrossability and leads to a polymer mobility which is not only too fast, but also qualitatively wrong. Introducing slip-springs restores correct polymer dynamics on almost all time scales as has been shown in the analysis of monomer MSDs and bond orientational autocorrelation functions. These results are rather close to reference MD calculations with full pairwise interactions, especially above the entanglement time $\tau_e \approx 2$ ns. The impact of slip-springs is similar on translational (MSDs) and reorientational motion (bond auto-correlation functions) and scaling cross-overs occur at the same characteristic times. Moreover, with slip-springs present, the end-to-end relaxation time τ_{ete} obeys the same power law relation to molar mass of PE, as seen in experiments and MD simulations, whereas the end-to-end relaxation time τ_{ete} of unmodified hPF-MD follows the Rouse-law for all molar masses. The entanglement effect however emerges at relatively short times in slip-spring hPF-MD simulations and the Rouse-like regime is compressed and hardly seen in either segmental translational or orientational characterizations. Thus, slip-springs seem to alter the dynamics at intermediate time and length scales. The dynamics at this scale, however, might be separately addressed, if needed, via modifying the equations of motion such as employing Langevin or Lowe-Andersen dynamics. For $t < \tau_e$, the dynamics is Rouse like and the motions are governed by the monomeric frictions in three dimensions ζ_{3D},[54,55,87,88] which has also been shown in CG polymer simulations.[89]

We seem to have found a working combination of the control parameters of the slip-springs. Yet, the underlying physics of some parameters such as the ratio of MD to MC steps and the number of slip-springs used in our present formalism may need further investigations. The MD/MC ratio has been found to impact the diffusion behavior in a similar way in a previous model proposed by our group,[28,90] namely by altering the effective Rouse time in one dimension (reptation) $\tau_{R,1D}$. This time is related to the one dimensional segmental friction coefficient ζ_{1D}[88] which is different from its three-dimensional counter part ζ_{3D}. Furthermore, the multi-chain slip-spring formulation and its incorporation with hPF-MD allow applications of the present model to problems specifically where the chemical details and intermolecular interactions have significant influences such as kinetics in complex morphologies of multicomponent polymeric materials[91–93] and dispersions of nanoparticles into polymer matrices.[94,95]

ACKNOWLEDGMENTS

Z. Wu thanks Prof. Martin Kröger for providing the Z1 code. The authors also thank our partners in the ROBERTO consortium (Prof. Toshihiro Kawakatsu and Prof. Yuichi Masubuchi) for many fruitful discussions along the project. This research is funded by the Deutsche

Forschungsgemeinschaft via the SFB-TRR 146 "Multiscale Simulation Methods for Soft Matter Systems", Project A8. Z. Wu gratefully acknowledges the computing time granted on the supercomputer Mogon at Johannes Gutenberg University Mainz. Open access funding enabled and organized by Projekt DEAL.

ORCID

Zhenghao Wu https://orcid.org/0000-0003-2862-4432

REFERENCES

[1] F. Müller-Plathe, *ChemPhysChem* **2002**, *3*(9), 754.
[2] G. Milano, T. Kawakatsu, *J. Chem. Phys.* **2009**, *130*(21), 214106.
[3] M. W. Matsen, M. Schick, *Phys. Rev. Lett.* **1994**, *72*(16), 2660.
[4] F. Drolet, G. H. Fredrickson, *Phys. Rev. Lett.* **1999**, *83*(21), 4317.
[5] A. De Nicola, T. Kawakatsu, G. Milano, *J. Chem. Theory Comput.* **2014**, *10*(12), 5651.
[6] S. Caputo, A. De Nicola, G. Donati, A. David, G. Raos, G. Milano, *J. Electrochem. Soc.* **2019**, *166*(9), B3309.
[7] A. De Nicola, Y. Zhao, T. Kawakatsu, D. Roccatano, G. Milano, *J. Chem. Theory Comput.* **2011**, *7*(9), 2947.
[8] G. Milano, T. Kawakatsu, A. D. Nicola, *Phys. Biol.* **2013**, *10*(4), 045007.
[9] G. J. Sevink, F. Schmid, T. Kawakatsu, G. Milano, *Soft Matter* **2017**, *13* (8), 1594.
[10] A. De Nicola, S. Hezaveh, Y. Zhao, T. Kawakatsu, D. Roccatano, G. Milano, *Phys. Chem. Chem. Phys.* **2014**, *16*(11), 5093.
[11] A. Pizzirusso, A. De Nicola, G. J. Sevink, A. Correa, M. Cascella, T. Kawakatsu, M. Rocco, Y. Zhao, M. Celino, G. Milano, *Phys. Chem. Chem. Phys.* **2017**, *19*(44), 29780.
[12] Y. L. Zhu, Z. Y. Lu, G. Milano, A. C. Shi, Z. Y. Sun, *Phys. Chem. Chem. Phys.* **2016**, *18*(14), 9799.
[13] S. L. Bore, H. B. Kolli, T. Kawakatsu, G. Milano, M. Cascella, *J. Chem. Theory Comput.* **2019**, *15*(3), 2033.
[14] H. B. Kolli, A. De Nicola, S. L. Bore, K. Schäfer, G. Diezemann, J. Gauss, T. Kawakatsu, Z. Y. Lu, Y. L. Zhu, G. Milano, M. Cascella, *J. Chem. Theory Comput.* **2018**, *14*(9), 4928.
[15] S. L. Bore, G. Milano, M. Cascella, *J. Chem. Theory Comput.* **2018**, *14* (2), 1120.
[16] J. T. Padding, W. J. Briels, *J. Chem. Phys.* **2001**, *115*(6), 2846.
[17] J. T. Padding, W. J. Briels, *J. Chem. Phys.* **2002**, *117*(2), 925.
[18] G. PAN, C. W. MANKE, *Int. J. Mod. Phys. B* **2003**, *17*(01n02), 231.
[19] J. D. Schieber, M. Andreev, *Annu. Rev. Chem. Biomol. Eng.* **2014**, *5* (1), 367.
[20] J. D. Schieber, J. Neergaard, S. Gupta, *J. Rheol.* **2003**, *47*(1), 213.
[21] A. E. Likhtman, *Macromolecules* **2005**, *38*(14), 6128.
[22] Y. Masubuchi, J.-I. Takimoto, K. Koyama, G. Ianniruberto, G. Marrucci, F. Greco, *J. Chem. Phys.* **2001**, *115*(9), 4387.
[23] T. Uneyama, Y. Masubuchi, *J. Chem. Phys.* **2012**, *137*(15), 154902.
[24] Y. Masubuchi, *Annu. Rev. Chem. Biomol. Eng.* **2014**, *5*(1), 11.
[25] Y. Masubuchi, *Macromolecules* **2018**, *51*(24), 10184.
[26] Y. Masubuchi, T. Uneyama, *Soft Matter* **2018**, *14*(29), 5986.
[27] V. C. Chappa, D. C. Morse, A. Zippelius, M. Müller, *Phys. Rev. Lett.* **2012**, *109*, 148302.
[28] M. Langeloth, Y. Masubuchi, M. C. Böhm, F. Müller-Plathe, *J. Chem. Phys.* **2013**, *138*(10), 104907.
[29] M. Langeloth, Y. Masubuchi, M. C. Böhm, F. Müller-Plathe, *J. Chem. Phys.* **2014**, *141*(19), 194904.
[30] A. Ramírez-Hernández, B. L. Peters, L. Schneider, M. Andreev, J. D. Schieber, M. Müller, J. J. De Pablo, *J. Chem. Phys.* **2017**, *146*(1), 014903.
[31] G. G. Vogiatzis, G. Megariotis, D. N. Theodorou, *Macromolecules* **2017**, *50*(7), 3004.
[32] Y. Masubuchi, M. Langeloth, M. C. Böhm, T. Inoue, F. Müller-Plathe, *Macromolecules* **2016**, *49*(23), 9186.
[33] M. Kröger, *Comput. Phys. Commun.* **2005**, *168*(3), 209.
[34] S. Shanbhag, M. Kröger, *Macromolecules* **2007**, *40*(8), 2897.
[35] R. S. Hoy, K. Foteinopoulou, M. Kröger, *Phys. Rev. E* **2009**, *80*, 031803.
[36] D. J. Read, K. Jagannathan, A. E. Likhtman, *Macromolecules* **2008**, *41* (18), 6843.
[37] J. Cao, Z. Wang, A. E. Likhtman, *Polymer* **2019**, *11*, 496.
[38] W. C. Swope, H. C. Andersen, P. H. Berens, K. R. Wilson, *J. Chem. Phys.* **1982**, *76*(1), 637.
[39] S. Nosé, *J. Chem. Phys.* **1984**, *81*(1), 511.
[40] S. L. Mayo, B. D. Olafson, W. A. Goddard, *J. Phys. Chem.* **1990**, *94* (26), 8897.
[41] J. Ramos, J. Vega, J. Martínez-Salazar, *Eur. Polym. J.* **2018**, *99*, 298.
[42] V. A. Harmandaris, V. G. Mavrantzas, D. N. Theodorou, M. Kröger, J. Ramírez, H. C. Ottinger, D. Vlassopoulos, *Macromolecules* **2003**, *36*(4), 1376.
[43] K. Foteinopoulou, N. C. Karayiannis, V. G. Mavrantzas, M. Kröger, *Macromolecules* **2006**, *39*(12), 4207.
[44] J. Ramos, J. F. Vega, D. N. Theodorou, J. Martinez-Salazar, *Macromolecules* **2008**, *41*(8), 2959.
[45] A. P. Sgouros, G. Megariotis, D. N. Theodorou, *Macromolecules* **2017**, *50*(11), 4524.
[46] D. Hossain, M. A. Tschopp, D. K. Ward, J. L. Bouvard, P. Wang, M. F. Horstemeyer, *Polymer* **2010**, *51*(25), 6071.
[47] Y. Zhao, A. De Nicola, T. Kawakatsu, G. Milano, *J. Comput. Chem.* **2012**, *33*(8), 868.
[48] A. De Nicola, T. Kawakatsu, F. Müller-Plathe, G. Milano, *Eur Phys J: Special Topics* **2016**, *225*(8–9), 1817.
[49] J. Baschnagel, K. Qin, W. Paul, K. Binder, *Macromolecules* **1992**, *25* (12), 3117.
[50] S. Neyertz, D. Brown, *J. Chem. Phys.* **2001**, *115*(2), 708.
[51] A. E. Likhtman, M. Ponmurugan, *Macromolecules* **2014**, *47*(4), 1470.
[52] Y. L. Zhu, H. Liu, Z. W. Li, H. J. Qian, G. Milano, Z. Y. Lu, *J. Comput. Chem.* **2013**, *34*(25), 2197.
[53] J. Schelten, D. Ballard, G. Wignall, G. Longman, W. Schmatz, *Polymer* **1976**, *17*(9), 751.
[54] M. Doi, S. Edwards, *The Theory of Polymer Dynamics*, Oxford University Press, New York, NY **1986**.
[55] R. S. Graham, A. E. Likhtman, T. C. B. McLeish, S. T. Milner, *J. Rheol.* **2003**, *47*(5), 1171.
[56] R. Everaers, S. K. Sukumaran, G. S. Grest, *Science* **2010**, *823* (2004), 823.
[57] C. Tzoumanekas, D. N. Theodorou, *Macromolecules* **2006**, *39*(13), 4592.
[58] J. Qin, S. T. Milner, *Soft Matter* **2011**, *7*(22), 10676.
[59] J. F. Vega, S. Rastogi, G. W. M. Peters, H. E. H. Meijer, *J. Rheol.* **2004**, *48*(3), 663.
[60] E. van Ruymbeke, D. Vlassopoulos, M. Kapnistos, C. Liu, C. Bailly, *Macromolecules* **2010**, *43*(1), 525.
[61] C.-Y. Liu, A. F. Halasa, R. Keunings, C. Bailly, *Macromolecules* **2006**, *39*(21), 7415.
[62] T. Kreer, J. Baschnagel, M. Müller, K. Binder, *Macromolecules* **2001**, *34*(4), 1105.
[63] K. Kremer, G. S. Grest, *J. Chem. Phys.* **1990**, *92*(8), 5057.
[64] M. Monkenbusch, A. Wischnewski, L. Willner, D. Richter, *Phys. B* **2004**, *350*(1), 214.
[65] J. Ramos, J. F. Vega, J. Martínez-Salazar, *Soft Matter* **2012**, *8*(23), 6256.
[66] H. P. Hsu, K. Kremer, *J. Chem. Phys.* **2016**, *144*(15), 154907.
[67] Z. Wang, A. E. Likhtman, R. G. Larson, *Macromolecules* **2012**, *45*(8), 3557.
[68] U. Ebert, L. Schäfer, A. Baumgärtner, *J. Stat. Phys.* **1998**, *90*(5–6), 1325.
[69] K. Hur, C. Jeong, R. G. Winkler, N. Lacevic, R. H. Gee, D. Y. Yoon, *Macromolecules* **2011**, *44*(7), 2311.

[70] K. Z. Takahashi, R. Nishimura, K. Yasuoka, Y. Masubuchi, *Polymer* **2017**, *9*(1), 1.
[71] A. P. Sgouros, A. T. Lakkas, G. Megariotis, D. N. Theodorou, *Macromolecules* **2018**, *51*(23), 9798.
[72] M. G. Brereton, *Macromolecules* **1990**, *23*(4), 1119.
[73] F. Vaca Chávez, K. Saalwächter, *Phys. Rev. Lett.* **2010**, *104*, 198305.
[74] F. Vaca Chávez, K. Saalwächter, *Macromolecules* **2011**, *44*(6), 1549.
[75] K. Adachi, T. Kotaka, *Macromolecules* **1984**, *17*(1), 120.
[76] K. Adachi, T. Kotaka, *Macromolecules* **1985**, *18*(3), 466.
[77] Y. Zhang, M. Zuo, Y. Song, X. Yan, Q. Zheng, *Comp. Sci. Technol.* **2015**, *106*, 39.
[78] E. Pilyugina, M. Andreev, J. D. Schieber, *Macromolecules* **2012**, *45* (14), 5728.
[79] J. P. Mont fort, G. Marin, P. Monge, *Macromolecules* **1984**, *17*(8), 1551.
[80] J. L. Viovy, M. Rubinstein, R. H. Colby, *Macromolecules* **1991**, *24*(12), 3587.
[81] S. T. Milner, T. C. B. McLeish, A. E. Likhtman, *J. Rheol.* **2002**, *45* (2), 539.
[82] M. E. Shivokhin, D. J. Read, D. Kouloumasis, R. Kocen, F. Zhuge, C. Bailly, N. Hadjichristidis, A. E. Likhtman, *Macromolecules* **2017**, *50* (11), 4501.
[83] V. A. Harmandaris, V. G. Mavrantzas, D. N. Theodorou, *Macromolecules* **1998**, *31*(22), 7934.
[84] T. Glomann, G. J. Schneider, A. R. Brás, W. Pyckhout-Hintzen, A. Wischnewski, R. Zorn, J. Allgaier, D. Richter, *Macromolecules* **2011**, *44*(18), 7430.
[85] Y. Matsumiya, K. Kumazawa, M. Nagao, O. Urakawa, H. Watanabe, *Macromolecules* **2013**, *46*(15), 6067.
[86] S. K. Sukumaran, A. E. Likhtman, *Macromolecules* **2009**, *42*(12), 4300.
[87] P. G. De Gennes, *J. Chem. Phys.* **1971**, *55*(2), 572.
[88] A. E. Likhtman, M. S. Talib, B. Vorselaars, J. Ramirez, *Macromolecules* **2013**, *46*(3), 1187.
[89] H. J. Qian, C. C. Liew, F. Müller-Plathe, *Phys. Chem. Chem. Phys.* **2009**, *11*, 1962.
[90] J. Schneider, L. D. Süss, F. Müller-Plathe, *J. Chem. Eng. Data* **2020**, *65* (3), 1264.
[91] M. Murat, G. S. Grest, K. Kremer, *Macromolecules* **1999**, *32*(3), 595.
[92] K. C. Daoulas, M. Müller, J. J. de Pablo, P. F. Nealey, G. D. Smith, *Soft Matter* **2006**, *2*, 573.
[93] M. Müller, *J. Stat. Phys.* **2011**, *145*(4), 967.
[94] I. G. Mathioudakis, G. G. Vogiatzis, C. Tzoumanekas, D. N. Theodorou, *IEEE Trans. Nanotechnol.* **2016**, *15*(3), 416.
[95] S. K. Kumar, V. Ganesan, R. A. Riggleman, *J. Chem. Phys.* **2017**, *147* (2), 020901.

SUPPORTING INFORMATION

Additional supporting information may be found online in the Supporting Information section at the end of this article.

How to cite this article: Wu Z, Kalogirou A, De Nicola A, Milano G, Müller-Plathe F. Atomistic hybrid particle-field molecular dynamics combined with slip-springs: Restoring entangled dynamics to simulations of polymer melts. *J Comput Chem*. 2021;42:6–18. https://doi.org/10.1002/jcc.26428

Supplemental Material for: Atomistic Hybrid Particle-Field Molecular Dynamics Combined with Slip-Springs: Restoring Entangled Dynamics to Simulations of Polymer Melts

Zhenghao Wu [*], Andreas Kalogirou[*], Antonio De Nicola [†], Giuseppe Milano[†], Florian Müller-Plathe[*]

September 16, 2020

Determining the Number of Slip-Springs from MD Simulations

This section provides more details about the determination of the number of slip-springs in our model. The number of slip-springs N_{ssp} per chain is expected to depend linearly on the chain length. In practice, we conduct slip-spring hPF-MD simulations with different concentrations of slip-springs $\rho_{ssp} = N_{ssp}^{\text{total}}/N^{\text{total}}$, where N_{ssp}^{total} is the total number of slip-springs and N^{total} is the number of atoms in the system. Then we compute the mean square displacements of the chain centers and extract the values of g_1^{mid} at $t = \tau_R$. After that, comparing $g_1^{\text{mid}}(\tau_R)$ of different ρ_{ssp} with the reference MD values, the optimum total number of slip-springs N_{ssp}^{total} for each chain length is identified. In this work, chain length $N = C_{150}$, C_{200}, C_{250}, C_{300} and C_{350} and values of ρ_{ssp} from 0.03 to 0.08 are chosen for determining the number of slip-springs. An example is shown in Figure S1 for the mean square displacements of chain centers of PE (C_{350}) with various ρ_{ssp} and the reference MD result. It is worth noting that the MD simulation shows the same qualitative behavior as the slip-spring hPF-MD simulations with different ρ_{ssp}. As seen in Figure S4, the number of slip-springs per chain N_{ssp} is found to follow the linear relation with the chain length quite well. The linear relation is shown below:

$$N_{ssp} = k\,N + b \tag{1}$$

where $k = 0.037$ and $b = 4.12$ are the fitting parameters. This linearity between the number of slip-springs per chain and the chain length is also found in other slip-spring models [1,2]. With this relation, the number of slip-springs can be extrapolated for long polymers.

[*]Eduard-Zintl-Institut für Anorganische und Physikalische Chemie, Technische Universität Darmstadt, Alarich-Weiss-Str. 8, 64287 Darmstadt, Germany

[†]Department of Organic Materials Science, Yamagata University, 4-3-16 Jonan Yonezawa, Yamagata-ken 992-8510, Japan

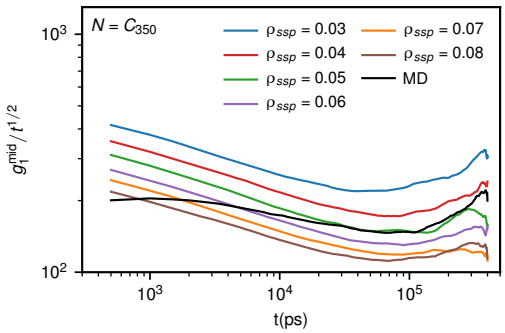

Figure S1: Mean square displacements of chain centers of PE (C_{350}) normalized by $t^{1/2}$ for slip-spring hPF-MD with various concentrations of slip-springs and the corresponding MD simulation.

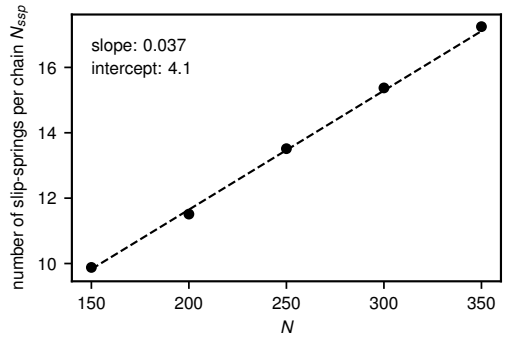

Figure S2: Dependence of the number of slip-springs per chain N_{ssp} on the polymer chain length N. The dashed line is a linear fit.

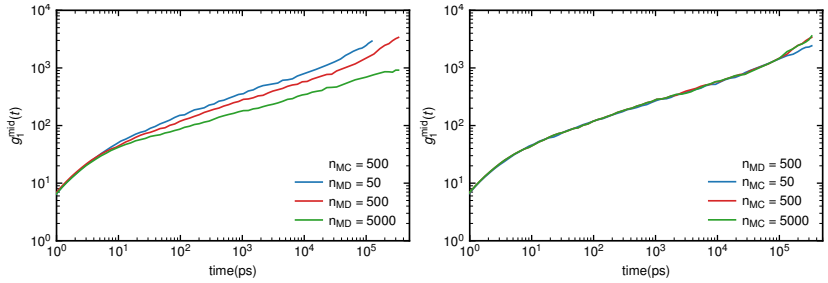

(a) (b)

Figure S3: Influence of sequence length of the molecular dynamics and Monte-Carlo blocks on the diffusive dynamics of polyethylene melts composed of 350 carbons.

Influence of Sequence Length of Molecular Dynamics and Monte-Carlo Blocks

The influence of the sequence length of Molecular Dynamics (n_{MD}) and Monte-Carlo (n_{MC}) blocks on polymer dynamics in the combination of slip-springs and the hybrid particle-field simulation is similar to the initial work of Langeloth et al., which introduces the slip-springs into the dissipative particle dynamics simulation. Basically, the number of MD steps between two MC blocks determines the duration time of the topological constraints (entanglement) imposed by the slip-springs on the polymer chains. Meanwhile, the number of MC steps between two MD blocks dictates the mobility of the slip-springs. In detail, we measure the mean square displacements of the chain center in polyethylene melts of chain length N=C_{350} to show the impact of different pairs of MD/MC sequence lengths. As seen in Figure 3(a), with the same MC block length $n_{\mathrm{MC}} = 500$, the mobility of the polymer melts is profoundly decreasing with increasing MD block length from $n_{\mathrm{MD}} = 50$ to $n_{\mathrm{MD}} = 5000$. On the other hand, the dynamics of polymer melts is expected not to be altered significantly by varying MC block length once it is larger than a critical value at which the slip-springs are mobile enough. Figure 3(b) shows the diffusive dynamics varying as the MC block length from $n_{\mathrm{MC}} = 50$ to $n_{\mathrm{MC}} = 5000$. when $n_{\mathrm{MC}} = 50$, the diffusive dynamics is unchanged in the short time regime, while slightly slower than that of both $n_{\mathrm{MC}} = 500$ and $n_{\mathrm{MC}} = 5000$ in the long time regime. The overlap of the mean square displacements of $n_{\mathrm{MC}} = 500$ and $n_{\mathrm{MC}} = 5000$ indicates that $n_{\mathrm{MC}} = 500$ sufficiently ensures that the slip-springs are mobile enough in our current systems. To achieve better computational efficiency, we employ $n_{\mathrm{MC}} = 500$ for all slip-spring hPF-MD simulations.

Parameters in Slip-Spring Hybrid Particle-Field Simulation

Table 1: Parameters in slip-spring hybrid particle-field simulation

parameters	explanation	units
T	temperature of the system	K
$\chi_{i,j}$	density-field interaction parameter between particles of type i and j	kJ/mol
κ	compressibility factor	1/(kJ/mol)
N	number of carbons of the polymer chain	-
M	number of polymer chains in the system	-
ρ	density of the system	kg/m^3
K_{ssp}	slip-spring bond force constant	kJ/mol
$r_{0,ssp}$	equilibrium distance of the slip-spring bond	nm
N_{ssp}	number of slip-springs in the system	-
n_{MD}	time steps for one molecular dynamics block between Monte-Carlo blocks	-
n_{MC}	time steps for one Monte-Carlo block between molecular dynamics blocks	-

Relationship between the Entanglement Length and Number of Slip-Springs per Chain

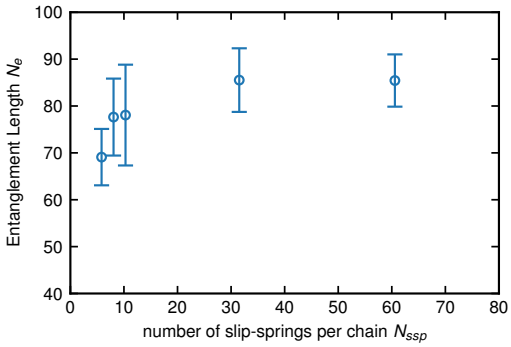

Figure S4: Dependence of the entanglement length N_e on the number of slip-springs per chain N_{ssp}.

References

1. Langeloth, M.; Masubuchi, Y.; Böhm, M. C. and Müller-Plathe, F., *The Journal of Chemical Physics*, 2014, **141**(19), 194904.

2. Sgouros, A. P.; Megariotis, G. and Theodorou, D. N., *Macromolecules*, 2017, **50**(11), 4524–4541.

3.2 Combination of Hybrid Particle-Field Molecular Dynamics and Slip-Springs for the Efficient Simulation of CG Polymer Models: Static and Dynamic Properties of Polystyrene Melts

JCTC Journal of Chemical Theory and Computation

pubs.acs.org/JCTC Article

Combination of Hybrid Particle-Field Molecular Dynamics and Slip-Springs for the Efficient Simulation of Coarse-Grained Polymer Models: Static and Dynamic Properties of Polystyrene Melts

Zhenghao Wu, Giuseppe Milano, and Florian Müller-Plathe*

Cite This: J. Chem. Theory Comput. 2021, 17, 474−487 Read Online

ACCESS | Metrics & More | Article Recommendations | Supporting Information

ABSTRACT: A quantitative prediction of polymer-entangled dynamics based on molecular simulation is a grand challenge in contemporary computational material science. The drastic increase of relaxation time and viscosity in high-molecular-weight polymeric fluids essentially limits the usage of classic molecular dynamics simulation. Here, we demonstrate a systematic coarse-graining approach for modeling entangled polymers under the slip-spring particle-field scheme. Specifically, a frequency-controlled slip-spring model, a hybrid particle-field model, and a coarse-grained model of polystyrene melts are combined into a hybrid simulation technique. Via a rigorous parameterization strategy to determine the parameters in slip-springs from existing experimental or simulation data, we show that the reptation behavior is clearly observed in multiple characteristics of polymer dynamics, mean-square displacements, diffusion coefficients, reorientational relaxation, and Rouse mode analysis, consistent with the predictions of the tube theory. All dynamical properties of the slip-spring particle-field models are in good agreement with classic molecular dynamics models. Our work provides an efficient and practical approach to establish chemical-specific coarse-grained models for predicting polymer-entangled dynamics.

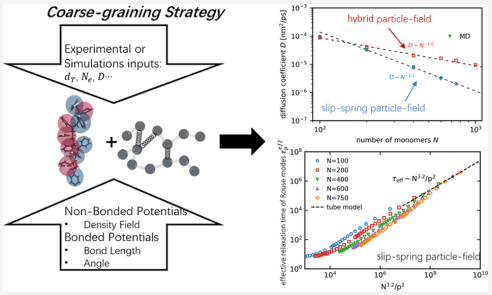

INTRODUCTION

During the last half century, the comprehensive understanding of the structure/property relationship in polymer melts has been advanced by extensive theoretical and experimental studies.[1] However, the bottom-up prediction of dynamical and rheological behavior of high-molecular-weight polymers continues to be a grand challenge. All-atom (AA) molecular dynamics (MD) simulations have emerged as one of the most powerful tools to obtain the molecular-level understanding of the structure/property relationship in many areas of polymeric materials. However, the drastic increase in relaxation times and viscosity of polymers with increasing molecular weight essentially limits the usage of AA simulations. This requires modeling techniques that can access extended time and length scales while retaining chemical specificity, such as the atomistic-derived coarse-grained (CG) models.[2,3]

Numerous systematic coarse-graining methods have been proposed during the last 2 decades, most of which focus on optimizing the effective pair potential to reproduce some particular structural or thermodynamic properties calculated from the underlying AA counterpart. A prevalently used approach is to derive CG force-fields by performing inversions of target AA probability distributions, such as iterative Boltzmann inversion (IBI)[4,5] and inverse Monte Carlo.[6] Other structure-based approaches include the multiscale coarse-graining,[7,8] relative entropy method,[9] conditional reversible work,[10] and integral equation coarse-graining theory.[11] Structural properties of polymers such as radius of gyration and end-to-end distance are successfully depicted by these coarse-graining models. However, the dynamics of these models is accelerated due to the smoother free-energy landscape of CG models. The effect of this spurious acceleration is twofold: on the one hand, it makes comparisons of dynamical quantities to experiments inevitably difficult; on the other hand, it benefits the modeling polymeric systems with their inherently slow dynamics to reach equilibration and extract dynamical properties in a qualitatively correct way. Many works have attempted to predict the dynamical acceleration factor of these CG models relative to AA models.[9,12−14] This acceleration factor is often defined as the ratio of the diffusion coefficients of CG and AA models: $\alpha = D_{CG}/D_{AA}$. Previous studies have reported that α is nearly independent of chain length N for long polymer chains.[15,16]

Received: September 16, 2020
Published: December 4, 2020

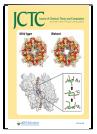

https://dx.doi.org/10.1021/acs.jctc.0c00954
J. Chem. Theory Comput. 2021, 17, 474−487

One can perform dynamic time rescaling with this acceleration factor to correct the CG dynamics.[15,17] For instance, Harmandaris and Kremer reported a hierarchical multiscale model of polystyrene melts,[15] where one monomer is mapped to two CG beads. The fast equilibration of CG models allowed them to simulate polystyrene melts of several entanglement lengths, which is not reachable in AA models. By rescaling the dynamics obtained in CG models with a time-rescaling factor, self-diffusion coefficients of linear polystyrene melts composed of up to 500 monomers are well reproduced compared to the AA simulation and experimental data. Additionally, the entanglement molecular weight they calculated using primitive path analysis is close to the experimental data. However, the aforementioned low-to-moderately CG models, where one monomer is mapped to one or two CG beads, are still not sufficient to attain the length and time scales of long, entangled polymer chains within reasonable computation time.

Increasing the coarse-graining degree is a natural choice for extending the spatial and temporal scales. However, when the degree of coarse-graining is larger than some critical value, for instance, grouping tens of monomers into a single CG bead, the resulting CG pair potential will be so soft that atoms or bonds are allowed to cross through each other. Consequently, the dynamics of these CG models is not only accelerated but qualitatively incorrect, in particular, for entangled polymers. Additional topological constraints must be properly added for compensating for the influence of chain crossability, in order to make the dynamics physically realistic. One of the most successful theories to describe the topological constraint is the tube model.[1,18] It demonstrates that the motion of the polymer chain is confined into a tubular region by a mean-field potential formed by entanglements with its neighboring chains. Consequently, a chain can only reptate along the contour of its tube, while the lateral motion against the tube is suppressed. Besides reptation, modern versions of the tube model include extra relaxation mechanisms of contour-length fluctuations and constraint release.[18] Inspired by the phenomenological picture of tube-like dynamical constraints, recent developments in modeling techniques to predict the dynamics of high-molecular-weight polymers have been heavily involved. Examples include the CG blob MD simulations of Padding and Briels[19] and several versions of slip-link models at different levels of coarse-graining.[20−24] Multiple slip-spring simulations have also been developed over the recent years in the single-chain form by Likhtman and in the multichain form by Uneyama and Masubuchi,[25] Chappa et al.,[26] Langeloth et al.,[27] and Ramírez-Hernández et al.[28] However, intensive studies are still ongoing,[29−32] attempting to map properties of interest with these generic models at high-level coarse-graining to realistic polymers. More recently, Theodorou and co-workers developed a multiscale strategy that bridges detailed MD simulations to mesoscopic slip-spring-based Brownian dynamics simulations.[33,34] The combination of the slip-spring model with systematic highly CG polymer models offers a promising way to model the entangled polymers, retaining reasonable molecular information in spatial−temporal scales close to experiments.

Recently, the atomistic hybrid particle-field (hPF) approach has been combined with a multichain slip-spring model,[35] making it promising for studying dynamical properties of entangled polymers in a computationally efficient way. Here, we extend this methodology to incorporate a structure-based CG model and a modified model of slip-springs, in which almost all parameters can be extracted from MD reference calculations. We apply this model to mono-disperse polystyrene melts of chains of length between 100 monomers and 750 monomers, covering the unentangled to entangled regimes. In the hPF model, the bonded potentials are exactly the same as in its MD counterpart, while the non-bonded interactions are evaluated through a density-functional-field rather than in a pairwise fashion. This formulation massively improves the computational efficiency and makes it well-controlled to perform simulations at a desired resolution.[36] The CG model allows a larger time step and system size in comparison to the AA model, profoundly broadening the range of practical applications for the modeling of entangled polymers. To compensate for the reduced degree of freedom coming from the density-functional-field, an effective frictional term is added to the equation of motion, so that the dynamics of the unentangled polymers or short-time dynamics of entangled polymers in hPF simulations is consistent with their MD counterparts. The introduction of slip-springs to the chemical-specific polymer models successfully recovers the entangled dynamical behavior of long chains in the particle-field model, in contrast to most other slip-spring models.[25,26,28] Last, the combination of the slip-spring model, the particle-field formulation, and the CG polymer model provides a 20−30-fold improvement in the efficiency of MD simulations compared to classic MD algorithms probing the in-equilibrium dynamics of entangled polymers.

COARSE-GRAINING STRATEGY

As introduced above, our coarse-graining approach is based on the hPF model in which the intramolecular bonded potentials are atomistic or CG-derived from the fine-grained simulation models, and the intermolecular potentials are treated by a density-functional-field potential (see Figure 1). This density-functional-field potential is soft-core, causing effective amount of chain-crossing events in dense polymeric fluids. This artificial effect has been shown not to impact the equilibrium structures of polymer chains.[37−39] However, the important

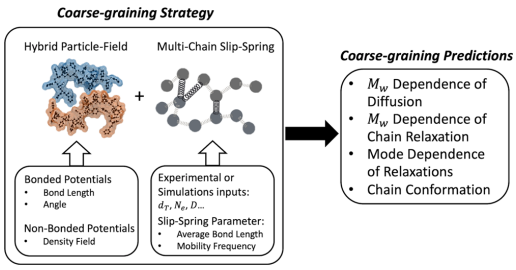

Figure 1. General procedure of the coarse-graining strategy based on the combination of the hPF and multichain slip-spring models. The bonded potentials used in the hPF models can be derived from quantum calculations or from CG models parameterized using atomistic simulations. The non-bonded potentials are calculated through the density-functional-field. The parameters of slip-springs (e.g., average slip-spring bond length, hopping frequency of slip-springs, and number of slip-springs) can be determined by the inputs of either experimental measurements or molecular dynamic simulations. The performance of the CG model of polystyrene melts is tested by calculating the MSDs, diffusion coefficients, end-to-end vector relaxations, and Rouse mode analysis.

https://dx.doi.org/10.1021/acs.jctc.0c00954
J. Chem. Theory Comput. 2021, 17, 474−487

dynamical mechanism related to the chain entanglements is lost. Similar problems have also been reported in simulations with soft-core intermolecular potentials such as dissipative particle dynamics simulations.[26,27] In theory, no matter how long the chain is, the (diffusion) dynamics in the entanglement-free (chain-crossing allowed) polymer melt can be universally described by the simple Rouse model

$$D = \frac{k_B T}{\zeta N} \sim N^{-1}$$

where, D and k_B are the center-of-mass diffusion coefficient and the Boltzmann constant, T and ζ are the temperature and the segmental friction, respectively, and N is the chain length of the polymer. This, however, disagrees with the observations of abundant experiments, which shows the domination of the chain entanglement on dynamics in long-chain polymer melts, as expected from the reptation theory developed long ago by de Gennes.[1] Specifically, the diffusion coefficient D scales with the chain length N^{-2} for polymer melts with noticeable entanglements. This picture is confirmed by our simulations of polystyrene melts using standard MD and hPF methods sharing the same intramolecular potentials (see details below). Figure 2 shows a comparison of hPF and MD models,

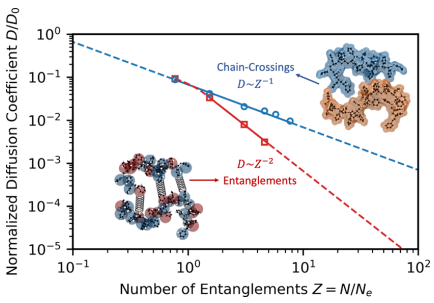

Figure 2. Normalized diffusion coefficients as a function of number of entanglements per chain for hPF and MD simulations (T = 500 K, ρ = 0.96 g cm^{-3}). The dashed and solid lines are the power-law fits of Rouse and reptation predictions. The entanglements between polymer chains in MD simulations are considered as binary contacts and visualized as virtual springs. D_0 is the diffusion coefficient of a monomer fluid at the same density.

involving entanglements which come from hard-core pair interactions. This comparison reveals the same dynamical behavior at the regime of few entanglements but an increasing disparity with more entanglements between the models with or without entanglements. Meanwhile, the scaling behavior in polymer melts with and without entanglements is consistent with the theoretical predictions.

To recover the entangled dynamics in hPF simulations, the chain entanglements are modeled as slip-springs (see Slip-Spring Model for details). The dynamics at short and long time is dictated by segmental friction ζ and chain entanglements (slip-springs), respectively. We then start from determining the segmental friction in the hPF model in Segmental Friction in Particle-Field Model. Next, the procedure to extract the slip-spring parameters from experiments or reference MD simulations is introduced in Slip-Spring Model. Following that, the influence of the mobility of slip-springs on the entangled dynamics is discussed.

Segmental Friction in Particle-Field Model. The dynamics of any CG model is accelerated due to the loss of degrees of freedom in comparison to the atomistic model. In our hPF model, the non-bonded interactions are additionally replaced by interactions with the density-functional field, which further smoothens the free-energy landscape compared to the pairwise potentials in the reference MD simulation. Consequently, the dynamics of the hPF system is further accelerated. The artificial acceleration can be remedied by including frictional and stochastic forces.[40] We adopt a Langevin equation of motion with a friction term to compensate for the smoother free-energy landscape

$$m\frac{\mathbf{dv}}{t} = \mathbf{F}_C - \zeta\cdot\mathbf{v} + \mathbf{F}_R$$

where $\mathbf{F}_C$ is the conservative force acting on the particle from bonded, non-bonded and slip-springs, ζ is the friction coefficient, and $\mathbf{F}_R$ is a uniformly distributed random force. The magnitude of $\mathbf{F}_R = 6k_BT\zeta/\delta t$ is chosen via the fluctuation−dissipation theorem to be consistent with the friction coefficient and temperature. In order to determine the friction coefficient for the hPF model, multiple pure hPF simulations of unentangled polystyrene melts ($N \approx 0.8 \times N_e$ = 100 monomers) with various friction coefficients are performed. The same qualitative behavior of the mean-square displacements (MSDs) is observed in Figure 3. The friction

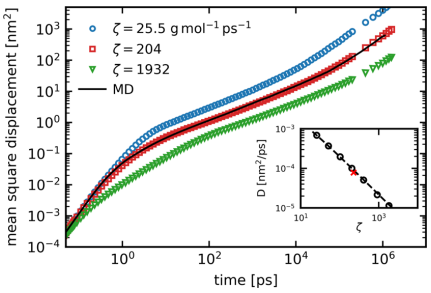

Figure 3. Center-of-mass MSDs of polystyrene chains of 100 monomers in hPF simulations with friction coefficients ζ = 25.5 (blue), 204 (red), and 1932 (green) g mol^{-1} ps^{-1} and corresponding MD simulations (black line). In the inset, the diffusion coefficients D of particle-field simulations are plotted as a function of friction coefficient ζ. The red star is the reference MD value. The dashed line is the power law fit.

coefficient ζ = 204 g mol^{-1} ps^{-1} is chosen when the diffusion coefficient matches the target value of the reference MD simulation, as seen in the inset of Figure 3. We note that the selected chain length should be long enough to eliminate the effect of the chain end but shorter than the entanglement length N_e to avoid the effect of entanglements. This chain length (N = 100) is also where the time-scaling factor reaches a plateau in the work of Harmandaris and Kremer,[15] implicating that the segmental friction starts to become chain-length independent.

Slip-Spring Model. *Designing the Potential Form of Slip-Springs.* The density-functional treatment of non-bonded interactions is effectively soft-core, causing the reptation dynamics in long polymer melts to be lost in the original hPF method. In order to restore this important dynamic

https://dx.doi.org/10.1021/acs.jctc.0c00954
J. Chem. Theory Comput. 2021, 17, 474−487

mechanism, a multichain slip-spring model similar to refs[25,27,33] is introduced into the hPF model. The slip-springs mimic the interchain confinement of the surrounding chains imposed on the probed chain. In practice, they are modeled as transient bonds connecting chain segments belonging to different chains. The length of the slip-spring in the equilibrium state is assumed to be equivalent to the tube diameter $d_T/2$. The restoring entanglement force is finite at the length-scale above the tube diameter, similar to the anharmonic idea of the topological constraints implied from the recent theoretical model.[41] The potential form of the slip-spring adopted in this work is in the form of

$$U(l_{ss}) = -0.5K_{ss}R_{max}^{\ 2}\ln\left[1-\left(\frac{l_{ss}}{R_{max}}\right)^2\right]$$

where R_{max} is the maximum length of the slip-spring, and K_{ss} represents the force constant of the slip-spring. The potential is cut at $l_{ss} = 0.95 \times R_{max}$ and continued linearly (Figure 4). R_{max}

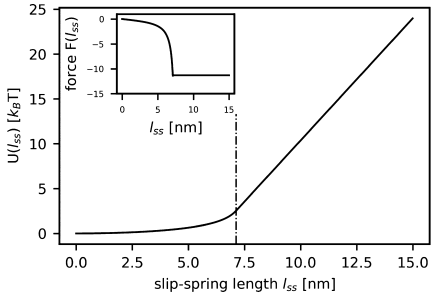

Figure 4. Potential of the slip-spring as a function of the slip-spring length with K_{ss} = 0.52 kJ/mol and R_{max} = 7.5 nm in the unit of k_BT. Inset: the slip-spring force as a function of the slip-spring length. The dash-dotted line is the length, where the slip-spring bond potential is cut off, l_{ss} = 7.125 nm.

is chosen as d_T, and K_{ss} is adjusted until the mean equilibrium length of slip-springs $\langle l_{ss}^2\rangle = (d_T/2)^2$. Specifically, the equilibrium length of slip-springs $\langle l_{ss}\rangle$ decreases with the slip-spring bond strength K_{ss} at fixed R_{max}. For instance, Figure 5 shows the distribution of slip-spring lengths of varying K_{ss} in polystyrene chains composed of 400 monomers. In the inset of Figure 5, a logarithm equation is fitted to the slip-spring length $\langle l_{ss}\rangle$ and K_{ss} for data smoothing and interpolation. In a prior MD simulation study of polystyrene melts,[5] $d_T \approx 7.5$ nm was determined via the CRETA[42] algorithm (topological primitive path analysis), so that we obtain the value of K_{ss} = 0.52 kJ/(mol nm^2), and this parameter is fixed to be the same in all slip-spring particle-field (SSPF) model of polystyrene melts in this work.

Monte-Carlo Movements of Slip-Springs. The slip-springs are initially placed randomly in the system, satisfying the distance criteria $l_{ss} < 0.9R_{max}$. To update the configurations of the slip-spring, a version of discrete Monte-Carlo move is employed, where the slip-spring jumps between adjacent beads along both polymer chains. One slip-spring connects two different chains, resulting in two attachments per slip-spring. The probability of a discrete hop of a slip-spring is $P_{hop} = \nu_{hop}\Delta t_{MC}\exp[U(l_{ss})/k_BT]$, where Δt_{MC} is the time interval between MC moves and ν_{hop} is the hopping frequency,

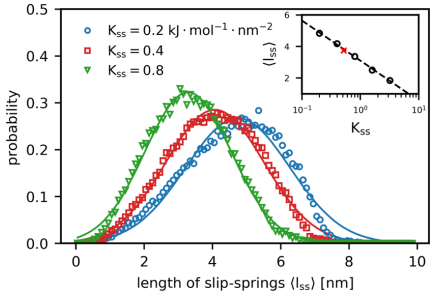

Figure 5. Probability distribution of the slip-spring lengths in equilibrium in polystyrene melt of 400 monomers with slip-spring bond strength K_{ss} = 0.2 (blue), 0.4 (red), and 0.8 (green) kJ mol^{-1} nm^{-2}. In the inset, the mean slip-spring lengths are plotted as a function of K_{ss}. The red cross is $\langle l_{ss}\rangle = d_T/2$. The dashed line is a logarithm fit.

determined by the comparison to experimental or MD simulation data. Indeed, the chain dynamics is found not to be influenced significantly by Δt_{MC} within the range of 50−500 time steps (1.5−15 ps). Thus, we choose Δt_{MC} = 100 time steps (3 ps) for all SSPF simulations. When one of the slip-spring attachments moves out of the chain, this slip-spring is destroyed. In the equilibrium state, the average number of entanglements in the polymer melt is constant. Accordingly, the number of slip-springs also remains unchanged. Thus, a new slip-spring is created randomly in the system, one attachment of which is forced located at a chain end. Indeed, the implementation of destruction and creation of the slip-springs is similar to other versions of slip-spring (link) models,[25,26,33] essentially capturing the relaxation mechanism of constraint release in the modern tube model.[18]

Another important parameter is the length between adjacent slip-spring attachments N_e^{ss}, related to specific chemistry. This parameter is empirically chosen as $N_e/2$, where N_e is the conventional entanglement length between entanglements along the chain. The conventional entanglement length N_e of polystyrene melts was analyzed from classical MD simulations using the CRETA algorithm by Spyriouni et al.,[5] giving $N_e \approx 127$. With the length between adjacent slip-spring attachments N_e^{ss} known, the total number of slip-springs Z_t is calculated as

$$Z_t = \frac{(N/N_e^{ss} - 1)}{2} \times M$$

where M is the number of chains in the simulation box. We note here that the relation between N_e^{ss} and N_e is still not determined analytically, albeit extensive discussions in the literature suggest $N_e^{ss} < N_e$ in the slip-spring model.[43,44]

Influence of Slip-Spring Hopping Frequency on Dynamics. As noted before, the hopping frequency ν_{hop} effectively determines the mobility of the slip-springs. The higher mobility the slip-springs have, the weaker interchain constraints the polymer chains will experience. In the limit of extremely high mobility of the slip-springs, the dynamics of SSPF models will be reduced to that of the pure hPF model, which has no topological constraints between chains. In contrast, the slip-springs can be envisaged as chemical cross-links between polymer chains when they do not move over the entire simulation time. However, the exact relationship between the hopping frequency ν_{hop} and the polymer dynamics

https://dx.doi.org/10.1021/acs.jctc.0c00954
J. Chem. Theory Comput. 2021, 17, 474−487

is still not analytically derived. In this case, the hopping frequency ν_{hop} is determined by demanding the target dynamics of reference systems (MD models in this case) at different chain lengths to be consistent with the SSPF models. Specifically, we perform SSPF simulations with varying hopping frequencies and then make comparisons with the target property. Here, we compare the diffusion coefficient of the SSPF models with the corresponding MD models at various chain lengths. Figure 6 displays the MSDs of SSPF

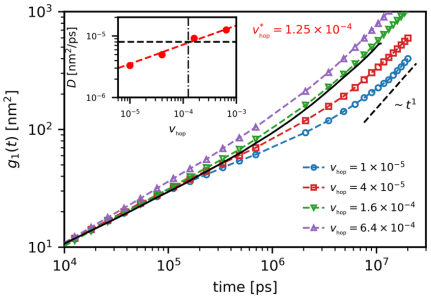

Figure 6. Monomer MSDs of the SSPF simulations of polystyrene melts (N = 400) with hopping frequencies $\nu_{hop} = 1 \times 10^{-5}$ (blue), $\nu_{hop} = 4 \times 10^{-5}$ (red), $\nu_{hop} = 1.6 \times 10^{-4}$ (green), and $\nu_{hop} = 6.4 \times 10^{-4}$ (purple). The black line is the monomer MSD of reference MD simulations. Inset: diffusion coefficients extracted from the center-of-mass MSDs of varying hopping frequencies. The red dashed line is the power-law fit with exponent 0.302. The black dashed line is the value of the MD counterpart, and the dot dash line is where the hopping frequency is taken for the productive SSPF simulations.

models with four different hopping frequencies. We find that the MSDs are indeed decreasing for systems with smaller ν_{hop}. The diffusion coefficients extracted from the MSDs of chain center-of-mass as a function of ν_{hop} are shown in the inset of Figure 6. The diffusion coefficient D increase with ν_{hop} in a nonlinear fashion. In order to determine the required ν^*_{hop}, we naively fit the data using a power-law equation, although we know that there should be a plateau value at high ν_{hop}, close to D_{hPF} of pure hPF models. By applying the same procedure for systems of various chain lengths, the derived hopping frequency ν_{hop} is found to be almost chain-length independent.

CG Model and Simulation Details. *Polystyrene CG Model.* The CG model of polystyrene employed in the present work has been developed by Qian and co-workers.[45] The schematic figure of the CG model is shown in Figure 7. In this CG model, a repeating unit is replaced by a single bead placed at its center of mass. Two different bead types (R and S) are defined to account for the tacticity of the polymer chain. The sequence of R and S beads of the polymer chain is generated randomly for coarse-graining atactic polystyrene melts. Specifically, the CG-bonded interactions, that is, bonds, angles, and dihedrals, are derived by preserving their probability distribution functions of all-atomistic references using the IBI method. In the hPF method used here,[36] the CG non-bonded interactions are computed through the density-functional field. In such a field, each bead experiences an effective interaction which is equivalent to an external potential $V(\mathbf{R})$. The resulting potential energy for a particle of species of K at position $\mathbf{R}$ is given by

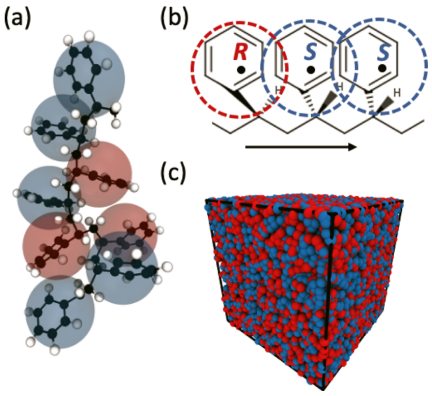

Figure 7. Coarse-graining mapping (a) from the atomistic model to the CG model from the mapping rule (b). One CG bead corresponds to one polystyrene monomer, which is located at the center of mass of the corresponding atomistic chemical structure. Bead types R and S are defined in accordance with the configuration of the monomer given by the asymmetric −CHR− group, which is defined against the direction of the backbone indicated by the arrow. (c) Snapshot of the simulated CG system, rendered by VMD.[48]

$$V_K(\mathbf{R}) = \frac{1}{\phi_0}\left[k_B T \sum_L \chi_{K,L}\phi_L(\mathbf{R}) + \frac{1}{\kappa}\left(\sum_K \phi_K(\mathbf{R}) - \phi_0\right)\right]$$

where $\chi_{K,L}$ is the mean field coupling term between particle species K and L, κ is the compressibility factor dictating the local fluctuations of density, $\phi_K(\mathbf{R})$ is the number density of particle species K at position $\mathbf{R}$, and ϕ_0 is the average number density of the whole system. $\chi_{K,L}$ has a value of zero for homopolymer melts, and κ is fixed at 0.1 kJ^{-1} mol in all particle-field simulations. The density field is chosen to be updated every single hPF-MD step in GALAMOST.[46,47] This field treatment of non-bonded interactions speeds up the calculations remarkably, with the structural properties well-preserved, except the pair correlation function at very short length scales (see details in Statistics of Slip-Springs and Polymer Chains). The detailed information about the hPF approach and the development of the CG model can be found in prior studies.[36,37,45] It should be noted that the compressibility parameter κ must have an impact on the structural and dynamical behaviors of polymer chains. We tested the values of κ from 0.05 to 0.2 kJ^{-1} mol in polystyrene melts with chains of N = 100 monomers, giving us deviations of ∼2 and ∼5% for the diffusion coefficients and the chain size, respectively (see Table S1 in the Supporting Information). The corresponding CG MD and hPF simulations are performed for comparison, the details of which can be found in the Supporting Information.

Simulation Methods. All our simulations are carried out using the GALAMOST software package (version 3.1.1).[46] Details about systems of SSPF, MD, and hPF simulations are summarized in Table 1. Periodic boundary conditions are applied in all directions to simulate the bulk properties of polystyrene melts. A timestep Δt of 4 and 30 fs is chosen for the MD and particle-field simulations (hPF and SSPF), respectively. The temperature of all simulated systems are kept at T = 500 K via the Nosé−Hoover thermostat. More

https://dx.doi.org/10.1021/acs.jctc.0c00954
J. Chem. Theory Comput. 2021, 17, 474−487

Table 1. Simulation Details[a]

system code	N	M	t_{sim} [ps]	Z_t	ν_{hop} [ps^{-1}]
SSPF-PS100	100	300	1.31×10^7	86	1.25×10^{-4}
SSPF-PS200	200	150	1.31×10^7	161	1.25×10^{-4}
SSPF-PS400	400	75	2.62×10^7	199	1.25×10^{-4}
SSPF-PS600	600	50	2.62×10^7	211	1.25×10^{-4}
SSPF-PS750	750	40	2.62×10^7	216	1.25×10^{-4}
MD-PS100	100	300	1.27×10^6		
MD-PS200	200	150	1.60×10^6		
MD-PS400	400	75	1.12×10^7		
MD-PS600	600	50	1.60×10^7		
MD-PS750	750	40	1.60×10^7		
hPF-PS100	100	300	1.31×10^7		
hPF-PS200	200	150	1.31×10^7		
hPF-PS400	400	75	1.31×10^7		
hPF-PS600	600	50	1.31×10^7		
hPF-PS750	750	40	1.31×10^7		
hPF-PS1000	1000	30	1.31×10^7		

[a] N: number of monomers per chain; M: number of chains in the system; t_{sim}: total simulation time; Z_t: total number of slip-springs in the system; ν_{hop}: hopping frequency of slip-springs.

details about the simulation methods can be found in the Supporting Information.

Simulation Analysis. The dynamics of the polymer melts is measured by means of the MSD of all monomers $g_1(t)$ and chain centers of mass $g_3(t)$

$$g_1(t) = \langle (\mathbf{R}_i(t) - \mathbf{R}_i(0))^2 \rangle$$

$$g_3(t) = \langle (\mathbf{R}_{com}(t) - \mathbf{R}_{com}(0))^2 \rangle$$

where $\mathbf{R}_i(t)$ and $\mathbf{R}_{com}(t)$ are position vector of monomer i and the chain center-of-mass at time t, respectively.

The self-diffusion coefficient D is computed from the MSD of the chain center-of-mass $g_3(t)$, by

$$D = \lim_{t\to\infty} \frac{\langle (\mathbf{R}_{com}(t) - \mathbf{R}_{com}(0))^2 \rangle}{6t}$$

The reorientational relaxation is quantified via the end-to-end vector autocorrelation function

$$C_1(t) = \langle \mathbf{e}_i(t) \cdot \mathbf{e}_i(0) \rangle$$

where $\mathbf{e}_i(t) = \mathbf{R}_N(t) - \mathbf{R}_1(t)$ is the end-to-end unit vector of chain i at time t. The relaxation time τ_{ete} is determined as follows: we first fit all $C_1(t)$ for times, after the initial fast relaxation process is complete, to an exponential functional form, $C_1(t) = A \exp(-t/\tau_1)$, where A and τ_1 are fitting parameters. We define the end-to-end vector relaxation time as $\tau_{ete} = \tau_1$. Typical exponential function fits to the end-to-end vector autocorrelation function are shown in Figure 8.

The internal relaxation of the chain for a polymer melt of chain length N is characterized by means of Rouse-mode analysis. The Rouse modes ($p = 0, 1, 2, 3...N-1$) of a polymer chain composed of N monomers are defined as $\mathbf{X}_p = \left(\frac{2}{N}\right)^2 \sum_{i=1}^{N} \mathbf{R}_i \cos\left[\left(\frac{p\pi}{N}\right)\left(i - \frac{1}{2}\right)\right]$ where $\mathbf{R}_i(t)$ is the position vector of monomer i. The normalized autocorrelation function of the Rouse modes is expressed as $\langle \mathbf{X}_p(t) \cdot \mathbf{X}_p(0) \rangle / \langle \mathbf{X}_p \rangle^2$, which can be fitted by the Kohlrausch–Williams–Watts (KWW) function[49]

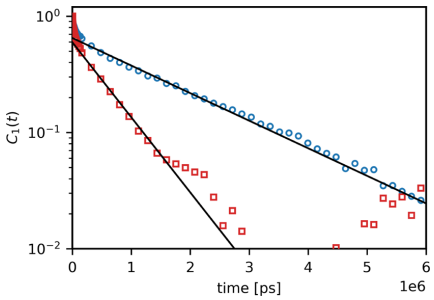

Figure 8. Exponential fits (solid lines) to the end-to-end vector autocorrelation function data for simulations of polystyrene melts of chain length $N = 200$ (red) and $N = 600$ (blue).

$$\langle \mathbf{X}_p(t) \cdot \mathbf{X}_p(0) \rangle / \langle \mathbf{X}_p \rangle^2 = \exp\left[-\left(\frac{t}{\tau_p^{KWW}} \right)^{\beta_p} \right]$$

where β_p and τ_p^{KWW} are the stretching exponent and the characteristic time of the relaxation, respectively. The effective relaxation time τ_p^{eff} of Rouse mode p can be computed by integrating the KWW relaxation function

$$\tau_p^{eff} = \int_0^\infty \exp\left[-\left(\frac{t}{\tau_p^{KWW}} \right)^{\beta_p} \right] dt = \left(\frac{\tau_p^{KWW}}{\beta_p} \right) \Gamma\left(\frac{1}{\beta_p} \right)$$

where Γ is the gamma function. The effective relaxation rate W_p^{eff} of mode p is defined as $W_p^{eff} = 3k_B T/\zeta b^2 = 1/[4\tau_p^{eff} \sin^2(p\pi/2N)]$, where ζ is the monomeric friction coefficient and b is the bond length of successive carbons of the backbone.

RESULTS

Capturing Polymer-Entangled Dynamics via Slip-Springs. First of all, we examine the effectiveness of our SSPF model in comparison to the translational diffusion behavior in the reference models of MD. To this end, we calculate the MSD of the monomers ($g_1(t)$) and that of chain center-of-mass ($g_3(t)$). The results of $g_1(t)$ of different chain lengths and $g_3(t)$ of PS750 are shown in Figure 9. The apparent overlaps of $g_1(t)$ between SSPF and MD suggest that

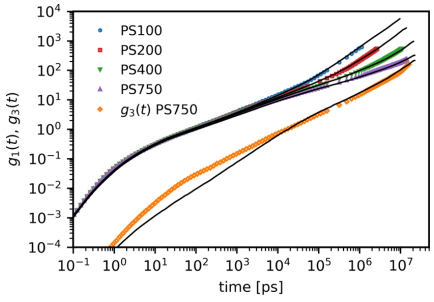

Figure 9. Monomer MSDs of the CG MD simulations (this work) of polystyrene melts $N = 100$ (blue), $N = 200$ (red), $N = 400$ (green), and $N = 750$ (purple). The yellow marker is the MSD of chain center-of-mass. The black lines are the fits from the SSPF simulations.

https://dx.doi.org/10.1021/acs.jctc.0c00954
J. Chem. Theory Comput. 2021, 17, 474−487

the SSPF model successfully reproduces the segmental translational diffusive behavior across a range of time scales. It is also observed that the discrepancy of $g_3(t)$ between SSPF and MD, particularly at the intermediate time scale from subpicosecond (t < 1 ps) to ∼20 ps, originates from the density-functional-field softening the collisions between chains. The distinct scaling relations of $g_1(t)$ correspond to the unique underlying dynamical mechanisms within the phenomenological theoretical framework of the tube model. For instance, $g_1(t)$ scales as $t^{1/2}$ at the short-time regime $t < \tau_e$, where τ_e is the characteristic time when the chain segments feel the topological constraints from the neighboring chains. In this time period, the dynamics of the chain segments can be well described by the Rouse model. Following that, chain segments can only move forward or backward in the tube-like region. In detail, at the length scale of the chain segments, we find $g_1(t) \sim t^{1/4}$ ($\tau_e < t < \tau_R$) and above this length scale, $g_1(t) \sim t^{1/2}$ ($\tau_R < t < \tau_d$), relating to the Rouse-like movement of tube segments (∼N_e). The characteristic times τ_R and τ_d are the Rouse time and terminal time, respectively. After τ_d, all chain segments diffuse freely with $g_1(t) \sim t$.

Figure 10 plots MSDs of the centermost monomer normalized by $t^{1/4}$ to compare with the postulation of scaling

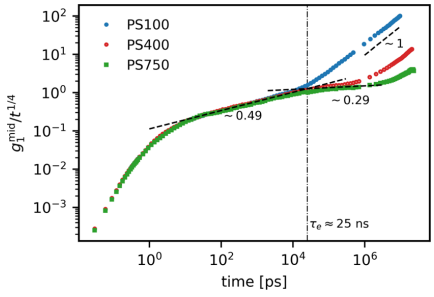

Figure 10. Monomer MSDs of the SSPF simulations of N = 100 (blue), N = 400 (red), and N = 750 (green) normalized by $t^{1/4}$. The dashed lines are the power law fits to Rouse regime ($g_1^{mid}(t) \sim t^{0.49}$) and constrained Rouse regime ($g_1^{mid}(t) \sim t^{0.29}$), respectively. The vertical dash-dotted line is the crossover between the two regimes at $t = \tau_e$.

relations of the tube model. Qualitatively, four distinct regimes appear stably for PS750, as predicted by the tube model. The plateau observed for PS750 at the intermediate times signals the strong entanglement effect. The fit to a power law ($g_1^{mid}(t) = g_0 t^b$) yields b = 0.49 for $t < \tau_e$ and b = 0.29 for $\tau_e < t < \tau_R$, respectively. The former value (0.49) is quite close to the Rouse model prediction (0.5), while the latter is slightly higher than the predicted one (0.25) of the reptation theory. This can be interpreted by two possible reasons. The chain may be not long enough. Namely, the entanglement in PS750 is not strong enough to completely constrain the chain segments to the one-dimensional reptation-like movements. The other reason may be the contour length fluctuations and constraint releases in the real polymer melts, which suggests that the theoretical value 1/4 cannot be reached no matter how long the chain is. Indeed, these two important dynamical mechanisms are naturally captured by our SSPF model. Our model is also able to predict the characteristic time of these different dynamical mechanisms. For instance, the crossover of the two power law relations $g_1(t) \sim t^{1/2}$ and $g_1(t) \sim t^{1/4}$ yields an entanglement time $\tau_e \approx$ 25 ns, close to the value obtained from the CG MD simulation of Chen et al.[50]

The diffusion coefficients of all systems of particle-field as well as MD are shown in Figure 11. First, we see the apparent

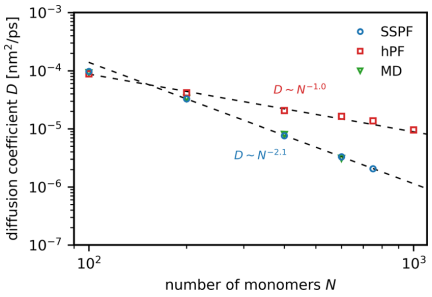

Figure 11. Diffusion coefficients of particle-field simulations with (blue) and without (red) slip-springs and the CG MD (this work) simulations (green) as a function of the chain length N. The dashed lines are the power law fits to the particle-field simulations with ($D \sim N^{-2.1}$) and without ($D \sim N^{-1.0}$) slip-springs for N > 200.

overlaps between the diffusion coefficients of SSPF and MD simulations, indicating the effectiveness of our model in reproducing the diffusive behavior. The diffusion coefficient D of particle-field with and without slip-springs and MD simulations shows two distinct scaling relations with respect to the chain length N. Specifically, D scales as ∼N^{-1} for all chain lengths in hPF simulations in accordance with Rouse model of (short-chain) polymer melts. In comparison, $D \sim N^{-2.1}$ for $N > N_e$ for the SSPF and MD models. In the case of PS100 ($N < N_e$), the diffusion coefficients of all models are the same, consistent with our expectation that the slip-springs do not alter the short-chain dynamics. Moreover, the diffusion coefficient of polystyrene melts was also measured via nuclear magnetic resonance at $T \approx$ 500 K. We replot the experimental data available in the literature with our simulation results rescaled by a time-scaling factor μ = 128.4, which is defined as the ratio of the diffusion coefficient of PS200 from our SSPF result and experimental data of Bachus and Kimmich,[51] $\mu = D_{SSPF}/D_{exp}$, displayed in Figure 12. These rescaled results of SSPF models are evidently consistent with the experimental measurements in a quantitative way.

The autocorrelation functions of the end-to-end vector $C_1(t)$ are shown in Figure 13. Generally, the chain-length-dependent relaxation is observed as the increasingly slow decay of $C_1(t)$ in the longer chain. Specifically, the autocorrelation functions of SSPF simulations sit on top of those of MD spanning all time regimes, indicating the intriguing effectiveness of the SSPF model in predicting the reorientational dynamics compared to the classical MD approach. Figure 14 presents the relaxation time of the end-to-end vector τ_{ete} as a function of the chain length N. The relaxation time τ_{ete} is determined via the procedure described in Simulation Analysis for all systems of particle-field and MD simulations from the autocorrelation functions in Figure 13. The data is almost separated into two distinct regimes for $N > N_e \approx$ 130, similar to the diffusion coefficient. Specifically, the relaxation time τ_{ete} of hPF follows a linear relation across all chain lengths under study. A fit to the power law equation yields $\tau_{ete} \sim N^{1.96}$. This scaling relation is

https://dx.doi.org/10.1021/acs.jctc.0c00954
J. Chem. Theory Comput. 2021, 17, 474−487

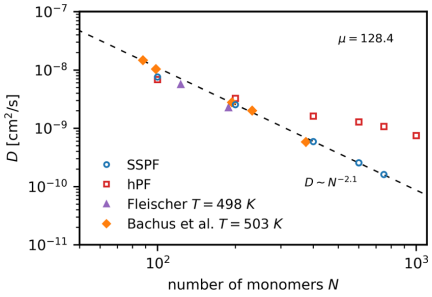

Figure 12. Diffusion coefficients of particle-field simulations with (blue) and without (red) slip-springs as a function of the chain length N shifted by a time-scaling factor μ = 128.4. The purple[52] and orange[51] markers are the experimental measurements. The dashed line is the power law fit to the data of the SSPF simulation for N > 200.

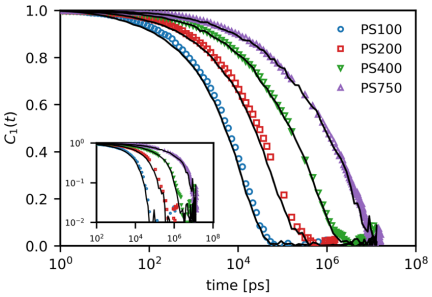

Figure 13. Autocorrelation functions of SSPF simulations (black line) and MD simulations (hollow symbols) for chain length ranging from N = 100 (blue), 200 (red), 400 (green), and 750 (purple). The inset is the replot in double logarithm scale.

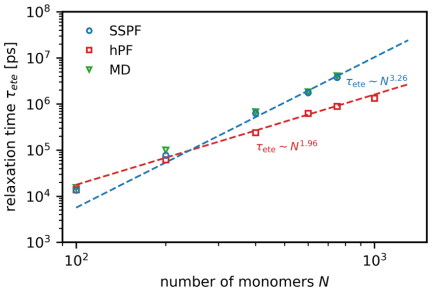

Figure 14. End-to-end relaxation time of particle-field simulations with (blue) and without (red) slip-springs and the CG MD simulations (green) as a function of the chain length N. The dashed lines are the power law fits to the relaxation time for N > 200.

in good agreement with the postulation of the Rouse model, indicating the absence of entanglements in this model. However, both SSPF and MD deviate from hPF, when N > 200. The relaxation time τ_{ete} increases much faster with respect to chain length in both cases in comparison to hPF. A fit to the power law yields $\tau_{ete} \sim N^{3.26}$ and $\tau_{ete} \sim N^{3.19}$ for SSPF and MD, respectively. As suggested from the modern tube model, the scaling factor of τ_{ete} with respect to chain length N is approximately 3.3, if taking the additional relaxation mechanisms of contour length fluctuation and constraint release into consideration. Our results of τ_{ete} from SSPF simulations are obviously consistent with this prediction. Exemplarily shown in Figure 8, the end-to-end vector correlation functions are approximately exponential following a transient at very short times.

To further understand how the internal relaxations of the chains depend on the length of the subchain in the slip-spring hPF models, we performed Rouse-mode analysis and compared the results with the original hPF model. The objective is to elucidate the significance of the topological constraints (slip-springs) on the entangled dynamics of polymer melts. The normalized autocorrelation functions $\langle X_p(t)X_p(0)\rangle/\langle X_p^2\rangle$ of different Rouse modes p for a polystyrene melt of chain length N = 750 are presented in Figure S1. All autocorrelation functions for Rouse modes of index from p = 1 to p = 30 decay to zero, indicating that the polymer chain of N = 750 is fully relaxed. The results are well fitted by a stretched exponential relaxation function, consistent with previous MD simulations.[53−56] The effective relaxation times τ_p of different chain lengths are plotted against N/p in Figure 15a for the particle-field simulations with and without

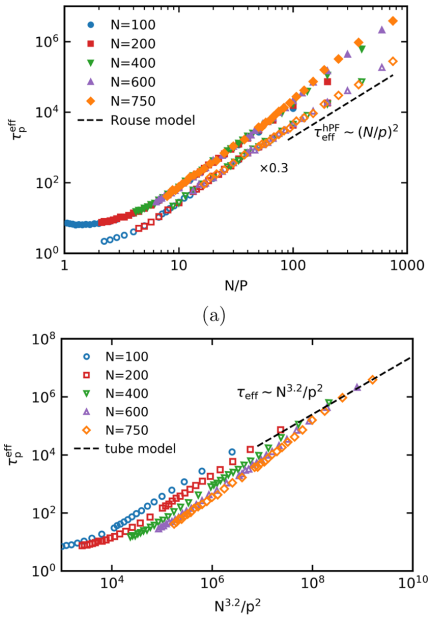

Figure 15. Effective relaxation times of polystyrene melts with various chain lengths: N = 100 (blue), N = 200 (red), N = 400 (green), N = 600 (purple), and N = 750 (orange) as a function of (a) sub-chain length scale (Rouse modes) N/p and (b) normalized sub-chain length scale $N^{3.2}/p^2$ motivated by the tube model. In figure (a), the filled markers are results from SSPF simulations and hollow markers are from hPF simulations. The results of hPF simulations are shifted by multiplying 0.3 for clarity. In figure (b), the dashed line is the fit to the results of the SSPF simulations at large $N^{3.2}/p^2$ with the tube model motivated equation.

https://dx.doi.org/10.1021/acs.jctc.0c00954
J. Chem. Theory Comput. 2021, 17, 474−487

slip-springs. We find that the effective relaxation times τ_p of chain lengths ranging from unentangled to entangled regimes fall on a master curve of $\tau_p^{\mathrm{hPF}} \sim (N/p)^2$ in the original hPF model, satisfying the predictions of the Rouse model. The deviations at small N/p are due to the chain stiffness and intramolecular correlations as revealed by prior MD studies.[53,54] In contrast to the original hPF, the effective relaxation times τ_p of SSPF models diverge from the master curve of $\tau_p \sim (N/p)^2$ at large N/p, implying the essential role of topological constraints (slip-springs) on the relaxations at large sub-chain length scales. These results, where the entanglements play a crucial role, are found to fall on a master curve motivated by the tube model,[53] especially for large N/P. Inspired by this idea, we replot the effective relaxation times τ_p of SSPF simulations at various chain lengths as a function of $N^{3.2}/p^2$ in Figure 15b. Here, the exponent $N^{3.2}$ is taken from the power law fit of relaxation times of end-to-end vectors with respect to the chain length N in Figure 14. As seen in Figure 15b, τ_p indeed falls on a master curve at large N/p, while the short chains follow Rouse behaviors. Only the polystyrene melts of chain length longer than $N = 200$ ($N \sim 2N_e$) start to experience the influence from the topological constraints (entanglements), in agreement with bead-spring MD simulations.[53]

To further characterize the impact of topological constraints (entanglements) by leveraging the Rouse mode analysis, we compute the effective relaxation rate W_p^{eff} based on the definition in Simulation Analysis. In Figure 16, the effective relaxation rates W_p^{eff} of slip-spring hPF models at different chain lengths are compared with those of the original hPF models. In both models, W_p^{eff} decreases with increasing N/p, whereas it forms a plateau after decreasing by a factor of 2 in the original hPF model. In contrast, W_p^{eff} decreases more profoundly in the slip-spring hPF model, in which the much lower plateau values of W_p^{eff} for the long chains are evidence for the addition of slip-springs significantly restraining chain motions. Additionally, the stretching exponent β_p is found to depend on the Rouse mode index. Specifically, the stretching exponent β_p is roughly stable at ~0.9 at short sub-chain length (large mode index p) and decreases with decreasing mode index p, reaching a minimum near $N/p \approx N_e$, independent of the chain length. The plateau value $\beta_p \sim 0.9$ is slightly larger than the value $\beta_p \sim 0.8$ observed in MD simulations,[19,53] this deviation being potentially related to soft intramolecular interactions as a result of the density-functional-field. The minimum value of β_p is not close to 0.5 as seen in bead-spring MD simulations of well-entangled polymer melts ($Z = N/N_e > 10$), implying that the minimum values of β_p are strongly affected by the topological constraints (slip-springs). In contrast, the location of the minimum β_p is in the vicinity of $N/p \approx N_e$, in good agreement with observations in previous MD simulations, underpinning its universality in entangled polymer melts.

Statistics of Slip-Springs and Polymer Chains. We first examine the statistics of the slip-springs in the system of different chain lengths. Figure 17 depicts the distribution of the length of the slip-springs l_{ss} in PS200 and PS600. The consistency between the distributions shows the independence of the slip-spring length from the chain length, which is expected in the current implementation since we use the same potential parameters of slip-springs for all systems. Gaussian probability function is found to fit the l_{ss} distribution well, consistent with the recent MD simulations which reveal a

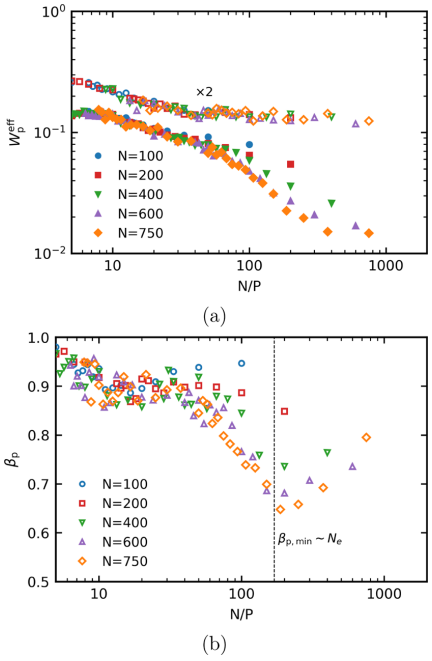

Figure 16. (a) Effective relaxation rate W_p^{eff} of polystyrene melts with various chain lengths: $N = 100$ (blue), $N = 200$ (red), $N = 400$ (green), $N = 600$ (purple), and $N = 750$ (orange) as a function of the sub-chain length scale (Rouse modes) N/p. Filled markers are results from SSPF simulations and hollow markers are from hPF simulations; (b) stretching exponents of SSPF models as a function of the sub-chain length scale (Rouse modes) N/p. The dot dashed line is the sub-chain length N/p where the stretching exponents close to the minimum.

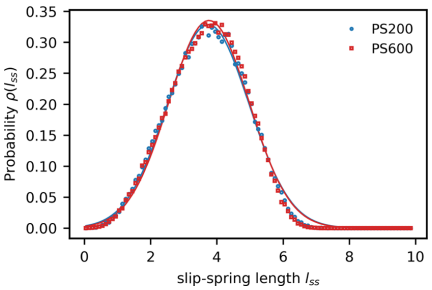

Figure 17. Probability distribution of the slip-spring lengths in equilibrium in polystyrene melt of $N = 200$ (blue) and $N = 600$ (red).

Gaussian-shaped transverse bead spreading under the iso-configurational ensemble. This is also observed in the recent slip-spring simulations of Vogiatzis et al.[33]

The slip-spring density $\rho_{ss}(i)$ along the chain can also be computed, which is defined as the probability to find a slip-spring attachment at monomer i at the time moment t. This is plotted in Figure 18 for PS200 and PS400. A striking feature in this plot is the slightly higher slip-spring density near the chain end in comparison to the center of the chain. The disparity

https://dx.doi.org/10.1021/acs.jctc.0c00954
J. Chem. Theory Comput. 2021, 17, 474−487

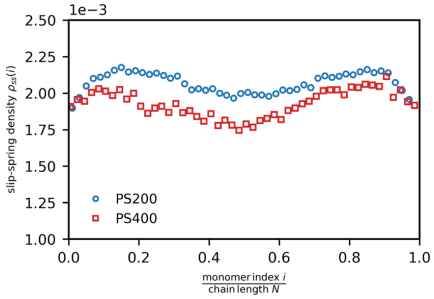

Figure 18. Slips-spring density along the chain in polystyrene melt of chain length $N = 200$ and $N = 400$.

between the chain end and center is slightly enhanced with increasing chain length. Indeed, the lower concentration of the slip-spring attachments in the chain center is counter-intuitive as the stronger confinements on dynamics are seen in, for example, (slower) MSDs of the chain central beads. Reminding ourselves that the slip-springs are to model the binary contacts (entanglements) between chains, actually this non-uniform distribution is also seen in the analysis of tight long-lived contacts between polymer chains in MD simulations by Likhtman and Ponmurugan.[57] The genuine relation between the slip-springs and the persistent contacts (entanglements) is still not clear.

The SSPF model is designed to capture the correct chain structures of polymer melts. Mean-square radius of gyration $\langle R_g^2 \rangle$ and mean-square end-to-end distance $\langle R_{ete}^2 \rangle$ are commonly taken to characterize the size of polymer chains. Both of them are presented as functions of the chain length N in Figure 19 in double logarithm scales. The results from the

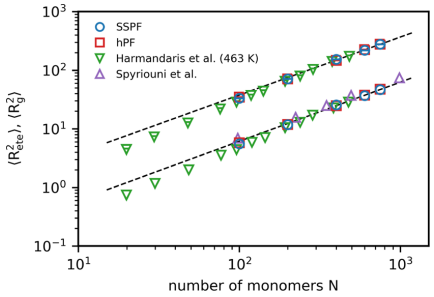

Figure 19. Mean-square radius of gyration and mean-square end-to-end distance of particle-field simulations with (blue) and without (red) slip-springs as a function of chain length N. The green[15] and purple[5] markers are results from the CG MD simulations of the reference. The dashed lines are the power law fits to the SSPF model.

current SSPF simulations and the pure hPF show good agreement with other simulation work of polystyrene melts.[5,15] Also consistent with the prior theoretical work, mean-square radius of gyration $\langle R_g^2 \rangle$ and end-to-end distance $\langle R_{ete}^2 \rangle$ scale linearly with the chain length N with exponents 1.01 and 0.99, respectively, for the SSPF model. The ratio of mean-square end-to-end distance $\langle R_{ete}^2 \rangle$ and mean-square radius of gyration $\langle R_g^2 \rangle$ is 6 for the ideal Gaussian chain. As expected for the ideal Gaussian chains, $\langle R_{ete}^2 \rangle / \langle R_g^2 \rangle$ of the longest chains simulated with the SSPF model is 5.97. Notably, the presence of slip-springs between chains has almost no effect on the chain dimensions, which is also seen in other slip-spring models.

The characteristic ratio C_N can be calculated from the end-to-end distance of polystyrene chains with the form

$$C_N = \langle R_{ete}^2 \rangle / nl^2$$

where n is the number of backbone bonds, and l is the carbon−carbon backbone bond length ($l = 1.54$ Å). The results about C_N together with values from other simulation studies are reported in Figure 20.[15,58] The characteristic ratio C_N first

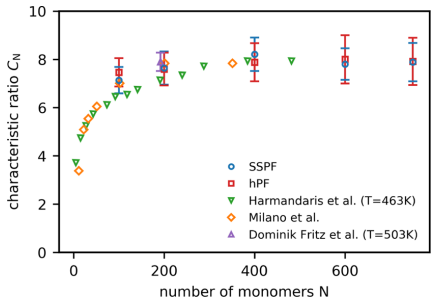

Figure 20. Characteristic ratio from particle-field simulations with (blue) and without (red) slip-springs as a function of chain length N at 500 K. The green,[15] orange,[58] and purple[59] symbols are results from CG MD simulations for comparison.

increases with chain length and reaches a plateau after the approximate chain length of 250 monomers. The plateau values of the characteristic ratio C_N obtained from our particle-field models is ∼8, consistent with the extrapolations of earlier simulation work of polystyrene melts. These properties can also be measured by experiments, yielding $C_\infty = 8.5$ at $T = 463$ K for high-molecular-weight polystyrene melts, again close to the results of our particle-field model.

The polymer chains are allowed to cross each other in prior hPF studies so that the advantages of density-functional-field potential cannot be used to study the entangled dynamics of the macromolecules. Figure 21 depicts the nonbonded radial distribution functions $g(r)$ of the centers of mass of monomers

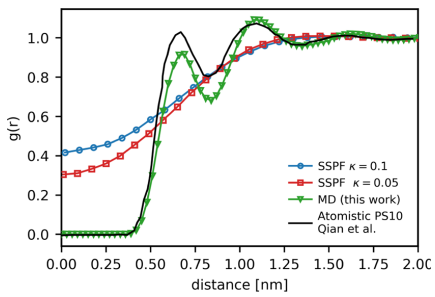

Figure 21. Intermolecular radial distribution function of particle-field simulations with (blue) and without (red) slip-springs and CG molecular dynamic simulation (this work) of polystyrene of 100 monomers. The solid line is the result from the atomistic simulation of polystyrene melt of 10 monomers.[40]

https://dx.doi.org/10.1021/acs.jctc.0c00954
J. Chem. Theory Comput. 2021, 17, 474−487

from particle-field simulations with different compressibility factor and the reference MD simulation. The radial distribution function $g(r)$ of particle-field simulations starts from non-zero values, indicating that some particle overlapping is possible. Compared to results from reference molecular dynamic simulations, oscillations of $g(r)$ at short distance are eliminated in particle-field simulations, but $g(r)$ converges to 1 at a similar length scale as MD simulations. All aspects of the behavior of $g(r)$ are well understood features of the hPF model.

Computational Efficiency. The essential advantage of the SSPF model is its computational efficiency. The gain in the computational speed mainly profits from the hPF model and algorithm to calculate the non-bond interactions, details of which have been discussed widely in prior studies.[60] The hPF model was later implemented on the novel computing architecture: graphical processing unit (GPU) via compute unified device architecture (CUDA) in GALAMOST.[46] The GPU considerably accelerates the computation of hPF simulations. Zhu et al.[46] showed that the performance of a system comprising one million particles on a single GPU is roughly comparable to that on 96 CPU cores. To show the performance of the hPF model after integrating slip-springs, we compare it with the original hPF model, which we use as an effective standard, in simulations of several system sizes on a single core of a CPU (Intel Xeon E5-2650 v4, 24 cores 2.2 GHz) and a single GPU (Nvidia GeForce GTX 1080 Ti, 3584 cuda cores). The performances of corresponding MD simulations using the same simulation package (GALAMOST) and computing resources are included as well. Figure 22

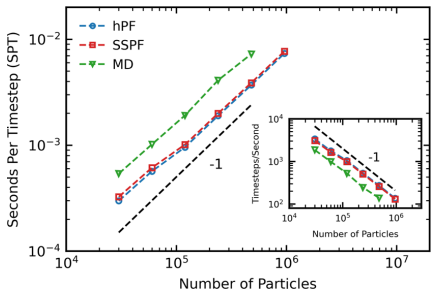

Figure 22. Seconds per timestep (SPT) of hPF (blue), SSPF (red), and MD (green) simulations of CG polystyrene melts as a function of number of CG beads in the system in double-logarithmic scaling. The inset: Timesteps per second as a function of number of CG beads in the system.

presents the consumed time (seconds) per timestep (SPT) of hPF, SSPF, and MD simulations of CG polystyrene melts in cubic simulation boxes with edge length ranging from ∼20 to ∼60 nm. The SPT of each simulation is recorded after the first 1×10^6 steps and averaged over another 1×10^6 steps. First, we find that SPTs of the SSPF simulations are almost comparable to the hPF values for all system sizes, in spite of a slight slowing-down seen due to the additional calculations of the slip-spring forces. This suggests that the introduction of slip-springs indeed requires little computation, satisfying our initiative to develop an efficient model for entangled polymers. In comparison to the classic MD simulations, the computing speed of the particle-field simulations is almost two-times faster than all systems tested in this work. All three simulation models show a good scaling of the computing speed with increasing number of particles up to ∼1 million, which may be attributed to the acceleration of GPUs. Moreover, the soft density-functional-field interactions allow a larger time-step (Δt = 0.03 ps for SSPF and hPF models) compared to the classic MD simulation with hard-core pair interactions (Δt = 0.004 ps for MD model). Figure 23 displays the timescale a

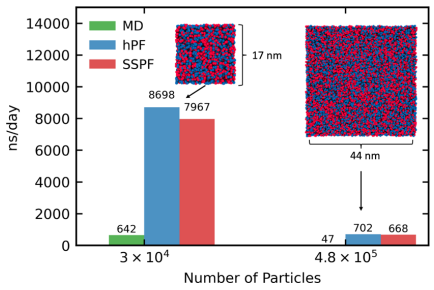

Figure 23. Timescale that a simulation is able to reach within one day of MD (green), hPF (blue), and SSPF (red) simulations for systems comprising 3×10^4 CG beads (left) and 4.8×10^5 CG beads (right) on a single GPU (Nvidia GeForce GTX 1080 Ti).

simulation is able to attain within 1 day in the unit of nanosecond for systems composed of 3×10^4 (box edge l = 17 nm) and 4.8×10^5 particles (box edge l = 44 nm). Taking the step length into consideration, the computing speed of particle-field simulations is around 15 times faster than the classic MD simulations, which are ∼9 and 0.6 ms, respectively. The computational efficiency of our SSPF model of polystyrene melts allows simulations containing detailed monomeric chemistry at the length scale of 50 nm and time scale of 100 ms with reasonable computational expense.

DISCUSSION AND CONCLUSIONS

We have established an efficient SSPF model for a CG treatment of entangled polymeric materials. This contribution evaluates its ability to reproduce static and dynamical features of polymer melts, as well as its computational performance. The particle-field scheme enables the novel combination of systematic CG polymer models and slip-spring models. In this way, the entanglements are modeled explicitly by the slip-springs in the hPF model, recovering the entangled dynamics at long times for high-molecular-weight polymers. By incorporating the systematic CG polymer model into our slip-spring-based approach, we show that it is able to directly predict the dynamics of entangled polymer melts and, at the same time, preserve the chemical specificity, making it differ from most other slip-spring models. We have demonstrated a rigorous procedure to determine the parameters of the slip-spring model from the existing experimental data or corresponding MD simulations with as few as possible fit parameters. The slip-spring hopping frequency is shown to have a strong influence on the dynamics of polymer melts in the long-time regime ($t > \tau_e$) without altering the dynamics at the short-time regime ($t < \tau_e$). This is consistent with the theoretical description of the entanglements between chains, which only affect the dynamics above the entanglement time τ_e. The entangled dynamics of polystyrene melts is

https://dx.doi.org/10.1021/acs.jctc.0c00954
J. Chem. Theory Comput. 2021, 17, 474−487

characterized by means of MSDs, diffusion coefficients, reorientational relaxations, and Rouse mode analysis. In all of these measurements, the dynamical properties are found to be consistent with the reference MD simulations quantitatively. The similar behavior between the slip-springs and "entanglement" provides supporting evidence of the validation to model topological constraints between polymer chains with slip-springs. Our model indeed provides a direct platform for comparing the behavior and properties of slip-springs with the "entanglements" in MD models, which can be measured by either Z1[61,62] and CRETA[42] algorithms or contact map analysis with isoconfigurational ensemble averaging.[57,63] Notably, it might be also possible to extract the slip-spring parameters from the reference MD simulations analytically based on the tube model or the (analytical) slip-link model.[24]

In addition, our model accurately predicts the chain structures of the polymer melt including the characteristic ratio, radius of gyration, and end-to-end distance. We have to note here that the intermolecular correlation at the sub-monomer length scale inherently deviates from the realistic condition because of the soft-core feature of the density-functional-field potential. Furthermore, the distribution of the lengths of the slip-springs is found well described by a simple Gaussian distribution, sharing connections with the Gaussian-shaped transverse bead spreading observed in recent MD simulations.[64] Similar to the recent findings of MD simulations,[57] more slip-springs are found near the chain end than near the chain center from the analysis of slip-spring density along the polymer chain, which is done for the first time to our knowledge. This similarity further indicates the strong connections between the slip-springs and the "entanglements" induced by hard−core pair interactions.

As our model essentially postulates a wide range of dynamical and structural properties of polystyrene melts, we expect our approach to be general for other polymers such as polyethylene and polyisoprene. Additionally, to further increase the computational efficiency to span a wider range of spatio-temporal scales, it is naturally to increase the degree of coarse-graining (the number of atoms per CG bead) of the polymer model. It is believed that the increasing degree of coarse-graining will cause decreasing segmental friction due to greater loss of the degree of freedom under coarse-graining. Although prior studies found that the slip-spring parameters scale well with the level of coarse-graining,[65,66] the effect of the coarse-graining degree on parameters of slip-springs in realistic polymeric systems is still not clear. We would expect the mobility (hopping frequency) of the slip-springs is strongly related to the degree of coarse-graining. Understanding and validating these effects as well as the relation between slip-springs and "entanglements" will be important and meaningful to establish more efficient modeling techniques and comprehensive theories for entangled polymers in the future.

■ ASSOCIATED CONTENT

Supporting Information

The Supporting Information is available free of charge at https://pubs.acs.org/doi/10.1021/acs.jctc.0c00954.

Simulation details of MD and particle-field models; influence of compressibility factor in particle-field simulations on the diffusion and radius of gyration of polystyrene melts; and normalized autocorrelation functions of various Rouse modes for polystyrene chains of 750 monomers (PDF)

■ AUTHOR INFORMATION

Corresponding Author

Florian Müller-Plathe − *Eduard-Zintl-Institut für Anorganische und Physikalische Chemie, Technische Universität Darmstadt, 64287 Darmstadt, Germany;* orcid.org/0000-0002-9111-7786; Email: f.mueller-plathe@theo.chemie.tu-darmstadt.de

Authors

Zhenghao Wu − *Eduard-Zintl-Institut für Anorganische und Physikalische Chemie, Technische Universität Darmstadt, 64287 Darmstadt, Germany;* orcid.org/0000-0003-2862-4432

Giuseppe Milano − *Department of Organic Materials Science, Yamagata University, Yonezawa 992-8510, Yamagata-ken, Japan*

Complete contact information is available at: https://pubs.acs.org/10.1021/acs.jctc.0c00954

Notes

The authors declare no competing financial interest.

■ ACKNOWLEDGMENTS

We thank our partners in the ROBERTO consortium (Prof. Toshihiro Kawakatsu and Prof. Yuichi Masubuchi) for many fruitful discussions along the project. This research is funded by the Deutsche Forschungsgemeinschaft via the SFB-TRR 146 "Multiscale Simulation Methods for Soft Matter Systems", Project A8. Z.W. gratefully acknowledges the computing time granted on the supercomputer Mogon at Johannes Gutenberg University Mainz and in part on the Lichtenberg high-performance computer of the TU Darmstadt.

■ REFERENCES

(1) de Gennes, P. G.; Leger, L. Dynamics of Entangled Polymer Chains. *Annu. Rev. Phys. Chem.* **1982**, *33*, 49−61.

(2) Müller-Plathe, F. Coarse-Graining in Polymer Simulation: From the Atomistic to the Mesoscopic Scale and Back. *ChemPhysChem* **2002**, *3*, 754−769.

(3) Padding, J. T.; Briels, W. J. Systematic coarse-graining of the dynamics of entangled polymer melts: the road from chemistry to rheology. *J. Phys.: Condens. Matter* **2011**, *23*, 233101.

(4) Reith, D.; Meyer, H.; Müller-Plathe, F. Mapping Atomistic to Coarse-Grained Polymer Models Using Automatic Simplex Optimization To Fit Structural Properties. *Macromolecules* **2001**, *34*, 2335−2345.

(5) Spyriouni, T.; Tzoumanekas, C.; Theodorou, D.; Müller-Plathe, F.; Milano, G. Coarse-Grained and Reverse-Mapped United-Atom Simulations of Long-Chain Atactic Polystyrene Melts: Structure, Thermodynamic Properties, Chain Conformation, and Entanglements. *Macromolecules* **2007**, *40*, 3876−3885.

(6) Lyubartsev, A. P.; Laaksonen, A. Calculation of effective interaction potentials from radial distribution functions: A reverse Monte Carlo approach. *Phys. Rev. E: Stat. Phys., Plasmas, Fluids, Relat. Interdiscip. Top.* **1995**, *52*, 3730−3737.

(7) Izvekov, S.; Voth, G. A. Multiscale coarse graining of liquid-state systems. *J. Chem. Phys.* **2005**, *123*, 134105.

(8) Izvekov, S.; Voth, G. A. A Multiscale Coarse-Graining Method for Biomolecular Systems. *J. Phys. Chem. B* **2005**, *109*, 2469−2473.

(9) Shell, M. S. The relative entropy is fundamental to multiscale and inverse thermodynamic problems. *J. Chem. Phys.* **2008**, *129*, 144108.

(10) Brini, E.; Marcon, V.; van der Vegt, N. F. A. Conditional reversible work method for molecular coarse graining applications. *Phys. Chem. Chem. Phys.* **2011**, *13*, 10468.
(11) Clark, A. J.; McCarty, J.; Lyubimov, I. Y.; Guenza, M. G. Thermodynamic Consistency in Variable-Level Coarse Graining of Polymeric Liquids. *Phys. Rev. Lett.* **2012**, *109*, 168301.
(12) Depa, P. K.; Maranas, J. K. Speed up of dynamic observables in coarse-grained molecular-dynamics simulations of unentangled polymers. *J. Chem. Phys.* **2005**, *123*, 094901.
(13) Rondina, G. G.; Böhm, M. C.; Müller-Plathe, F. Predicting the Mobility Increase of Coarse-Grained Polymer Models from Excess Entropy Differences. *J. Chem. Theory Comput.* **2020**, *16*, 1431−1447.
(14) Meinel, M. K.; Müller-Plathe, F. Loss of Molecular Roughness upon Coarse-Graining Predicts the Artificially Accelerated Mobility of Coarse-Grained Molecular Simulation Models. *J. Chem. Theory Comput.* **2020**, *16*, 1411−1419.
(15) Harmandaris, V. A.; Kremer, K. Dynamics of Polystyrene Melts through Hierarchical Multiscale Simulations. *Macromolecules* **2009**, *42*, 791−802.
(16) Peters, B. L.; Salerno, K. M.; Agrawal, A.; Perahia, D.; Grest, G. S. Coarse-Grained Modeling of Polyethylene Melts: Effect on Dynamics. *J. Chem. Theory Comput.* **2017**, *13*, 2890−2896.
(17) Salerno, K. M.; Agrawal, A.; Perahia, D.; Grest, G. S. Resolving Dynamic Properties of Polymers through Coarse-Grained Computational Studies. *Phys. Rev. Lett.* **2016**, *116*, 058302.
(18) Likhtman, A. E.; McLeish, T. C. B. Quantitative Theory for Linear Dynamics of Linear Entangled Polymers. *Macromolecules* **2002**, *35*, 6332−6343.
(19) Padding, J. T.; Briels, W. J. Time and length scales of polymer melts studied by coarse-grained molecular dynamics simulations. *J. Chem. Phys.* **2002**, *117*, 925−943.
(20) Shanbhag, S.; Larson, R. G.; Takimoto, J.; Doi, M. Deviations from Dynamic Dilution in the Terminal Relaxation of Star Polymers. *Phys. Rev. Lett.* **2001**, *87*, 195502.
(21) Shanbhag, S.; Larson, R. G. A Slip-Link Model of Branch-Point Motion in Entangled Polymers. *Macromolecules* **2004**, *37*, 8160−8166.
(22) Nair, D. M.; Schieber, J. D. Linear Viscoelastic Predictions of a Consistently Unconstrained Brownian Slip-Link Model. *Macromolecules* **2006**, *39*, 3386−3397.
(23) Schieber, J. D.; Horio, K. Fluctuation in entanglement positions via elastic slip-links. *J. Chem. Phys.* **2010**, *132*, 074905.
(24) Khaliullin, R. N.; Schieber, J. D. Analytic Expressions for the Statistics of the Primitive-Path Length in Entangled Polymers. *Phys. Rev. Lett.* **2008**, *100*, 188302.
(25) Uneyama, T.; Masubuchi, Y. Multi-chain slip-spring model for entangled polymer dynamics. *J. Chem. Phys.* **2012**, *137*, 154902.
(26) Chappa, V. C.; Morse, D. C.; Zippelius, A.; Müller, M. Translationally Invariant Slip-Spring Model for Entangled Polymer Dynamics. *Phys. Rev. Lett.* **2012**, *109*, 148302.
(27) Langeloth, M.; Masubuchi, Y.; Böhm, M. C.; Müller-Plathe, F. Recovering the reptation dynamics of polymer melts in dissipative particle dynamics simulations via slip-springs. *J. Chem. Phys.* **2013**, *138*, 104907.
(28) Ramírez-Hernández, A.; Peters, B. L.; Schneider, L.; Andreev, M.; Schieber, J. D.; Müller, M.; de Pablo, J. J. A multi-chain polymer slip-spring model with fluctuating number of entanglements: Density fluctuations, confinement, and phase separation. *J. Chem. Phys.* **2017**, *146*, 014903.
(29) Masubuchi, Y.; Uneyama, T. Multi-chain slip-spring simulations for polyisoprene melts. *Korea Aust. Rheol. J.* **2019**, *31*, 241−248.
(30) Schneider, J.; Süss, L. D.; Müller-Plathe, F. The Influence of Entanglements on the Dynamics of Flash Nanoprecipitation: A Slip-Spring Dissipative-Particle-Dynamics Investigation. *J. Chem. Eng. Data* **2020**, *65*, 1264−1272.
(31) Schneider, J.; Meinel, M. K.; Dittmar, H.; Müller-Plathe, F. Different Stages of Polymer-Chain Collapse Following Solvent Quenching−Scaling Relations from Dissipative Particle Dynamics Simulations. *Macromolecules* **2020**, *53*, 8889−8900.
(32) Becerra, D.; Córdoba, A.; Katzarova, M.; Andreev, M.; Venerus, D. C.; Schieber, J. D. Polymer rheology predictions from first principles using the slip-link model. *J. Rheol.* **2020**, *64*, 1035−1043.
(33) Vogiatzis, G. G.; Megariotis, G.; Theodorou, D. N. Equation of State-Based Slip-Spring Model for Entangled Polymer Dynamics. *Macromolecules* **2017**, *50*, 3004−3029.
(34) Sgouros, A. P.; Megariotis, G.; Theodorou, D. N. Slip-Spring Model for the Linear and Nonlinear Viscoelastic Properties of Molten Polyethylene Derived from Atomistic Simulations. *Macromolecules* **2017**, *50*, 4524−4541.
(35) Wu, Z.; Kalogirou, A.; Nicola, A.; Milano, G.; Müller-Plathe, F. Atomistic Hybrid Particle-Field Molecular Dynamics Combined with Slip-Springs: Restoring Entangled Dynamics to Simulations of Polymer Melts. *J. Comput. Chem.* **2020**, *42*, 6.
(36) Milano, G.; Kawakatsu, T. Hybrid particle-field molecular dynamics simulations for dense polymer systems. *J. Chem. Phys.* **2009**, *130*, 214106.
(37) De Nicola, A.; Kawakatsu, T.; Müller-Plathe, F.; Milano, G. Fast relaxation of coarse-grained models of polymer interphases by hybrid particle-field molecular dynamics: Polystyrene-silica nanocomposites as an example. *Eur. Phys. J.: Spec. Top.* **2016**, *225*, 1817−1841.
(38) Munaò, G.; Pizzirusso, A.; Kalogirou, A.; De Nicola, A.; Kawakatsu, T.; Müller-Plathe, F.; Milano, G. Molecular structure and multi-body potential of mean force in silica-polystyrene nanocomposites. *Nanoscale* **2018**, *10*, 21656−21670.
(39) Munaò, G.; De Nicola, A.; Müller-Plathe, F.; Kawakatsu, T.; Kalogirou, A.; Milano, G. Influence of Polymer Bidispersity on the Effective Particle-Particle Interactions in Polymer Nanocomposites. *Macromolecules* **2019**, *52*, 8826−8839.
(40) Qian, H.-J.; Liew, C. C.; Müller-Plathe, F. Effective control of the transport coefficients of a coarse-grained liquid and polymer models using the dissipative particle dynamics and Lowe−Andersen equations of motion. *Phys. Chem. Chem. Phys.* **2009**, *11*, 1962.
(41) Sussman, D. M.; Schweizer, K. S. Microscopic Theory of Entangled Polymer Melt Dynamics: Flexible Chains as Primitive-Path Random Walks and Supercoarse Grained Needles. *Phys. Rev. Lett.* **2012**, *109*, 168306.
(42) Tzoumanekas, C.; Theodorou, D. N. Topological Analysis of Linear Polymer Melts: A Statistical Approach. *Macromolecules* **2006**, *39*, 4592−4604.
(43) Everaers, R. Topological versus rheological entanglement length in primitive-path analysis protocols, tube models, and slip-link models. *Phys. Rev. E: Stat., Nonlinear, Soft Matter Phys.* **2012**, *86*, 022801.
(44) Likhtman, A. E.; Talib, M. S.; Vorselaars, B.; Ramirez, J. Determination of Tube Theory Parameters Using a Simple Grid Model as an Example. *Macromolecules* **2013**, *46*, 1187−1200.
(45) Qian, H.-J.; Carbone, P.; Chen, X.; Karimi-Varzaneh, H. A.; Liew, C. C.; Müller-Plathe, F. Temperature-Transferable Coarse-Grained Potentials for Ethylbenzene, Polystyrene, and Their Mixtures. *Macromolecules* **2008**, *41*, 9919−9929.
(46) Zhu, Y.-L.; Liu, H.; Li, Z.-W.; Qian, H.-J.; Milano, G.; Lu, Z.-Y. GALAMOST: GPU-accelerated large-scale molecular simulation toolkit. *J. Comput. Chem.* **2013**, *34*, 2197−2211.
(47) Zhu, Y.-L.; Lu, Z.-Y.; Milano, G.; Shi, A.-C.; Sun, Z.-Y. Hybrid particle−field molecular dynamics simulation for polyelectrolyte systems. *Phys. Chem. Chem. Phys.* **2016**, *18*, 9799−9808.
(48) Humphrey, W.; Dalke, A.; Schulten, K. VMD: Visual Molecular Dynamics. *J. Mol. Graphics* **1996**, *14*, 33−38.
(49) Williams, G.; Watts, D. C. Non-symmetrical dielectric relaxation behaviour arising from a simple empirical decay function. *Trans. Faraday Soc.* **1970**, *66*, 80.
(50) Chen, T.; Zhao, H.-Y.; Shi, R.; Lin, W.-F.; Jia, X.-M.; Qian, H.-J.; Lu, Z.-Y.; Zhang, X.-X.; Li, Y.-K.; Sun, Z.-Y. An unexpected N-dependence in the viscosity reduction in all-polymer nanocomposite. *Nat. Commun.* **2019**, *10*, 5552.
(51) Bachus, R.; Kimmich, R. Molecular weight and temperature dependence of self-diffusion coefficients in polyethylene and

polystyrene melts investigated using a modified n.m.r. field-gradient technique. *Polymer* **1983**, *24*, 964−970.
(52) Fleischer, G. Temperature dependence of self diffusion of polystyrene and polyethylene in the melt an interpretation in terms of the free volume theory. *Polym. Bull.* **1984**, *11*, 75−80.
(53) Kalathi, J. T.; Kumar, S. K.; Rubinstein, M.; Grest, G. S. Rouse Mode Analysis of Chain Relaxation in Homopolymer Melts. *Macromolecules* **2014**, *47*, 6925−6931.
(54) Pérez-Aparicio, R.; Alvarez, F.; Arbe, A.; Willner, L.; Richter, D.; Falus, P.; Colmenero, J. Chain Dynamics of Unentangled Poly(ethylene- alt -propylene) Melts by Means of Neutron Scattering and Fully Atomistic Molecular Dynamics Simulations. *Macromolecules* **2011**, *44*, 3129−3139.
(55) Richter, D.; Willner, L.; Zirkel, A.; Farago, B.; Fetters, L. J.; Huang, J. S. Onset of topological constraints in polymer melts: A mode analysis by neutron spin echo spectroscopy. *Phys. Rev. Lett.* **1993**, *71*, 4158−4161.
(56) Richter, D.; Willner, L.; Zirkel, A.; Farago, B.; Fetters, L. J.; Huang, J. S. Polymer Motion at the Crossover from Rouse to Reptation Dynamics. *Macromolecules* **1994**, *27*, 7437−7446.
(57) Likhtman, A. E.; Ponmurugan, M. Microscopic Definition of Polymer Entanglements. *Macromolecules* **2014**, *47*, 1470−1481.
(58) Milano, G.; Müller-Plathe, F. Mapping Atomistic Simulations to Mesoscopic Models: A Systematic Coarse-Graining Procedure for Vinyl Polymer Chains. *J. Phys. Chem. B* **2005**, *109*, 18609−18619.
(59) Fritz, D.; Harmandaris, V. A.; Kremer, K.; van der Vegt, N. F. A. Coarse-Grained Polymer Melts Based on Isolated Atomistic Chains: Simulation of Polystyrene of Different Tacticities. *Macromolecules* **2009**, *42*, 7579−7588.
(60) Zhao, Y.; De Nicola, A.; Kawakatsu, T.; Milano, G. Hybrid particle-field molecular dynamics simulations: Parallelization and benchmarks. *J. Comput. Chem.* **2012**, *33*, 868−880.
(61) Shanbhag, S.; Kröger, M. Primitive Path Networks Generated by Annealing and Geometrical Methods: Insights into Differences. *Macromolecules* **2007**, *40*, 2897−2903.
(62) Hoy, R. S.; Foteinopoulou, K.; Kröger, M. Topological analysis of polymeric melts: Chain-length effects and fast-converging estimators for entanglement length. *Phys. Rev. E: Stat., Nonlinear, Soft Matter Phys.* **2009**, *80*, 031803.
(63) Bisbee, W.; Qin, J.; Milner, S. T. Finding the Tube with Isoconfigurational Averaging. *Macromolecules* **2011**, *44*, 8972−8980.
(64) Qin, J.; Milner, S. T. Tubes, Topology, and Polymer Entanglement. *Macromolecules* **2014**, *47*, 6077−6085.
(65) Sukumaran, S. K.; Likhtman, A. E. Modeling Entangled Dynamics: Comparison between Stochastic Single-Chain and Multi-chain Models. *Macromolecules* **2009**, *42*, 4300−4309.
(66) Wang, Z.; Likhtman, A. E.; Larson, R. G. Segmental Dynamics in Entangled Linear Polymer Melts. *Macromolecules* **2012**, *45*, 3557−3570.

https://dx.doi.org/10.1021/acs.jctc.0c00954
J. Chem. Theory Comput. 2021, 17, 474−487

Supporting Information: Combination of Hybrid Particle-Field Molecular Dynamics and Slip-Springs for the Efficient Simulation of Coarse-Grained Polymer Models: Static and Dynamic Properties of Polystyrene Melts

Zhenghao Wu,[†] Giuseppe Milano,[‡] and Florian Müller-Plathe*[,†]

†*Eduard-Zintl-Institut für Anorganische und Physikalische Chemie, Technische Universität Darmstadt, Alarich-Weiss-Str. 8, 64287 Darmstadt, Germany*

‡*Department of Organic Materials Science, Yamagata University, 4-3-16 Jonan Yonezawa, Yamagata-ken 992-8510, Japan*

E-mail: f.mueller-plathe@theo.chemie.tu-darmstadt.de

Molecular Dynamics Simulation

We perform the molecular dynamics simulation using GALAMOST (GPU-accelerated large-scale molecular simulation toolkit).[1] The procedure for obatining the tabulated force field of the coarse-grained polystyrene model can be found in reference.[2] The initial random configurations of all systems are generated via the self-avoiding walk algorithm. The initial configurations are subject to an high-temperature pre-equilibration under the isothermal-isobaric (NPT) condition at $P = 1$ atm and $T = 800\ K$ for 10^7 steps. Next, the configurations are cooled down to $T = 500\ K$, after which the systems are equilibrated until the density

converged. The simulation box is then resized to the average density at $T = 500\ K$, as determined in previous step. Followed that, the systems are further equilibrated in the NVT ensembale for up to 4×10^8 steps. The internal distance of the polymer backbone is monitored throughout the final equilibration procedure. The temperature and the pressure are controlled via Nosé-Hoover thermostat and Andersen barostat, respectively, as implemented in GALAMOST with damping parameter equal to 0.4 ps and 4 ps. The equation of motion of the particle is integrated via the velocity-Verlet algorithm with a time step $\delta t = 4$ fs. Generally, the longest simulations are run up to $16,000$ ns, which take around 40 days on a single Geforce NVIDIA GTX1080Ti GPU.

Particle-Field Simulation

We perform the particle-field simulation using GALAMOST (GPU-accelerated large-scale molecular simulation toolkit),[1] with the module of self-consistent-field molecular dynamics. The initial configurations are obtained from the corresponding molecular dynamics simulations after density converged. We perform pure hybrid particle-field simulation to pre-equilibrate the system up to 4×10^8 steps, with grid size starting as $l_{\text{grid}} \approx 1$ nm then slowly decreasing to $l_{\text{grid}} \approx 0.55$ nm.[3] The internal distance of the polymer chain is monitored to make sure the fully equilibration of the system. Data are then collected from the simulation runs continued from these equilibrated systems with $l_{\text{grid}} \approx 0.55$ nm. Both hybrid particle-field simulations with and without slip-springs are run in NVT ensemble with Langevin thermostat for constant temperature.

Compressibility Factor Effect on Diffusion and Radius of Gyration of Polystyrene melts

Table 1: Square radius of gyration $\langle R_g^2 \rangle$ and diffusion coeffcients D of polystyrene melts with $N = 100$ monomers in hybrid particle-field systems with compressibility factor $\kappa = 0.05$, $\kappa = 0.1$ and $\kappa = 0.2$;

	$\kappa = 0.05$	$\kappa = 0.1$	$\kappa = 0.2$
$\langle R_g^2 \rangle$ [nm^2]	2.43 ± 0.03	2.47 ± 0.03	2.54 ± 0.03
D [nm^2/ps]	8.78×10^{-5}	9.24×10^{-5}	9.66×10^{-5}

Rouse Mode Analysis of Slip-Spring Particle-field Simulations of Polystyrene Melts

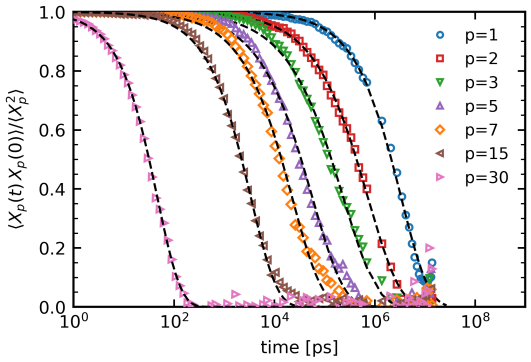

Figure S1: Normalized autocorrelation functions of Rouse modes p=1,2,3,5,7,15,30 for a polystyrene melt of chain length $N = 750$ at temperature $T = 500$ K. The dashed lines are the stretch exponential fits.

References

(1) Zhu, Y.-L.; Liu, H.; Li, Z.-W.; Qian, H.-J.; Milano, G.; Lu, Z.-Y. GALAMOST: GPU-accelerated large-scale molecular simulation toolkit. *Journal of Computational Chemistry* **2013**, *34*, 2197–2211.

(2) Qian, H.-J.; Carbone, P.; Chen, X.; Karimi-Varzaneh, H. A.; Liew, C. C.; Müller-Plathe, F. Temperature-Transferable Coarse-Grained Potentials for Ethylbenzene, Polystyrene, and Their Mixtures. *Macromolecules* **2008**, *41*, 9919–9929.

(3) De Nicola, A.; Kawakatsu, T.; Müller-Plathe, F.; Milano, G. Fast relaxation of coarse-grained models of polymer interphases by hybrid particle-field molecular dynamics: Polystyrene-silica nanocomposites as an example. *Eur. Phys. J. Spec. Top.* **2016**, *225*, 1817–1841.

3.3 Slip-Spring Hybrid Particle-Field Molecular Dynamics for Coarse-Graining Branched Polymer Melts: Polystyrene Melts as an Example

Submitted for review on 28/07/2021

Slip-Spring Hybrid Particle-Field Molecular Dynamics for Coarse-Graining Branched Polymer Melts: Polystyrene Melts as an Example

Zhenghao Wu and Florian Müller-Plathe*

Eduard-Zintl-Institut für Anorganische und Physikalische Chemie, Technische Universität Darmstadt, Alarich-Weiss-Str. 8, 64287 Darmstadt, Germany

E-mail: f.mueller-plathe@theo.chemie.tu-darmstadt.de

Abstract

The topology of chains significantly modifies dynamical properties of polymer melts. Here, we extend a recently developed efficient simulation method, namely, slip-spring hybrid particle-field model (SS-hPF), to study structural and dynamical properties of branched polymer melts. In the coarse-grained SS-hPF simulation of polymers, the bonded potentials are derived by Iterative Boltzmann Inversion from the underlying fine-grained model. The non-bonded potentials are computed from a density-functional-field instead of pair-wise interactions used in standard molecular-dynamics simulations, which increases the computational efficiency by a factor of $10 \sim 20$. The entangled dynamics is lost due to the soft-core nature of density-functional-field interactions. It is recovered by a multi-chain slip-spring model, which is rigorously parameterized from existing experimental or simulation data. For quantitatively predicting the relaxation and diffusion of branched polymers, which are dominated by arm retraction rather than

chain reptation, the slip-spring algorithm is augmented to improve the polymer dynamics near the branch point. Multiple dynamical observables, e.g., diffusion coefficients, arm relaxations and tube survival probabilities, are characterized in the example coarse-grained model of symmetric and asymmetric star-shaped polystyrene melts. Consistent dynamical behaviors are identified and compared with theoretical predictions. With a single rescaling factor, the prediction of diffusion coefficients agrees well with the available experimental measurements. In this work, an efficient approach is provided to build chemistry-specific coarse-grained models for predicting the dynamics of branched polymers.

Introduction

Molecular topology can significantly influence structural, dynamical and rheological properties of polymers. Theoretical studies aiming to comprehensively understand the structure/property relation of various types of topological polymers such as star,[1–3] comb,[4–6] bottlebrush[7–9] and ring[10–12] polymers have been advanced during the last three decades. The first topological architecture to receive intensive studies was a star polymer with a single branch point. Pioneered by the work of De Gennes[1] and Doi and Kuzuu,[13] Pearson and Helfand proposed a first-passage formulation to derive the free energy barrier for the arm retraction process,[14] results of which are consistent with the experimentally observed exponential dependence of the relaxation time on the arm molecular weight. However, the exponential dependence is predicted too strong by their model. Ball and McLeish improved this model via introducing the idea of dynamic tube dilation (DTD) to account for the constraint release.[2] This model was further developed by Milner and McLeish through detailed calculation of the first-passage process along with the DTD and the fast Rouse relaxation.[3]

The theoretical models mentioned above and the following developments[15–17] for star-shaped polymers provide reasonable predictions for the experimental measurements, e.g., stress relaxation, but the microscopic understanding is still incomplete. Molecular dynamics

simulations have served as an important technique to study the dynamical mechanisms in polymeric systems at the molecular level. The all-atom (AA) model is an ideal choice to obtain (quasi) first-principle predictions from MD simulation. However, the detailed description at the atom level in AA-MD models is computationally demanding, and it is almost unfeasible for this model to attain the time scale of full relaxations of high-molecular-weight polymers. Instead, coarse-grained (CG) polymer models, in which several atoms are lumped into a single CG bead, have become a route to increase the accessible length and time scales in MD simulations. A body of coarse-graining methods for polymeric systems has been developed during the last two decades. These methods can generally be divided into two categories: bottom-up and top-down methods. The bottom-up CG techniques mostly focus on constructing effective interactions from the underlying AA counterpart to reproduce certain physical properties evaluated from AA-MD simulations. Systematic CG methods such as Iterative Boltzmann Inversion,[18] Inverse Monte-Carlo[19] and Multiscale Coarse-Graining (force-matching)[20] have been widely used to build CG models for polymers. Their resolution is usually the monomer level. In the top-down approaches, a universal representation of polymers (e.g., a bead-spring model) is usually adopted that only carries limited relevant interactions, such as the connectivity along the polymer backbone and the segmental repulsion; The free energy function of such a CG system is postulatively constructed by directly optimizing the description of experimental observables. Typical CG models developed under the top-down scheme include the MARTINI force fields[21,22] and the statistical associating fluid theory CG models.[23,24] However, these CG models are still limited for predicting the dynamics of high-molecular-weight polymers and not able to sufficiently capture effects of molecular topology, even in the mildly entangled state.[25]

In order to reach longer time and length scales, one can continue along the path of coarse-graining with grouping even more atoms together into a CG bead. As the coarse-graining degree increases, the CG non-bonded potentials turn effectively soft, eventually leading to unphysical bond crossings. In consequence, these models cannot capture the entanglement

effects and thus predict qualitatively incorrect dynamics for high-molecular-weight polymers. The prime example of such a soft-core, non-entangled description is dissipative particle dynamics (DPD)[26]. Two major strategies have been proposed to overcome this limitation of such drastically CG models. Padding and Briels developed the TWENTANGLEMENT algorithm that explicitly detects imminent bond crossings and inserts entanglement points to prevent them.[27] Recently, this model has been extended to predict dynamics and stress relaxations of CG models of star-shaped polyethylene melts, where one CG bead represents 20 CH_2 units.[28] Later, Similar approaches such as the Soft Segmental Repulsive potential,[29,30] basically introducing additional soft repulsive forces between bonds, have also been shown to massively decrease the bond crossing events and postulate reasonable dynamical behaviors of entangled polymer melts. On the other hand, additional topological constraints have also been successfully modeled using so-called slip-links or slip-springs. The dynamics and rheology of linear polymers at mildly- and well-entangled states have been well predicted by these models.[31–34] Some of them have been further extended to branched polymers. For instance, Shanbhag and Larson proposed a slip-link model for star-shaped polymers, in which special attention was paid on the branch-point motion in asymmetric stars.[35] Masubuchi *et al.* also reported a series of multi-chain slip-link (primitive chain network) simulations for symmetric and asymmetric star-shaped polymers.[36,37] Using some sophisticated mapping procedures for specific chemistries, these slip-link models, with resolution at the entanglement segment level, are capable of predicting dynamical and rheological properties of experimental-scale polymer samples. Recently, Zhu *et al.* extended the single-chain slip-spring model of Likhtman[31] to study arm retraction dynamics of entangled star polymers.[38] The multi-chain slip-spring model has also been improved to simulate branched polymer melts.[39] One of ongoing directions of slip-link/slip-spring models is to endow these relatively high-level coarse-grained generic models with more chemical details. More recently, systematic coarse-graining has been attempted involving slip-spring models.[40–42] Alternatively, hierarchical multi-scale simulations have been proposed for quantitatively predicting poly-

mer dynamics,[43,44] e.g., all-atom model → monomer-level CG model → slip-link/slip-spring model.

In this work, we generalize the recently proposed efficient systematic coarse-graining strategy for high-molecular-weight linear polymers to model branched ones using the combination of hybrid particle-field simulation and slip-springs.[42,45] This coarse-graining strategy allows simulations of systems at large spatial-temporal scales and, at the same time, it provides sufficiently detailed chemistry for the mapping scheme. The generalization on the hPF side is straightforward, in which the procedure to parameterize the bonded and non-bonded potential is exactly the same as that for linear polymers. Specifically, the CG bonded potentials are obtained via Iterative Boltzmann Inversion to match the target distributions, e.g., bond and angle, of the underlying fine-grained atomistic model. The non-bonded interactions are computed from a density-functional-field, sufficiently enhancing the computational efficiency in comparison with pair-wise interactions used in standard MD simulations.[46,47] However, it becomes complicated on the slip-spring side for branched polymers. Special consideration has to be given to the slip-springs around the branch point since the relaxation and diffusion of branched polymers typically proceed through arm retraction, rather than chain reptation in linear polymers. For this reason, we refine our multi-chain slip-spring model by introducing two new elementary steps for the slip-spring motion, namely, bouncing-back and moving-over branch-point, to incorporate the aforementioned theoretical pictures of arm retraction and hierarchical relaxations. It is noted that the algorithm, which allows the slip-spring transit across the branch-point, is similar to the one incorporated in the multi-chain slip-spring model of Masubuchi *et al.* for branched polymers.[39] As an example system, we choose the CG model of symmetric and asymmetric atactic polystyrene star-shaped polymer melts to demonstrate the effectiveness of our generalized model. Benefiting from the computational efficiency of SS-hPF method, we simulate the PS melts for times over 1×10^2 μs in CG time units or 1×10^4 μs in real time after using a single time-rescaling factor. The translational and reorientational dynamics as well as the molecular size of 4-arm symmetric

and 3-arm asymmetric PS stars are characterized, and they are compared with results from standard MD simulations and available experimental measurements.

Methodology

CG Model of Star-Shaped Polystyrene Melts

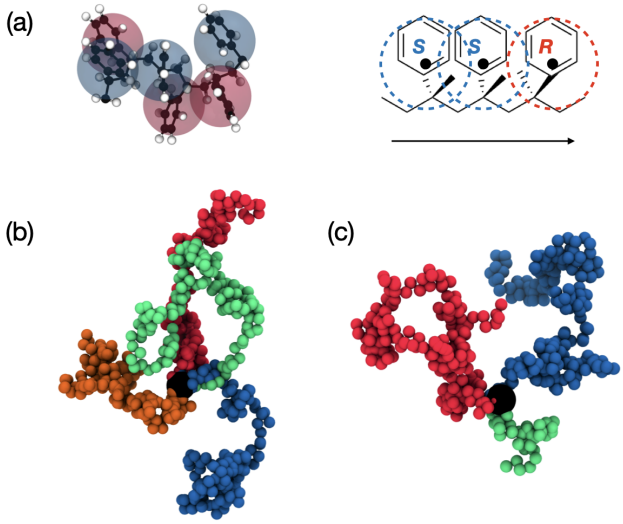

Figure 1: (a) Coarse-graining mapping: one coarse-grained bead represents one polystyrene monomer. The coarse-grained bead is positioned at the center of mass of the corresponding atomistic chemical structure. The bead types R and S are defined according to the monomer configuration, particularly, the asymmetric -CHR- group, against the direction of the backbone indicated by the arrow. Snapshots (rendered by VMD[48]) of CG representations for a single molecule: (b) 4-arm symmetric star PS melts with arm length $N_{\mathrm{arm}} = 150$ monomers and (c) 3-arm asymmetric star PS melts with long arm $N_{\mathrm{arm}} = 200$ monomers and short arm $N_{\mathrm{arm}} = 50$ monomers. The arms of the star polymer are painted with different colors. The black bead represents the branch point.

The CG model of star-shaped polystyrene melts employed in the present study is built upon a recent developed CG-hPF model of linear PS melts.[42] In this CG model, a one-bead-per-monomer scheme is applied to map the fine-grained all-atom model, where two different

bead types (R and S) are defined to account for the tacticity of the polymer chain. A schematic figure of symmetric and asymmetric star-shaped CG-PS models with various arm lengths is displayed in Figure 1. Specifically, the CG bonded interactions, namely bond and angle potentials, are derived by retaining their respective probability distribution functions of all-atom references using the iterative Boltzmann inversion method.[49] Different from the pairwise non-bonded interactions of standard MD simulation, in the hPF scheme the CG non-bonded interactions are computed through the density-functional field.[46] In this field representation of non-bonded interactions, the total interaction energy for the whole system $W[\phi(\mathbf{R})]$ depends on the local particle number densities:

$$W[\phi(\mathbf{R})] = \frac{1}{\phi_0}\left[\sum_{K<L}\chi_{K,L}\phi_K(\mathbf{R})\phi_L(\mathbf{R}) + \frac{1}{2\kappa}\left(\sum_L \phi_L(\mathbf{R}) - \phi_0\right)^2\right] \tag{1}$$

where $\chi_{K,L}$ is the mean field coupling term between particle species K and L, κ is the compressibility factor dictating the local fluctuations of the density; $\phi_K(\mathbf{R})$ is the number density of particle species K at position $\mathbf{R}$ and ϕ_0 is the average number density of the whole system. The corresponding external potential $V_K(\mathbf{R})$ for a particle of species of K at position $\mathbf{R}$, is given by:

$$V_K(\mathbf{R}) = \frac{1}{\phi_0}\left[\sum_L \chi_{K,L}\phi_L(\mathbf{R}) + \frac{1}{\kappa}\left(\sum_L \phi_L(\mathbf{R}) - \phi_0\right)\right] \tag{2}$$

For efficient computation of local particle densities, the simulation box is initially partitioned into a fine grid. The particle density is first calculated by mapping particles on the grid, and the resulting potential grid is then interpolated linearly back to the individual particle positions. The grid size is chosen as $\sim$ 0.56 nm for the model of star PS melts, slightly larger than the average bond length $l_b \approx 0.52$ nm between successive monomers; The compressibility parameter κ and density-field interaction parameter χ are fixed at 0.1 $\mathrm{kJ}^{-1}\cdot\mathrm{mol}$ and 0.0 $\mathrm{kJ}\cdot\mathrm{mol}^{-1}$ (only repulsive interactions (I am not very clear about this comment.)), respectively, in all hPF simulations. It is important to note that the choice of

these parameters is the same as our previous work on the linear PS melts.[42] It presumes the transferability among topological variants, e.g., from linear to branched polymers. More details of the hPF technique can be found in references.[42,45,46]

Langevin Equation of Motion

The particle-to-field representation makes the non-bonded interactions effectively soft-core, bringing about a rather smooth energy landscape, even if compared with the reference CG-MD model. As a result, the mobility of the hPF model is accelerated over that of a traditional MD simulation. In previous studies, this accelerated dynamics has been utilized to quickly obtain relaxed structures in systems such as AA-MD models of large-molecular-weight polymer melts[50] and coarse-grained models of large-scale polymer nanocomposites.[51] However, it is necessary to mitigate this artificial acceleration in order to construct an efficient CG model which is also dynamically consistent with the reference CG-MD model. In order to effective control of the dynamics in coarse-grained models, the Langevin equation of motion is commonly adopted to add frictions or stochastic forces,[52] which is given by:

$$m\frac{d\mathbf{v}}{dt} = \mathbf{F}_C - \zeta \cdot \mathbf{v} + \mathbf{F}_R \tag{3}$$

where $\mathbf{F}_C$ is the conservative force acting on the particle from bonded, non-bonded and slip-spring interactions, ζ is the friction coefficient and $\mathbf{F}_R$ is a uniformly distributed random force. The magnitude of $\mathbf{F}_R = 6k_BT\zeta/\delta t$ is chosen via the fluctuation-dissipation theorem to be consistent with the friction coefficient and the temperature. In this way, we are able to control the mobility of polymer chains in CG models by tuning a single parameter, the friction coefficient ζ. In hPF simulations, an appropriate friction coefficient is chosen to reproduce the dynamics (e.g. diffusion coefficient) of a reference CG-MD simulations. Notably, for calibrating the friction coefficient, the polymer melt system has to be of unentangled or weakly entangled molecular weight, due to the loss of chain incrossability in such a soft

model. In this way, the friction coefficient has been determined using linear CG-PS melts with chain length $N = 100$ monomers, giving $\zeta = 204\,\mathrm{g\,mol^{-1}\,ps^{-1}}$. The global topology of the polymer chain is expected to hardly influence the segmental friction, which is a local property. Thus the same value is employed to model star PS melts of various molecular weights.

Multi-Chain Slip-Spring Model

Soft models such as dissipative particle dynamics and hPF models are by construction not able to reproduce the entangled dynamics of high-molecular-weight polymer melts because their non-bonded interactions are too soft to avoid chains interpenetrating each other. Recently, however, entangled dynamics has been successfully restored in the hPF model of linear polymer melts by combining it with a multi-chain slip-spring model (SS-hPF).[42,45] However, the current SS-hPF model can not be directly transferred to simulate branched polymer melts since the dynamical mechanisms have changed due to the branch point. Here, we aim to extend the formulation of the multi-chain slip-spring model to branched polymer chains, e.g., star polymers. This extension is not trivial. Several new slip-spring movements have been implemented to incorporate the branch-point induced mechanisms such as dynamic tube dilation and arm retraction.

The soft FENE interaction form, same as for linear polymers,[42] is adopted to describe the potential of slip-springs:

$$U(l_{ss}) = -0.5 K_{ss} R_{\max}^2 \ln\left[1 - (\frac{l_{ss}}{R_{\max}})^2\right] \tag{4}$$

where $R_{\max}$ and K_{ss} denote the maximum length and the force constant of the slip-spring, respectively. To avoid extremely large forces, the slip-spring potential is cut at $l_{\mathrm{ss}} = 0.95 \times R_{\max}$ and continued linearly. The maximum length of the slip-spring $R_{\max}$ is chosen as the tube diameter d_T and the force constant K_{ss} is tuned until the equilibrium

mean length of slip-springs $\langle l_{\mathrm{ss}} \rangle = d_T/2$. In the previous study,[42] the force constant K_{ss} was determined as $= 0.52$ kJ/(mol $\cdot$ nm^2) with the tube diameter being $d_T \approx 7.5$ nm for linear polystyrene melts.[53] In this work, the same slip-spring parameters are employed for modeling star PS melts.[42]

The initial configurations of slip-springs are randomly created in the system for pairs of beads separated by $l_{\mathrm{ss}} < 0.9 \times R_{\mathrm{max}}$. As seen in the schematic of Figure 2, a single slip-spring

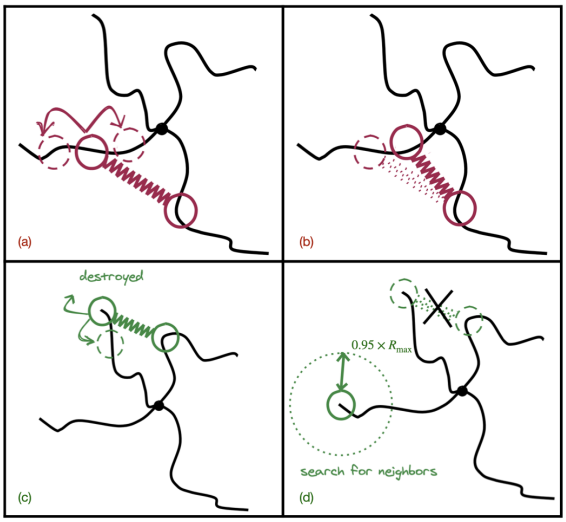

Figure 2: Schematic of the multi-chain slip-spring model for a star-shaped polymer molecule: (a) and (b) describes the hopping movement of slip-springs; (c) and (d) describes the destruction and recreation of slip-springs at arm end.

in star polymers is allowed to connect two different arms whether they belong to the same molecule or not. It is noted that slip-springs in the current implementation can not connect beads of the same arm, thus self-entanglements are avoided. Figure 2 (a)-(b) illustrate the hopping movement of slip-springs, where one of the two attachments of a slip-spring is chosen to move either left or right by one monomer with equal possibility. When one attachment of a slip-spring sits at the end of an arm, it has an equal possibility to move out of the arm (being destroyed) or move backwards toward the branch point, as shown in Figure 2

(c). In equilibrium state, the number of chain entanglements is expected to be statistically constant. Therefore, if a slip-spring is destroyed when it leaves one arm, a new one will be created simultaneously, whose one attachment is forced to locate at a randomly chosen arm end. The other attachment will be found within its radial distance $d < 0.95 \times R_{\max}$ (Figure 2 (d)). We note that the slip-spring mechanisms of hopping, destruction and creation are exactly the same as those employed for linear PS melts.[42]

In star polymers, the relaxation and diffusion of molecules proceed through arm retraction instead of snake-like chain reptation. Thus the movements of slip-springs around the branch point require careful considerations. As described in theoretical models,[2,3,54] the branch point strongly hinders the dynamical progressing of topological entanglements. Moreover, the hierarchical relaxation[54] implies that the time scales of the relaxation and diffusion of polymer segments are separated due to the dominance of branch points that differ in their shortest distances from a free chain end. In other words, the shorter arm is able to favor the relaxation of longer arms in a branched polymer. Accordingly, (Figure 3 (a)-(b)) in our augmented model, the slip-springs are reflected from a branch point to another arm, which carries at least one slip-spring. The arm is considered to be fully relaxed when there is no slip-spring on it. The slip-spring is allowed to move over the branch point only if the arm receiving it is fully relaxed (no slip-springs) (Figure 3 (c)-(d)). Notably, no additional parameter is required for the current implementation of slip-spring movements near branch points.

The total number of slip-springs Z_t is held constant in the system at the equilibrated state, given by:

$$Z_t = M \times \sum \frac{(N_{\text{arm}}/N_e^{ss} - 1)}{2} \tag{5}$$

where M denotes the number of molecules; N_{arm} and N_e^{ss} represent the number of monomers per arm and the average length between adjacent slip-spring attachments, respectively. Here, $N_e^{ss} = 64$ monomers is chosen as half of the entanglement length $N_e = 127$ monomers measured by CReTA[53] in the CG model of PS melts.[55] The configuration of slip-springs

is updated using a Monte-Carlo algorithm every 100 hPF steps ($\Delta t_{\mathrm{MC}} = 100\Delta t_{\mathrm{hPF}} = 3$ ps). As implemented in previous SS-hPF work for linear polymers, the dynamics of the slip-springs is controlled by a single parameter of hopping frequency v_{hop}. Here, the hopping frequency in star PS melts is chosen to be equivalent to be the value used in linear PS melts $v_{\mathrm{hop}} = 1.25 \times 10^{-}4$ ps^{-1}. More details about the slip-spring algorithm can be found in the reference.[42]

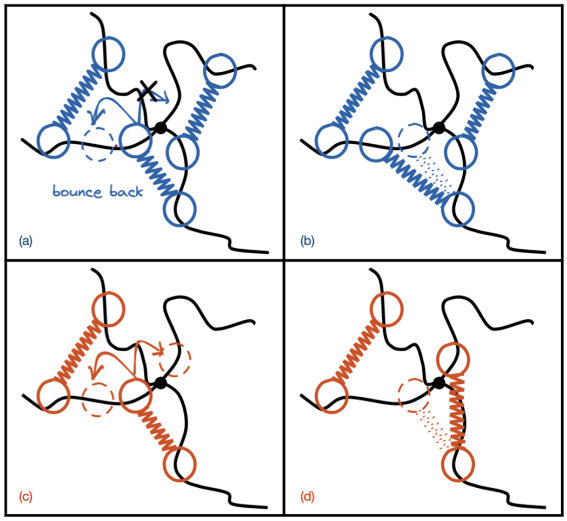

Figure 3: Schematic of the multi-chain slip-spring model for a star-shaped polymer molecule: (a) and (b) describes the bouncing-back of slip-spring when trying to move over the branch-point; (c) and (d) describes the slip-spring move over a branch-point to another branch without any slip-springs.

Simulation Details

We perform SS-hPF simulations of star PS melts using the GPU-accelerated large-scale molecular simulation toolkit (GALAMOST) package (version 3.1.1), with corresponding hPF (without slip-spring) and standard CG-MD simulations conducted as well for comparison. Periodic boundary conditions are applied to all directions to simulate bulk properties.

Timesteps $\Delta t = 0.03$ ps and $\Delta t = 0.004$ ps are chosen for particle-field simulations (hPF and SS-hPF) and standard CG-MD simulations, respectively. Details about the systems simulated are summarized in Table 1. The initial configurations of SS-hPF and hPF simulations are obtained from the corresponding CG-MD simulations after their density converged. These configurations are subjected to an initial equilibration in NVT ensemble with temperature controlled by a Langevin thermostat at $T = 500$ K for 1×10^8 steps (3×10^6 ps). Subsequently, these systems are further equilibrated ($1 \times 10^7 \sim 2 \times 10^8$ steps) until the radius of gyration of the star polymers converged. The linear momentum of the system is zeroed every 100 time steps, in order to ensure that there is no momentum accumulation within the system.

Table 1: Simulation Details[1].

Model	Topology	System Code	N_{arm}	M	N_t	Z_t
SS-hPF; hPF	Symmetric 4 arm star	PS50	50×4	100	20100	0
		PS100	100×4	100	40100	114
		PS150	150×4	100	60100	272
		PS200	200×4	50	40050	214
		PS250	250×4	50	50050	293
		PS300	300×4	50	60050	372
		PS350	350×4	50	70050	451
		PS400	400×4	50	80050	529
SS-hPF; CG-MD	Asymmetric 3 arm star	PS(10,200×2)	$10, 200 \times 2$	75	30825	161
		PS(20,200×2)	$20, 200 \times 2$	75	31575	161
		PS(30,200×2)	$30, 200 \times 2$	75	32325	161
		PS(50,200×2)	$50, 200 \times 2$	75	33825	161
		PS(100,200×2)	$100, 200 \times 2$	75	37575	182
		PS(150,200×2)	$150, 200 \times 2$	75	41325	212

[1] N_{arm}: number of monomers per arm; M: number of star molecules in the system; N_t: total number of monomers; Z_t: total number of slip-springs in the system.

Results

Comparison with Reference Simulations

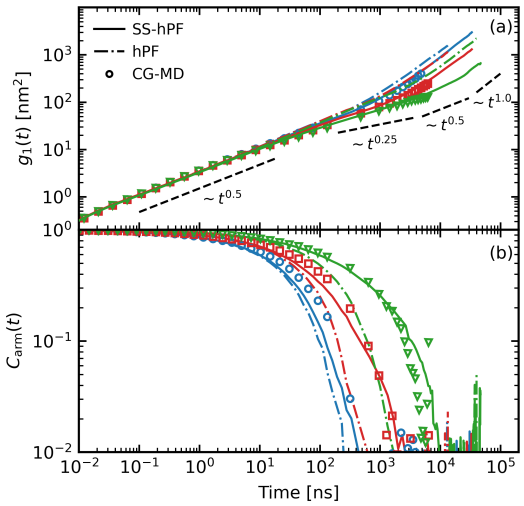

Figure 4: (a) Mean-square displacements $g_1(t)$ averaged over all monomers and (b) arm end-to-end-vector auto-correlation function $C_{\text{arm}}(t)$ as a function of time from SS-hPF (solid lines), hPF (dot dashed lines) and CG-MD (symbols) simulations of 4-arm symmetric star PS melts with arm length $N = 100$ (blue), $N = 150$ (red) and $N = 250$ (green).

We first examine the effectiveness of SS-hPF model of star PS melts by comparing it with corresponding hPF and CG-MD simulations. The monomer mean-square displacement (MSD) and auto-correlation function (ACF) of arm end-to-end (from branch-point to arm-end) vectors of 4-arm symmetric star PS melts with arm length $N = 100 \sim 250$ monomers are shown in Figure 4. Quantitative agreement is observed at short timescale $t < 20$ ns in both MSDs and ACFs from all of these simulation models, indicating the successful recovery of segmental mobility via the parameterization of segmental friction introduced in Section **Langevin Equation of Motion**. Profound slow-down in both translational and reorientational dynamics is seen after integrating slip-springs to the hPF models, especially those of high molecular weight at long times. Consistent dynamical behavior in both molecular diffusion and arm relaxation over the entire time range is then found between SS-hPF

and CG-MD models showing that introducing slip-springs can effectively restore entangled dynamics to the hPF description.

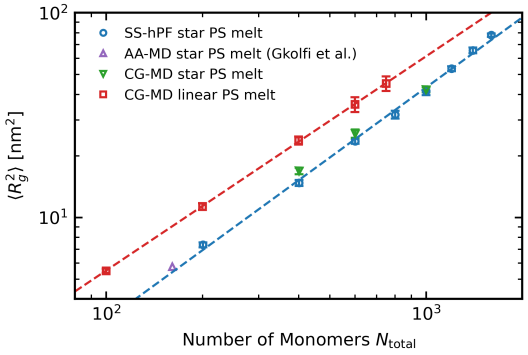

Figure 5: Ensemble-averaged square radius of gyration $\langle R_g^2 \rangle$ as a function of number of monomers in SS-hPF (blue) and MD (green) models of 4-arm symmetric star PS melts as well as the MD model of linear PS (red) melts. The red and blue dashed lines are the power law fits ($\langle R_g^2 \rangle \sim N_{\text{total}}^{\alpha}$) to MD simulations of linear PS melts ($\alpha \approx 0.46$) and SS-hPF simulations of 4-arm symmetric star PS melts ($\alpha \approx 0.49$), respectively. The purple triangle is the result from recent all-atom MD simulations of 4-arm symmetric star PS melts with arm length $N = 40$ monomers[56]

The hPF model, leveraging the density-functional-field for efficiently computing non-bonded interactions, has been reported to predict accurate structural properties in diverse polymeric systems except the local structure (e.g. pair distribution function) at the length scale of few monomer diameters ($\sim$ 1 nm in the CG-PS model). In prior studies,[42,45] integrating slip-springs into hPF models of linear polymers to recover entangled dynamics has been shown to barely affect the chain structures. The molecular dimension, i.e., radius of gyration, of 4-arm symmetric star PS molecules in the SS-hPF simulation is compared with its AA-MD[56] and CG-MD counterparts in Figure 5. Results from corresponding linear ones are also included. It is found that the ensemble-averaged square radius of gyration $\langle R_g^2 \rangle$ of 4-arm symmetric star PS molecules in the SS-hPF simulation is in quantitative agreement with those from standard MD simulations. Additionally, the star PS molecules are more compact than their linear counterparts at the same molecular weight, consistent with previous simulation observations.[39,57]

Self-Diffusion Coefficient

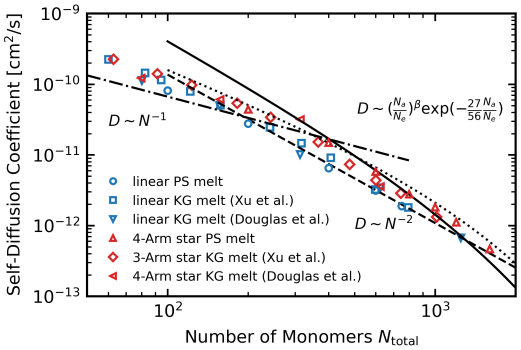

Figure 6: Self-diffusion coefficients of star (red) and linear PS (blue) melts as a function of number of monomers per molecule from the SS-hPF model (circles), Kremer-Grest model of Xu *et al.*[58] (squares) and Chremos *et al.*[57] (triangles). The dot dashed line and dashed line are predictions from Rouse model for unentangled polymers and the tube theory for entangled linear polymers,[59] respectively. The dotted line and solid line are the Frischknech-Milner model[60] for entangled star polymers with dilated ($\beta = -3/2$) and undilated ($\beta = -29/14$) tubes, respectively.

The self-diffusion coefficient D is a common observable to measure the mobility of polymer chains. Theoretically, the self-diffusion coefficient of star polymers can be computed by the mean-square displacement a branch point is able to hop during an arm retraction time: $D = (pa)^2/6\tau_{\text{arm}}$, where a and p denote the tube diameter and a constant of order unity, respectively. Frischknecht and Milner, utilizing the idea of dynamic tube dilation developed by Milner and McLeish,[3] derived quantitative analytical expressions for the self-diffusion coefficient of star polymers:[60]

$$D \sim (\frac{N_{\text{arm}}}{N_e})^{\beta} \exp\left(-\frac{27 N_{\text{arm}}}{56 N_e}\right) \tag{6}$$

where, N_{arm} and N_e are the arm length and entanglement length, respectively; The branch-point hops a distance of a dilated tube diameter with $\beta = -3/2$ and an undilated tube diameter with $\beta = -29/14$.[60,61] It is noted that the tube dilation effect is expected to be significant in the limit of extremely entangled polymer melts. However, previous

experimental studies show that the diffusion coefficients of star PS melts well conform to the case of undilated tube over a range of $N_{\text{arm}} = 135 \sim 1400$ monomers.[61] In simulations, the self-diffusion coefficient D can be computed from the chain center-of-mass MSD $g_3(t)$ using Einstein relation:

$$D = \lim_{t\to\infty} \frac{g_3(t)}{6t} \tag{7}$$

The self-diffusion coefficient D is plotted as a function of number of monomers per molecule in Figure 6. The results of Kremer-Grest (KG) models from Xu *et al.*[58] and Chremos *et al.*[57] are also included. To facilitate comparison, the number of beads in the KG model N_{KG} is translated to the number of monomers of PS melts with a conversion factor $N_{e,\text{PS}}/N_{e,\text{KG}}$, where $N_{e,\text{KG}} \approx 65$ beads and $N_{e,\text{PS}} \approx 127$ monomers are the entanglement length of the KG model[62] and CG model of PS melts,[55] respectively. At small number of monomers, the diffusion coefficients of linear PS melts deviates slightly from the Rouse predictions for unentangled polymer melts. This may be due to the influence of chain stiffness of our CG-PS models. For a larger number of monomers per molecule, the reptation motion induced by chain entanglements, starts to dominate the dynamics of linear polymers. As predicted by the naive tube model, the diffusion coefficients of linear PS melts scale with the number of monomers as $D \sim N^{-2}$. The polymer dynamics is altered significantly by the molecular architecture (e.g., star vs linear). At a small numnber of monomers per chain, the mobility of star PS melts is faster than the respective linear PS melts in SS-hPF simulations, similar as observed in the KG models. For arms with large number of monomers, arm entanglements start to play a significant role in suppressing the motion of star polymers. The exponential dependence of self-diffusion coefficients on the number of monomers per arm has been observed in polymeric systems experimentally,[61,63] but it has not yet, to our knowledge, been clearly seen in KG simulations of star polymers reported in previous literature. The computational diffusion coefficients from SS-hPF model of star PS melts are also compared with the theoretical prediction of Frischknecht and Milner.[60] Overall, the simulation results are consistent with the postulates of the analytical model, showing the effectiveness of the

augmented SS-hPF model to predict diffusive dynamics of star polymers. Specifically, it is found that in the high-molecular-weight regime the simulation results are located roughly between the predictions of stars diffusing in dilated and undilated tubes. This disparity will be further discussed through comparisons between rescaled simulation results and experimental measurements in the next section.

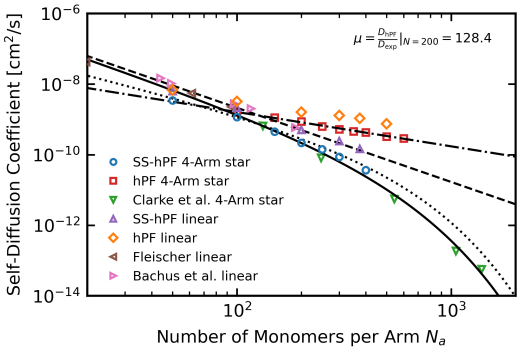

Figure 7: Self-diffusion coefficients of star (blue) and linear PS (purple) melts as a function of number of monomers per arm from the SS-hPF model shifted by a time-rescaling factor $\mu = 128.4$. The brown,[64] pink[65] and green[61] are experimental measurements for linear and 4-arm symmetric star PS melts. The dot dashed and dashed lines are the predictions of Rouse model and the tube model, respectively. The dotted and solid lines are Frischknecht-Milner expressions[60] of arm-length dependent self-diffusion coefficient for entangled star-shaped polymers with and without dilated tube, respectively.

While the SS-hPF model quantitatively reproduces the dynamics of CG-MD counterparts, it is still found to be too fast in comparison with experimental measurements. Thus we introduced an empirical time-rescaling factor μ to resolve this gap.[42] It is defined as the ratio between the chain diffusion coefficients computed from the SS-hPF simulation and the experimental values such as obtained by pulsed field gradient nuclear magnetic resonance for PS melts with the same molecular weight. Here, this time-rescaling factor $\mu \approx 128.4$ was estimated from linear PS melts with $N = 200$ monomers.[42] In this way, all simulation results (shifted by this rescaling factor) and experimental results available[61,64,65] for linear PS and 4-arm symmetric star PS melts are displayed in Figure 7. It is noted that the experimental results from Clarke *et al.*[61] are shifted to a single temperature $T = 500$ K

using the WLF form shift factors determined from the viscosity experiments.[61] The details about the determination of this shift factor can be found in the **Supporting Information**. Deviations between self-diffusion coefficients of linear PS and star PS melts from both simulation and the experimental measurements are clearly observed in PS melts with number of monmers per arm $N_{\text{arm}} > 100$. The scaling relation $D \sim N^{-2.1}$ previously determined from SS-hPF models of linear PS melts[42] is not able to reproduce the diffusive behavior of star PS melts with arm lengths longer than the entanglement length $N_e \approx 127$.[55] It is found that diffusion coefficients from SS-hPF model of 4-arm symmetric star PS melts are in good agreement with the experimental measurements at the intermediate range of arm molecular weight $N_{\text{arm}} = 100 \sim 300$ monomers. However, the SS-hPF model predicts a slightly greater diffusion coefficient for 4-arm symmetric star PS melts with $N_{\text{arm}} > 300$ monomers than the experimental results, which were reported to well conform to the theoretical prediction of the undilated tube model over the range of $3.5 < N/N_e < 9$.[61] This discrepancy implies that the SS-hPF model predicts a faster dynamic tube dilation process, which potentially requires future refinements. Additionally, the diffusion coefficients of linear and star PS melts from hPF models, in which chain entanglements are missing due to soft non-bonded interactions, follow the same scaling relations $D \sim N_{\text{arm}}^{-1}$, indicating the topological constraint from the branch point alone does not qualitatively alter the dynamics of polymer melts in the star polymers with small number (≤ 4) of arms.

Mean-Square Displacement

The monomer MSD of star PS melts is calculated through $g_1(t) = \langle(\mathbf{r}_i(t) - \mathbf{r}_i(0)^2)\rangle$, where $\mathbf{r}_i(t)$ and $\mathbf{r}_i(0)$ are the position of particle i at time t and 0, respectively. Figure 8 depicts MSDs of star PS melts with various arm lengths in SS-hPF simulations. The result of linear PS melts from the previous publication[42] is also included for comparison. Firstly, multiple scaling relations are distinctly observed in both linear PS and star PS melts. Below the entanglement time τ_e, the topological constraint of entanglements is unimportant and the

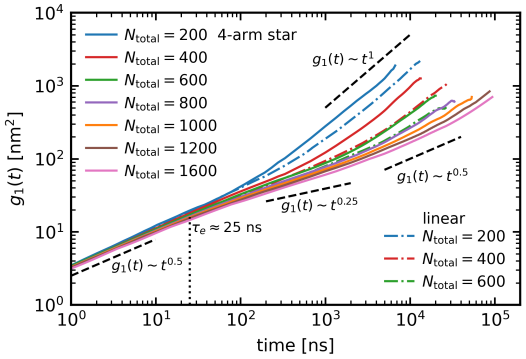

Figure 8: Monomer MSD of star (solid lines) and linear PS (dot dashed lines) melts with various number of monomers $N_{\text{total}} = 200$ (blue), $N_{\text{total}} = 400$ (red), $N_{\text{total}} = 600$ (green), $N_{\text{total}} = 800$ (purple), $N_{\text{total}} = 1000$ (orange), $N_{\text{total}} = 1200$ (brown) and $N_{\text{total}} = 1600$ (pink) from SS-hPF simulations. The vertical dot line is the estimated entanglement time τ_e. Dashed lines are indications of scaling relations predicted by the tube theory.

motion of monomers are similar to unentangled ones, which are well-described by the Rouse model. Indeed, in both linear PS and star PS melts, the scaling $g_1(t) \sim t^{0.5}$ is clearly seen at short time scales ($t < 10$ ns), implying that the branch-point in star-shaped polymer melts imposes negligible influence on the short-time dynamics of polymer segments. The entanglement time τ_e, known as transition time from free Rouse motion $g_1(t) \sim t^{0.5}$ to constrained Rouse motion $g_1(t) \sim t^{0.25}$, can be estimated by the time at the intersection between power-law fits of these two regimes. It yields $\tau_e \approx 25$ ns for both linear PS melts and star PS melts, respectively. These close values suggest that the branch-point has little impact on the entanglement time of polystyrene melts. This coincidence further indicates that the entanglement length is barely affected by the branch point, a posteriore justifying the transferability of slip-spring parameters from linear PS melts to star PS melts with a few arms. At time scale $\tau_e < t < \tau_R$, monomers of linear PS and star PS melts start to feel entanglements from confinements of the neighboring chains (arms), manifesting scaling relations of $g_1(t) \sim t^{0.25}$ in the limit of ideal long enough chains. A scaling law of $g_1(t) \sim t^{0.5}$, predicted from the tube theory, is clearly observed at time scales $\tau_R < t < \tau_d$ in star PS melts with arm length $N_{\text{arm}} > 200$. However, this region is often not observed in simulations of

linear chain melt, because τ_R and τ_d are proportional to the square and cube of the molecular weight, respectively. It is noted that although the scaling relation of star PS melts within the tested molecular-weight range is similar to that of linear PS melts, it could be different for star-shaped polymers with higher molecular weight since the diffusion and relaxation of stars proceed through arm retractions rather than chain reptation due to the existence of branch points.

Arm Relaxation

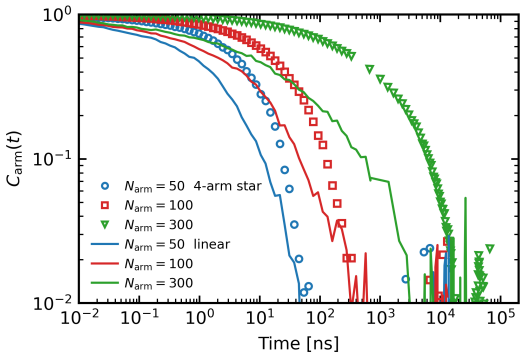

Figure 9: Autocorrelation function $C_{\text{arm}}(t)$ of arm end-to-end vectors (branch point to the end monomer) for SS-hPF models of linear PS (lines) and star PS (symbols) melts with arm length $N_{\text{arm}} = 50$ (blue), $N_{\text{arm}} = 100$ (red) and $N_{\text{arm}} = 300$ (green).

The arm relaxation is quantified via the autocorrelation function (ACF) of arm end-to-end vectors, which is given by:

$$C_1(t) = \langle \mathbf{e_i}(t) \cdot \mathbf{e_i}(0) \rangle \tag{8}$$

where $\mathbf{e_i}(t)$ is the unit vector from the branch point to the end monomer of arm i at time t. Figure 9 presents ACFs from SS-hPF models of 4-arm symmetric star PS melts with various arm lengths. The results from linear PS melts, which are considered as 2-arm symmetric stars, with corresponding arm lengths are also included for comparison. Clearly, the ACF of the star PS melt decays considerably slower than that of its linear counterpart, especially for

long arms, due to the dynamical restraint from the branch point. The arm relaxation times $\tau_{d,\mathrm{arm}}$ are determined as follows: The ACF ($C_1(t)$) for times, after the initial fast relaxation process is complete, is fitted to an exponential functional form, $C_1(t) = A\exp(t/\tau_1)$, where A and τ_1 are fitting parameters; The arm relaxation time is then defined as $\tau_{d,\mathrm{arm}} = \tau_1$. Examples of the exponential fits can be found in the **Supporting Information**. The results including both star and linear PS melts are shown in Figure 10. Firstly, it is evident that the arm relaxation times $\tau_{d,\mathrm{arm}}$ of star PS melts are larger than their linear PS counterparts at the same arm length, consistent with the observations in diffusion coefficients discussed in previous sections. McLeish and co-workers[2,3] proposed a dynamic tube dilation ansatz to analytically solve for the arm retraction or arm relaxation time, which depends exponentially on the number of entanglements per arm N_{arm}/N_e:

$$\tau_{\mathrm{arm}} = \tau_0(\frac{N_{\mathrm{arm}}}{N_e})^{29/14}\exp\left(\frac{27N_{\mathrm{arm}}}{56N_e}\right) \tag{9}$$

where τ_0 is a fitting parameter. A fit of Equation 9 to the arm relaxation times computed from SS-hPF models of star PS melts yields τ_0. Specifically, the computational arm relaxation times are generally in good agreement with the theoretical prediction in the range of long arm length $N_{\mathrm{arm}} > 200$ monomers. The theoretical model of McLeish and co-workers is found to perform much worse for star PS melts with arm lengths below $N_{\mathrm{arm}} \approx 200$ monomers, a transition length close to the entanglement length of linear PS melts $N_e \approx 127$ monomers. This deviation is indeed anticipated from the theoretical underpinnings since the arm retraction and the related dynamic tube dilation are assumed to dictate the dynamics of star-shaped polymer melts in the limit of long arms.

Tube Relaxation

In order to gain more insights in the relaxation behavior of star PS melts from SS-hPF simulations, we conduct further analysis on tube relaxations by means of tube survival

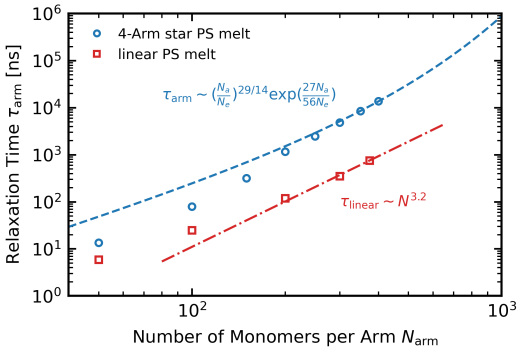

Figure 10: Relaxation times of arm end-to-end vectors for 4-arm symmetric star PS (blue) and linear PS (red) melts with various arm lengths. The dashed line is the fit of Milner-McLeish model and the dot dashed line is the fit of tube model for linear polymers.

probability $\Psi(t)$ following the original idea of Doi and Edwards.[66] Firstly, we compute the tube segment (local) survival probability. In molecular dynamics simulations, this can be computed for each arm of stars via the formulation:[67,68]

$$p(x,t) = \left\langle \frac{\partial \mathbf{R_i}(x,0)}{\partial x} \cdot \left(\mathbf{R}_{\mathrm{ete,i}}(t) - \frac{1}{f-1} \sum_{i \neq j}^{f} \mathbf{R}_{\mathrm{ete,j}}(t) \right) \right\rangle \tag{10}$$

where $\partial \mathbf{R_i}(x,0)/\partial z$ denotes the tangent vector of xth segment of arm i at time 0; $\mathbf{R}_{\mathrm{ete,i}}(t)$ and $\mathbf{R}_{\mathrm{ete,j}}(t)$ are arm end-to-end vectors for arm i and arm j at time t, respectively. The summation term involves $\mathbf{R}_{\mathrm{ete}}(t)$ from all other arms within the same star, enabling it to include cross-correlation effects between different arms. The bracket $\langle ... \rangle$ represents the ensemble average over all arms of all molecules in the system. This tangent correlation function for the arm segment is employed as an approximation for the relaxation for a certain tube fraction. Here, we directly use the chain coordinates instead of the mean path (tube) coordinate because only the fast motion of segments is averaged over in the representation of mean path and this fast motion does not affect the relaxation of arm segments significantly.[69] In essence, the long-time relaxation behavior of arm segments is equivalent to that of tube segments. The segments of each arm are defined as follows:

Starting from the branch point, every 10 monomers are grouped together and labeled as one segment $x = 0, 1, ...$ The end-to-end vector of each segment $\mathbf{R}_{\text{ete}}(x)$ is used to approximate the tangent vector $\partial\mathbf{R}(x)/\partial x$. The tube segment survival probability functions $p(x,t)$ of two example systems, star PS melts with $N_{\text{arm}} = 100$ and $N_{\text{arm}} = 400$ monomers, are shown in Figure S3. The stretched exponential or Kohlrausch-Williams-Watts (KWW) function $p(x,t) = \exp(-(t/\tau_K)^{\beta})$, where τ_K and β are fitting parameters, is employed to fit the tube segment survival probability function $p(x,t)$. In order to compare the tube survival probability between stars with different arms, we define a new normalized variable, namely, tube fractional distance s ($0 < s = x/L < 1$ with $s = 0$ at the branch point, where L denotes the arm length in segments). The characteristic time $\tau(s)$ for a certain tube fraction $s = x/L$ being fully relaxed can be calculated through the integration of the KWW fit over the whole time regime: $\tau(s) = (\tau_{K,s}/\beta_s)\Gamma(1/\beta_s)$. Essentially, we now obtain a discretized representation of the time $t = \tau(s)$ for relaxing an arm segment at a different position s_x along the arm from $s = 1$ (arm free end) to $s = s_x$ for each arm. Since the arm lengths are equal for our symmetric stars, the tube survival probability $\Psi(t)$ for a 4-arm symmetric star is equivalent to the tube fractional distance $s(t)$ as a function of characteristic relaxation time $t = \tau(s)$ averaged over four arms: $\Psi(t) = \sum_{n=4} s_i(t)/4$. As shown in Figure 11, we plot the tube survival probability $\Psi(t)$ of 4-arm symmetric stars with various arm lengths as a function of the characteristic relaxation time. Generally, the relaxation time needed for relaxing the same tube fractional distance s is observed to increase dramatically with increasing the arm length of the 4-arm symmetric star PS melts in SS-hPF simulations. The theoretical model of McLeish and co-workers[3,70] also provides an analytical expression for the tube survival probability in star polymer melts. The detailed derivation can be found in the **Supporting Information**. It is noted that the entanglement length input in the theoretical model was estimated from the rheological measurements in the original work.[70] This entanglement length N_e^{rheo} is found to be ~ 2 times smaller than the one estimated from the simulations using topological analysis (N_e^{topo}) such as CReTA:[71] $N_e^{\text{topo}} \approx 2N_e^{\text{rheo}}$.

Therefore, we use $N_e = N_e^{\text{topo}}/2 \approx 65$ as the input parameter for the theoretical model. The tube survival probability from previous simulations of Kremer-Grest models of $3 \sim 5$-arm symmetric star polymers with each arm carrying 5 entanglements was found to be consistent with the theoretical prediction above the timescale of τ_R.[68] Here, the SS-hPF simulation results for the tube survival probability are also validated and compared with the theoretical predictions as displayed in Figure 11. Large deviations are clearly seen between theoretical and SS-hPF models in the 4-arm symmetric star PS melt with $N_{\text{arm}} = 100$ monomers. The deviation between the theory and simulation results is narrowing when the arm length N_{arm} increases. In the largest star we are currently able to simulate with $N_{\text{arm}} = 400$ monomers, the theoretical prediction is in reasonable agreement with the SS-hPF simulation results covering the whole time regimes, except the deep region near the branch point due to p(x,t) of this region not fully relaxed within the current simulation time.

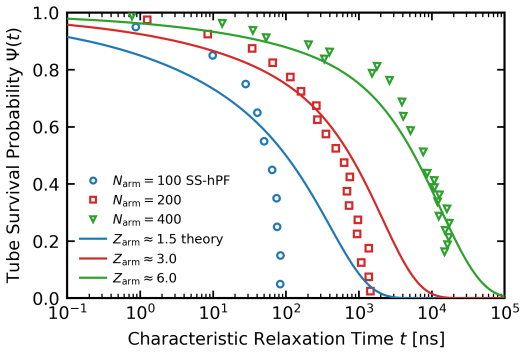

Figure 11: Tube survival probability $\Psi(t)$ against the characteristic relaxation time $t = \tau(s)$ from SS-hPF simulations (symbols) and Milner-McLeish theoretical model[3] (solid lines) for 4-arm symmetric PS melts with $N_{\text{arm}} = 100$ monomers (blue), $N_{\text{arm}} = 200$ monomers (red) and $N_{\text{arm}} = 400$ monomers (green).

Slip-Spring Moving-Over Branch-Point

It is crucial for slip-springs to be able to hop across the branch point, especially for asymmetric star-shaped polymers with significantly different arm lengths or, more importantly,

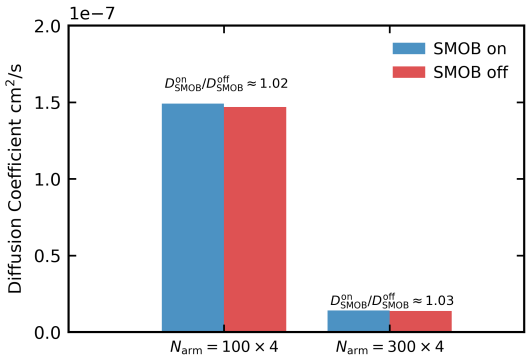

Figure 12: Self-diffusion coefficients of SS-hPF models with (blue) and without (red) slip-spring moving across branch-point for 4-arm symmetric star PS melts with arm length $N_{\mathrm{arm}} = 100$ and $N_{\mathrm{arm}} = 300$ monomers.

polymers with multiple branch points. For example, the conformations of slip-springs can not be properly equilibrated in H-shaped polymers on condition that slip-springs are only allowed to move between two branch-points. Therefore, an additional algorithm allowing the slip-spring move over the branch-point, which is described in detail in Section **Multi-Chain Slip-Spring Model**, is implemented to remedy this limitation. We firstly examine the influence of this mechanism on the dynamics of symmetric star-shaped polymer melts. As exhibited in Table 12, we compare the self-diffusion coefficients of two example systems of star PS melts with arm length $N_{\mathrm{arm}} = 100$ and $N_{\mathrm{arm}} = 300$ monomers with and without slip-springs moving over branch-point. The diffusive dynamics is found to be barely affected in symmetric star PS melts with unentangled and mildly entangled arm length, consistent with previous slip-spring simulations of generic star-shaped polymer models.[39,72] This indicates that the SMOB algorithm can be practically turned off to increase computational efficiency for future SS-hPF simulations of symmetric star-shaped polymers.

The inclusion of this move has a stronger effect on the self-diffusion coefficients of asymmetric 3-arm star PS melts. The chain length of the two long arms is kept the same ($N = 200$ monomers) while the chain length of the short arm is varied from $N = 20$ to 150 monomers, from SS-hPF simulations with and without allowing slip-springs moving over branch-point

(SMOB), are displayed in Figure 13. The results from the reference MD simulations are also included for evaluating the effectiveness of SMOB algorithm. SMOB profoundly accelerates the diffusive dynamics of asymmetric 3-arm star PS melts in comparison with those without SMOB, especially for those with a very short third arm. As short arm's length increases, the acceleration from the SMOB is decreasing, and eventually disappears. This observation is consistent with the theoretical picture that fast-relaxed short arms act as source for diluting entanglement networks (tube), which accelerates the relaxation of long arms. Additionally, the self-diffusion coefficients from reference CG-MD simulations are found to be smaller than those from SS-hPF simulations with SMOB in systems with significantly different arm lengths ($N_{\mathrm{arm},s} < 100$ monomers). This disparity could be interpreted by the free volume theory, which attributes the chain length dependence of segmental friction to the excess free volume of free chain ends.[66,73] Specifically, the segmental friction used in all SS-hPF simulations is parameterized through systems of linear PS melts with $N = 100$ monomers. We chose this chain length since previous studies found that the segmental friction becomes almost constant for linear PS melts with chain length larger than this value.[73] However, the chain ends of short arms in systems such as $3 - \mathrm{SPS}(10, 200 \times 2)$ provide additional excess free volume, which requires larger segmental frictional coefficient to recover the dynamics to its reference MD model. It results in faster diffusive dynamics of the SS-hPF model in comparison with its CG-MD counterpart. Additionally, the average number of slip-springs carried by a short arm is calculated(Figure S4). At least one slip-spring can be found on a short arm with chain length above approximately $N_{\mathrm{arm},s} \sim 75$ monomers, close to the average number of monomers separated by a slip-spring $N_e^{ss} = 64$ monomers. This also implies that the observed fast relaxation is mainly associated with the segmental friction instead of the chain entanglement.

Furthermore, we calculate the arm relaxation time τ_{arm} for long and short arms separately in the asymmetric 3-arm star PS melts of both SS-hPF and MD simulation models, as shown in Figure 14. It is observed that the arm relaxation times of short arms (even as

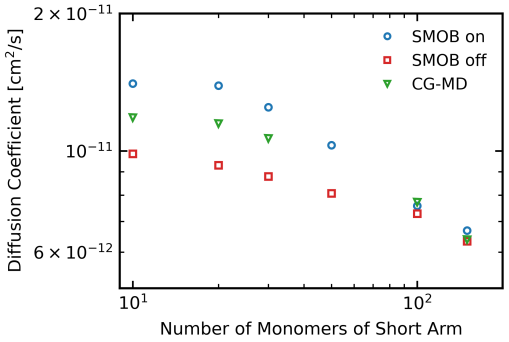

Figure 13: Self-diffusion coefficients of SS-hPF models with (blue) and without (red) slip-spring moving-over branch-point and reference CG-MD models (green) for 3-arm asymmetric star PS melts with short arm length ranging from $N_{\mathrm{arm},s} = 10$ to $N_{\mathrm{arm},s} = 150$ monomers. The long-arm length is $N_{\mathrm{arm},l} = 200$ for all systems.

short as $N_{\mathrm{arm},s} = 10$ and 20) from SS-hPF simulations with and without SMOB algorithm evidently overlap, indicating that SMOB algorithm hardly affects the short-arm dynamics. However, notable increase of long-arm relaxation time in SS-hPF simulations with SMOB turned off in asymmetric 3-arm star PS melts with significantly differing arm lengths such as $N_{\mathrm{arm},s} = 10$ and 20. This deviation decreases with increasing short-arm lengths, similar as for the diffusion coefficients. This again demonstrates that the short arms can indeed accelerate the relaxation of the long arms, in agreement with the idea of a hierarchical relaxation of branched polymers. The complete agreement of the relaxation times of long arms from SS-hPF simulations with SMOB algorithm and reference CG-MD simulations shows the good reproduction of reorientational dynamics in these arm lengths. The relaxation times of short arms such as $N_{\mathrm{arm},s} = 10$ and 20 in SS-hPF simulations with and without SMOB algorithm are clearly smaller than those from reference CG-MD simulations. This difference is similar to the deviations seen in the behavior of diffusion coefficients from reference CG-MD and SS-hPF models discussed in previous section.

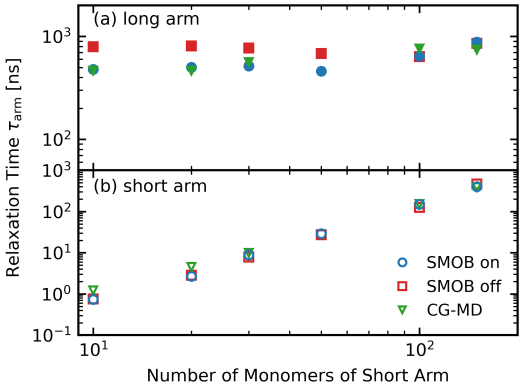

Figure 14: Arm relaxation times of short (hollow symbols) and long arms (filled symbols) from SS-hPF models with (blue) and without (red) slip-spring moving-over branch-point and reference CG-MD models (green) for 3-arm asymmetric star PS melts with short arm length ranging from $N_{\mathrm{arm},s} = 10$ to $N_{\mathrm{arm},s} = 150$ monomers. The long-arm length is $N_{\mathrm{arm},l} = 200$ for all systems.

Discussion and Conclusion

We have generalized the recently developed slip-spring hybrid particle-field (SS-hPF) simulation approach for linear entangled polymers[42,45] to be capable of modeling branched ones. We systematically evaluated the performance of this generalized model by validating the dynamical and structural properties of an example coarse-grained (CG) model of star PS melts in comparison with corresponding standard MD simulations and available experimental measurements. The particle-field treatment of non-bonded interactions preserves the chemistry-specific mapping of systematic coarse-graining procedures, here iterative Boltzmann Inversion. Its combination with the multi-chain slip-spring model, which explicitly mimics the entanglements between polymer chains, enables direct prediction of the dynamical properties of high-molecular-weight polymer melts in a wide range of time scales, e.g., from femtosecond (fs) to microsecond (μs). This integration of slip-springs with systematically coarse-grained polymer models makes the SS-hPF model different from most other slip-spring/link models.[31,32,35,36,74]

The SS-hPF Model of star-shaped PS melts essentially employs the parameterisation extracted from systems of linear PS melts. Due to the topological constraints of branch points, branched polymers diffuse and relax stresses through arm retraction rather than chain reptation. Therefore, two new slip-springs moves have been implemented into the original SS-hPF models to improve the prediction of polymer entangled dynamics around the branch point. The molecular dimensions, measured by the radius of gyration, of star PS melts from SS-hPF models are found to be intact in comparison with the reference coarse-grained and all-atom models, indicating topological transferability of the SS-hPF model for reproducing the structural properties of polymer melts. The polymer dynamics is characterised by means of diffusion coefficient, mean-square displacement and arm relaxations. Specifically, the arm-molecular-weight dependence of the diffusion coefficients of 4-arm symmetric star PS melts predicted by the generalized SS-hPF model is in good agreement with the theoretical prediction[60] and simulation results.[57,58] Moreover, after using a single scaling factor, the generalized SS-hPF model predicts the diffusion coefficients of both linear and star PS melts, which quantitatively agree with the experimental measurements.[61]

The dynamics of asymmetric star PS melts is also discussed, mainly focusing on the effect of allowing slip-spring transitions across the branch point (SMOB). We find that the short-arm length of asymmetric 3-arm star PS melts has a profound influence on both diffusive and reorientational dynamics, consistent with previous simulations.[38,39,75] More importantly, the SMOB mechanism is found to accelerate the dynamics of asymmetric 3-arm star PS melts with one significantly shorter arm. In contrast, it carries negligible effects on symmetric stars. Benefiting from the available CG-MD simulations, we notice that the friction coefficient parameterized from linear PS melts with $N = 100$ monomers is not sufficient to reproduce the dynamics of asymmetric stars with arm length $N_{\mathrm{arm}} < 100$ monomers. It is also possible to control the dynamics of asymmetric stars via regulating the possibility of a successful SMOB event if necessary in the future work. Thus, further refinements are required to build dynamically consistent CG models for branched polymers with short side

chains. Moreover, the hPF model is found to be transferable between linear and star-shaped polymers to predict the correct molecular dimensions compared with reference CG-MD and AA-MD models. The slip-spring model, using the same parameters extracted from the linear polymers, successfully recovers the entangled dynamics in star-shaped polymers with high-molecular-weight arms, demonstrating a good transferability of the slip-spring model from linear to 3- and 4-arm star-shaped polymers. It is noted that the slip-spring parameters may need careful examinations when modeling more complicated topological polymers such as comb and bottlebrush polymers[76] since the entanglement diameter/mesh size is found to be altered by side chains in these types of polymers.[6] We are currently able to establish chemistry-specific CG models for predicting dynamics of both linear and branched homopolymers via the SS-hPF model. It is promising for the SS-hPF approach to model the blends of linear and branched polymer for ,e.g., examination of the molecular picture of dynamic tube dilation process with detailed chemistry at the monomer level.[77–80]

Acknowledgement

We thank our partners in the ROBERTO consortium (Prof. Giuseppe Milano and Prof. Yuichi Masubuchi) for many fruitful discussions along the project. This research is funded by the Deutsche Forschungsgemeinschaft via the SFB-TRR 146 "Multiscale Simulation Methods for Soft Matter Systems", Project A8. Z. Wu is grateful to Jurek Schneider for many fruitful discussions and gratefully acknowledges the computing time granted on the supercomputer Mogon at Johannes Gutenberg University Mainz.

References

(1) De Gennes, P. Reptation of stars. *J. Phys. France* **1975**, *36*, 1199–1203.

(2) Ball, R. C.; McLeish, T. C. B. Dynamic dilution and the viscosity of star-polymer melts. *Macromolecules* **1989**, *22*, 1911–1913.

(3) Milner, S. T.; McLeish, T. C. B. Parameter-Free Theory for Stress Relaxation in Star Polymer Melts. *Macromolecules* **1997**, *30*, 2159–2166.

(4) Inkson, N. J.; Graham, R. S.; McLeish, T. C. B.; Groves, D. J.; Fernyhough, C. M. Viscoelasticity of Monodisperse Comb Polymer Melts. *Macromolecules* **2006**, *39*, 4217–4227.

(5) Liang, H.; Cao, Z.; Wang, Z.; Sheiko, S. S.; Dobrynin, A. V. Combs and Bottlebrushes in a Melt. *Macromolecules* **2017**, *50*, 3430–3437.

(6) Wijesinghe, S.; Perahia, D.; Grest, G. S. Polymer Topology Effects on Dynamics of Comb Polymer Melts. *Macromolecules* **2018**, *51*, 7621–7628.

(7) Paturej, J.; Sheiko, S. S.; Panyukov, S.; Rubinstein, M. Molecular structure of bottlebrush polymers in melts. *Sci. Adv.* **2016**, *2*, e1601478.

(8) Liang, H.; Morgan, B. J.; Xie, G.; Martinez, M. R.; Zhulina, E. B.; Matyjaszewski, K.; Sheiko, S. S.; Dobrynin, A. V. Universality of the Entanglement Plateau Modulus of Comb and Bottlebrush Polymer Melts. *Macromolecules* **2018**, *51*, 10028–10039.

(9) Liang, H.; Wang, Z.; Sheiko, S. S.; Dobrynin, A. V. Comb and Bottlebrush Graft Copolymers in a Melt. *Macromolecules* **2019**, *52*, 3942–3950.

(10) Pasquino, R. et al. Viscosity of Ring Polymer Melts. *ACS Macro Lett.* **2013**, *2*, 874–878.

(11) Lee, E.; Kim, S.; Jung, Y. Slowing Down of Ring Polymer Diffusion Caused by Inter-Ring Threading. *Macromol. Rapid Commun.* **2015**, *36*, 1115–1121.

(12) Parisi, D.; Costanzo, S.; Jeong, Y.; Ahn, J.; Chang, T.; Vlassopoulos, D.; Halverson, J. D.; Kremer, K.; Ge, T.; Rubinstein, M.; Grest, G. S.; Srinin, W.; Gros-

berg, A. Y. Nonlinear Shear Rheology of Entangled Polymer Rings. *Macromolecules* **2021**, *54*, 2811–2827.

(13) Doi, M.; Kuzuu, N. Y. Rheology of star polymers in concentrated solutions and melts. *J. Polym. Sci. B Polym. Lett. Ed.* **1980**, *18*, 775–780.

(14) Pearson, D. S.; Helfand, E. Viscoelastic properties of star-shaped polymers. *Macromolecules* **1984**, *17*, 888–895.

(15) van Ruymbeke, E.; Keunings, R.; Bailly, C. Prediction of linear viscoelastic properties for polydisperse mixtures of entangled star and linear polymers: Modified tube-based model and comparison with experimental results. *J. Nonnewton Fluid Mech.* **2005**, *128*, 7–22.

(16) Das, C.; Inkson, N. J.; Read, D. J.; Kelmanson, M. A.; McLeish, T. C. B. Computational linear rheology of general branch-on-branch polymers. *J. Rheol.* **2006**, *50*, 207–234.

(17) Wang, Z.; Chen, X.; Larson, R. G. Comparing tube models for predicting the linear rheology of branched polymer melts. *J. Rheol.* **2010**, *54*, 223–260.

(18) Reith, D.; Pütz, M.; Müller-Plathe, F. Deriving effective mesoscale potentials from atomistic simulations: Mesoscale Potentials from Atomistic Simulations. *J. Comput. Chem.* **2003**, *24*, 1624–1636.

(19) Soper, A. Empirical potential Monte Carlo simulation of fluid structure. *Chem. Phys.* **1996**, *202*, 295–306.

(20) Noid, W. G.; Chu, J.-W.; Ayton, G. S.; Krishna, V.; Izvekov, S.; Voth, G. A.; Das, A.; Andersen, H. C. The multiscale coarse-graining method. I. A rigorous bridge between atomistic and coarse-grained models. *J. Chem. Phys.* **2008**, *128*, 244114.

(21) Marrink, S. J.; Risselada, H. J.; Yefimov, S.; Tieleman, D. P.; de Vries, A. H. The

MARTINI Force Field: Coarse Grained Model for Biomolecular Simulations. *J. Phys. Chem. B* **2007**, *111*, 7812–7824.

(22) Souza, P. C. T. Martini 3: a general purpose force field for coarse-grained molecular dynamics. *Nature Methods* **2021**, *18*, 11.

(23) Papaioannou, V.; Lafitte, T.; Avendaño, C.; Adjiman, C. S.; Jackson, G.; Müller, E. A.; Galindo, A. Group contribution methodology based on the statistical associating fluid theory for heteronuclear molecules formed from Mie segments. *J. Chem. Phys.* **2014**, *140*, 054107.

(24) Rahman, S.; Lobanova, O.; Jiménez-Serratos, G.; Braga, C.; Raptis, V.; Müller, E. A.; Jackson, G.; Avendaño, C.; Galindo, A. SAFT- Force Field for the Simulation of Molecular Fluids. 5. Hetero-Group Coarse-Grained Models of Linear Alkanes and the Importance of Intramolecular Interactions. *J. Phys. Chem. B* **2018**, *122*, 9161–9177.

(25) Padding, J. T.; Briels, W. J. Systematic coarse-graining of the dynamics of entangled polymer melts: the road from chemistry to rheology. *J. Phys.: Condens. Matter* **2011**, *23*, 233101.

(26) Groot, R. D.; Warren, P. B. Dissipative particle dynamics: Bridging the gap between atomistic and mesoscopic simulation. *J. Chem. Phys.* **1997**, *107*, 4423–4435.

(27) Padding, J. T.; Briels, W. J. Time and length scales of polymer melts studied by coarse-grained molecular dynamics simulations. *J. Chem. Phys.* **2002**, *117*, 925–943.

(28) Liu, L.; den Otter, W. K.; Briels, W. J. Coarse-Grained Simulations of Three-Armed Star Polymer Melts and Comparison with Linear Chains. *J. Phys. Chem. B* **2018**, *122*, 10210–10218.

(29) Sirk, T. W.; Slizoberg, Y. R.; Brennan, J. K.; Lisal, M.; Andzelm, J. W. An enhanced

entangled polymer model for dissipative particle dynamics. *J. Chem. Phys.* **2012**, *136*, 134903.

(30) Iwaoka, N.; Hagita, K.; Takano, H. Multipoint segmental repulsive potential for entangled polymer simulations with dissipative particle dynamics. *J. Chem. Phys.* **2018**, *149*, 114901.

(31) Likhtman, A. E. Single-Chain Slip-Link Model of Entangled Polymers: Simultaneous Description of Neutron SpinEcho, Rheology, and Diffusion. *Macromolecules* **2005**, *38*, 6128–6139.

(32) Chappa, V. C.; Morse, D. C.; Zippelius, A.; Müller, M. Translationally Invariant Slip-Spring Model for Entangled Polymer Dynamics. *Phys. Rev. Lett.* **2012**, *109*, 148302.

(33) Andreev, M.; Khaliullin, R. N.; Steenbakkers, R. J. A.; Schieber, J. D. Approximations of the discrete slip-link model and their effect on nonlinear rheology predictions. *J. Rheol.* **2013**, *57*, 535–557.

(34) Langeloth, M.; Masubuchi, Y.; Böhm, M. C.; Müller-Plathe, F. Recovering the reptation dynamics of polymer melts in dissipative particle dynamics simulations via slip-springs. *J. Chem. Phys.* **2013**, *138*, 104907.

(35) Shanbhag, S.; Larson, R. G. A Slip-Link Model of Branch-Point Motion in Entangled Polymers. *Macromolecules* **2004**, *37*, 8160–8166.

(36) Masubuchi, Y.; Ianniruberto, G.; Greco, F.; Marrucci, G. Primitive chain network simulations for branched polymers. *Rheol. Acta* **2006**, *46*, 297–303.

(37) Masubuchi, Y.; Yaoita, T.; Matsumiya, Y.; Watanabe, H. Primitive chain network simulations for asymmetric star polymers. *J. Chem. Phys.* **2011**, *134*, 194905.

(38) Zhu, J.; Likhtman, A. E.; Wang, Z. Arm retraction dynamics of entangled star polymers: A forward flux sampling method study. *J. Chem. Phys.* **2017**, *147*, 044907.

(39) Masubuchi, Y. Multichain Slip-Spring Simulations for Branch Polymers. *Macromolecules* **2018**, *51*, 10184–10193.

(40) Vogiatzis, G. G.; Megariotis, G.; Theodorou, D. N. Equation of State Based Slip Spring Model for Entangled Polymer Dynamics. *Macromolecules* **2017**, *50*, 3004–3029.

(41) Sgouros, A. P.; Megariotis, G.; Theodorou, D. N. Slip-Spring Model for the Linear and Nonlinear Viscoelastic Properties of Molten Polyethylene Derived from Atomistic Simulations. *Macromolecules* **2017**, *50*, 4524–4541.

(42) Wu, Z.; Milano, G.; Müller-Plathe, F. Combination of Hybrid Particle-Field Molecular Dynamics and Slip-Springs for the Efficient Simulation of Coarse-Grained Polymer Models: Static and Dynamic Properties of Polystyrene Melts. *J. Chem. Theory Comput.* **2021**, *17*, 474–487.

(43) Becerra, D.; Córdoba, A.; Katzarova, M.; Andreev, M.; Venerus, D. C.; Schieber, J. D. Polymer rheology predictions from first principles using the slip-link model. *J. Rheol.* **2020**, *64*, 1035–1043.

(44) Behbahani, A. F.; Schneider, L.; Rissanou, A.; Chazirakis, A.; Bačová, P.; Jana, P. K.; Li, W.; Doxastakis, M.; Polińska, P.; Burkhart, C.; Müller, M.; Harmandaris, V. A. Dynamics and Rheology of Polymer Melts via Hierarchical Atomistic, Coarse-Grained, and Slip-Spring Simulations. *Macromolecules* **2021**, *54*, 2740–2762.

(45) Wu, Z.; Kalogirou, A.; De Nicola, A.; Milano, G.; Müller-Plathe, F. Atomistic hybrid particle-field molecular dynamics combined with: Restoring entangled dynamics to simulations of polymer melts. *J. Comput. Chem.* **2021**, *42*, 6–18.

(46) Milano, G.; Kawakatsu, T. Hybrid particle-field molecular dynamics simulations for dense polymer systems. *J. Chem. Phys.* **2009**, *130*, 214106.

(47) Zhao, Y.; Nicola, A. D.; Kawakatsu, T.; Milano, G. Hybrid particle-field molecular dynamics simulations: Parallelization and benchmarks. *J. Comput. Chem.* **2012**, *33*, 868–880.

(48) Humphrey, W.; Dalke, A.; Schulten, K. VMD – Visual Molecular Dynamics. 1996.

(49) Qian, H.-J.; Carbone, P.; Chen, X.; Karimi-Varzaneh, H. A.; Liew, C. C.; Müller-Plathe, F. Temperature-Transferable Coarse-Grained Potentials for Ethylbenzene, Polystyrene, and Their Mixtures. *Macromolecules* **2008**, *41*, 9919–9929.

(50) De Nicola, A.; Kawakatsu, T.; Milano, G. Generation of Well-Relaxed All-Atom Models of Large Molecular Weight Polymer Melts: A Hybrid Particle-Continuum Approach Based on Particle-Field Molecular Dynamics Simulations. *J. Chem. Theory Comput.* **2014**, *10*, 5651–5667.

(51) De Nicola, A.; Kawakatsu, T.; Müller-Plathe, F.; Milano, G. Fast relaxation of coarse-grained models of polymer interphases by hybrid particle-field molecular dynamics: Polystyrene-silica nanocomposites as an example. *Eur. Phys. J. Spec. Top.* **2016**, *225*, 1817–1841.

(52) Qian, H.-J.; Liew, C. C.; Müller-Plathe, F. Effective control of the transport coefficients of a coarse-grained liquid and polymer models using the dissipative particle dynamics and Lowe–Andersen equations of motion. *Phys. Chem. Chem. Phys.* **2009**, *11*, 1962.

(53) Tzoumanekas, C.; Theodorou, D. N. Topological Analysis of Linear Polymer Melts: A Statistical Approach. *Macromolecules* **2006**, *39*, 4592–4604.

(54) McLeish, T. C. B. Hierarchical Relaxation in Tube Models of Branched Polymers. *Europhys. Lett.* **1988**, *6*, 511–516.

(55) Spyriouni, T.; Tzoumanekas, C.; Theodorou, D.; Müller-Plathe, F.; Milano, G. Coarse-Grained and Reverse-Mapped United-Atom Simulations of Long-Chain Atactic

Polystyrene Melts: Structure, Thermodynamic Properties, Chain Conformation, and Entanglements. *Macromolecules* **2007**, *40*, 3876–3885.

(56) Gkolfi, E.; Bačová, P.; Harmandaris, V. Size and Shape Characteristics of Polystyrene and Poly(ethylene oxide) Star Polymer Melts Studied By Atomistic Simulations. *Macromol. Theory Simul.* **2021**, *30*, 2000067.

(57) Chremos, A.; Douglas, J. F. Influence of Branching on the Configurational and Dynamical Properties of Entangled Polymer Melts. *Polymers* **2019**, *11*, 1045.

(58) Xu, X.; Chen, J.; An, L. Simulation studies on architecture dependence of unentangled polymer melts. *J. Chem. Phys.* **2015**, *142*, 074903.

(59) de Gennes, P. G.; Leger, L. Dynamics of Entangled Polymer Chains. *Annu. Rev. Phys. Chem.* **1982**, *33*, 49–61.

(60) Frischknecht, A. L.; Milner, S. T. Self-Diffusion with Dynamic Dilution in Star Polymer Melts. *Macromolecules* **2000**, *33*, 9764–9768.

(61) Clarke, N.; Colley, F. R.; Collins, S. A.; Hutchings, L. R.; Thompson, R. L. Self-Diffusion and Viscoelastic Measurements of Polystyrene Star Polymers. *Macromolecules* **2006**, *39*, 1290–1296.

(62) Wang, Z.; Likhtman, A. E.; Larson, R. G. Segmental Dynamics in Entangled Linear Polymer Melts. *Macromolecules* **2012**, *45*, 3557–3570.

(63) Colley, F. R.; Collins, S. A.; Richards, R. W. Tracer diffusion of four arm polystyrene star molecules into linear and star polymer matrices from nuclear reaction analysis. *J. Mater. Chem.* **2003**, *13*, 2765–2770.

(64) Fleischer, G. Temperature dependence of self diffusion of polystyrene and polyethylene in the melt an interpretation in terms of the free volume theory. *Polymer Bulletin* **1984**, *11*, 75–80.

(65) Bachus, R.; Kimmich, R. Molecular weight and temperature dependence of self-diffusion coefficients in polyethylene and polystyrene melts investigated using a modified n.m.r. field-gradient technique. *Polymer* **1983**, *24*, 964–970.

(66) Doi, M.; Edwards, S. F. *The theory of polymer dynamics*; Clarendon Press: Oxford, 2007.

(67) Stephanou, P. S.; Baig, C.; Tsolou, G.; Mavrantzas, V. G.; Kröger, M. Quantifying chain reptation in entangled polymer melts: Topological and dynamical mapping of atomistic simulation results onto the tube model. *J. Chem. Phys.* **2010**, *132*, 124904.

(68) Holler, S.; Moreno, A. J.; Zamponi, M.; Bačová, P.; Willner, L.; Iatrou, H.; Falus, P.; Richter, D. The Role of the Functionality in the Branch Point Motion in Symmetric Star Polymers: A Combined Study by Simulations and Neutron Spin Echo Spectroscopy. *Macromolecules* **2018**, *51*, 242–253.

(69) Bačová, P.; Hawke, L. G. D.; Read, D. J.; Moreno, A. J. Dynamics of Branched Polymers: A Combined Study by Molecular Dynamics Simulations and Tube Theory. *Macromolecules* **2013**, *46*, 4633–4650.

(70) Milner, S. T.; McLeish, T. C. B. Arm-Length Dependence of Stress Relaxation in Star Polymer Melts. *Macromolecules* **1998**, *31*, 7479–7482.

(71) Everaers, R. Topological versus rheological entanglement length in primitive-path analysis protocols, tube models, and slip-link models. *Phys. Rev. E* **2012**, *86*, 022801.

(72) Zhu, J. Multiscale Computer Simulation Studies of Entangled Branched Polymers. **2017**, PhD thesis, University of Reading.

(73) Harmandaris, V. A.; Kremer, K. Dynamics of Polystyrene Melts through Hierarchical Multiscale Simulations. *Macromolecules* **2009**, *42*, 791–802.

(74) Uneyama, T.; Masubuchi, Y. Multi-chain slip-spring model for entangled polymer dynamics. *J. Chem. Phys.* **2012**, *137*, 154902.

(75) Zhou, Q.; Larson, R. G. Direct Molecular Dynamics Simulation of Branch Point Motion in Asymmetric Star Polymer Melts. *Macromolecules* **2007**, *40*, 3443–3449.

(76) Abbasi, M.; Faust, L.; Wilhelm, M. Comb and Bottlebrush Polymers with Superior Rheological and Mechanical Properties. *Adv. Mater.* **2019**, *31*, 1806484.

(77) Watanabe, H.; Yoshida, H.; Kotaka, T. Viscoelastic relaxation of a linear chain in star matrixes: examination of the constraint release mechanism in star matrixes. *Macromolecules* **1992**, *25*, 2442–2446.

(78) Shivokhin, M. E.; van Ruymbeke, E.; Bailly, C.; Kouloumasis, D.; Hadjichristidis, N.; Likhtman, A. E. Understanding Constraint Release in Star/Linear Polymer Blends. *Macromolecules* **2014**, *47*, 2451–2463.

(79) Desai, P. S.; Kang, B.-G.; Katzarova, M.; Hall, R.; Huang, Q.; Lee, S.; Shivokhin, M.; Chang, T.; Venerus, D. C.; Mays, J.; Schieber, J. D.; Larson, R. G. Challenging Tube and Slip-Link Models: Predicting the Linear Rheology of Blends of Well-Characterized Star and Linear 1,4-Polybutadienes. *Macromolecules* **2016**, *49*, 4964–4977.

(80) Malo de Molina, P.; Alegría, A.; Allgaier, J.; Kruteva, M.; Hoffmann, I.; Prévost, S.; Monkenbusch, M.; Richter, D.; Arbe, A.; Colmenero, J. Tube Dilation in Isofrictional Polymer Blends Based on Polyisoprene with Different Topologies: Combination of Dielectric and Rheological Spectroscopy, Pulsed-Field-Gradient NMR, and Neutron Spin Echo (NSE) Techniques. *Macromolecules* **2020**, *53*, 5919–5936.

Supporting Information: Slip-Spring Hybrid Particle-Field Model for Coarse-Graining Branched Polymer Melts: Polystyrene Melts as An Example

Zhenghao Wu and Florian Müller-Plathe*

Eduard-Zintl-Institut für Anorganische und Physikalische Chemie, Technische Universität Darmstadt, Alarich-Weiss-Str. 8, 64287 Darmstadt, Germany

E-mail: f.mueller-plathe@theo.chemie.tu-darmstadt.de

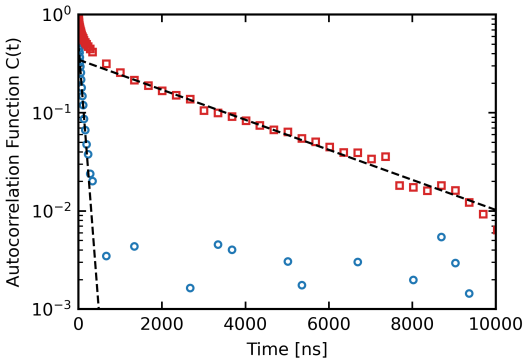

Figure S1: Exponential fits (dashed lines) to the autocorrelation functions of end-to-end vectors from branch-point to arm end for simulations of star polystyrene melts with arm length $N_{\mathrm{arm}} = 100$ (blue) and $N_{\mathrm{arm}} = 250$ (red).

Determine WLF Shift Factor

We employ the WLF equation to determine the shift factor for the diffusion coefficients at temperature $T = 500$ K.

$$\log(a_{\mathrm{T}}) = \frac{-C_1(T - T_{\mathrm{ref}})}{C_2 + (T - T_{\mathrm{ref}})} \tag{1}$$

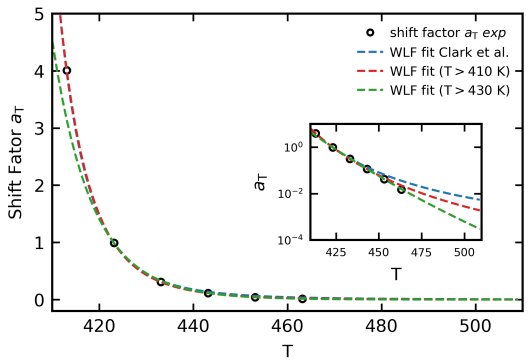

Figure S2: Shift factors as a function of temperature from viscosity measurements (black symbols) scaled using WLF equation with a reference temperature 423 K. The blue line is a fit of Equation 1 with $C_1 = 4.5$ and $C_2 = 84.7$ from the reference.[1] The red line is a fit of Equation 1 to the data extracted from reference[1] with $C_1 = 6.37$ and $C_2 = 115.04$. The green line is a fit of Equation 1 to the data extracted from reference[1] when T> 430 K with $C_1 = 21.86$ and $C_2 = 446.80$.

Tube Survival Probability Function

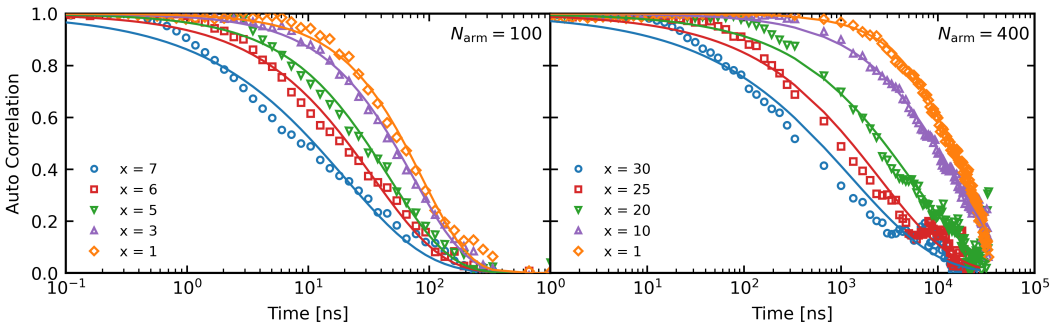

Figure S3: Tube survival probability functions for example systems: 4-arm symmetric stars with $N_{arm} = 100$ and $N_{arm} = 400$ from SS-hPF simulations. The symbols represent the simulation results and the lines are the KWW fits.

Analytical Expression of Tube Survival Probability

In the model of Mcleish and coworkers,[2,3] two time regimes are considered to derive the characteristic relaxation time of the whole arm. In the early-time regime $\tau_{early} < \tau_R$, the arm free end does not yet feel the effect from the branch point, and its motion is governed by the Rouse dynamics down the tube. The relaxation time at the early time $\tau_{early}(s)$ is successfully calculated via the mean-square displacement of the arm end, expressed by:[2]

$$\tau_{early}(s) = 225\pi^3/256\tau_e(N_{arm}/N_e)^4(1-s)^4 \tag{2}$$

where τ_e and N_e are the entanglement time and length, respectively, for the polymer chemistry under study. At later times, the arm retraction is activated. In this dynamical mode, arm free end is considered as a random walker in an effective potential U_{eff}, given by:

$$U_{eff}(s) = \frac{15N_{arm}}{4N_e}\frac{1-s^{1+a}[1+(1+a)(1-s)]}{(1+a)(2+a)} \tag{3}$$

where a is the scaling exponent, arguably chosen as 1 or 4/3.[2] Now, the relaxation time $\tau_{\text{late}}(s)$ at later times or deeper arm retration can be computed via solving the first-passage problem for the free end of a star arm diffusing in an effective potential field U_{eff} in the range between $s = s'$ and $s = 1$ (branch point). After the detailed derivation with some approximations, the relaxation time $\tau_{\text{late}}(s)$ is found to be:

$$\tau_{\text{late}}(s) \approx \tau_e(\frac{N}{N_e})^{3/2}(\frac{\pi^5}{30})^{1/2} \times \frac{\exp(U_{\text{eff}}(s))}{(1-s)\left[s^{2a} + \left(\left(\frac{4N_e}{15N}\right)(1+a)\right)^{2a/(a+1)} \Gamma\left(\frac{1}{a+1}\right)^{-2}\right]^{1/2}} \quad (4)$$

Where Γ denotes the Gamma function. The final solution is obtained via the combination of these two relaxation modes, namely, Rouse-like and activated arm retraction relaxations, giving a crossover formula:

$$\tau(s) \approx \frac{\tau_{\text{early}}(s)\exp[U_{\text{eff}}(s)]}{1 + \exp[U_{\text{eff}}(s)]\tau_{\text{early}}(s)/\tau_{\text{late}}(s)} \quad (5)$$

and the total tube survival probability can be computed from the integral over the starting and final positions:[4]

$$\Psi(t) = \int_0^1 \exp(-(t/\tau(s)))ds \quad (6)$$

The input parameters to derive the tube survival probability basically include the entanglement length N_e, arm length N_{arm} and the entanglement time τ_e. These values can be easily determined from our SS-hPF simulations such as $\tau_e \approx 25$ ns from the segmental mean-square displacements. It is noted that the entanglement length N_e can be determined by various methods in molecular dynamics simulations. The entanglement length N_e employed in the original theoretical work is related to the one determined normally by experiments, e.g., the rheological measurement (N_e^{rheo}). The entanglement length $N_e = 127$ monomers for the CG-PS models mentioned in the main text is measured by the topological numerical method[5] (N_e^{topo}). As discussed in reference,[6] the value of N_e^{topo} is commonly half of the value of N_e^{rheo}, thus we input $N_e \approx 65$ to the theoretical model described above.

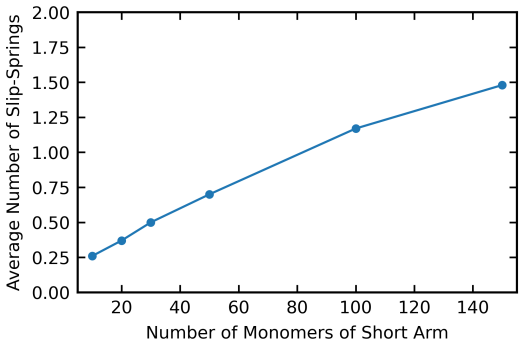

Figure S4: Average number of slip-springs for a short arm of a polystyrene asymmetric 3-arm star as a function of number of monomers of the short arm. The arm length of another two long arms is $N_{\mathrm{arm},l} = 200$.

References

(1) Clarke, N.; Colley, F. R.; Collins, S. A.; Hutchings, L. R.; Thompson, R. L. Self-Diffusion and Viscoelastic Measurements of Polystyrene Star Polymers. *Macromolecules* **2006**, *39*, 1290–1296.

(2) Milner, S. T.; McLeish, T. C. B. Parameter-Free Theory for Stress Relaxation in Star Polymer Melts. *Macromolecules* **1997**, *30*, 2159–2166.

(3) Milner, S. T.; McLeish, T. C. B. Arm-Length Dependence of Stress Relaxation in Star Polymer Melts. *Macromolecules* **1998**, *31*, 7479–7482.

(4) McLeish, T. C. B. Tube theory of entangled polymer dynamics. *Advances in Physics* **2002**, *51*, 1379–1527.

(5) Spyriouni, T.; Tzoumanekas, C.; Theodorou, D.; Müller-Plathe, F.; Milano, G. Coarse-Grained and Reverse-Mapped United-Atom Simulations of Long-Chain Atactic Polystyrene Melts: Structure, Thermodynamic Properties, Chain Conformation, and Entanglements. *Macromolecules* **2007**, *40*, 3876–3885.

(6) Everaers, R. Topological versus rheological entanglement length in primitive-path analysis protocols, tube models, and slip-link models. *Phys. Rev. E* **2012**, *86*, 022801.

3.4 Knotting Behaviour of Polymer Chains in the Melt State for Soft-Core Models with and without Slip-Springs

Both first authors contributed equally to this work with their different expertise. The knotting behavior of two different soft-core models, slip-spring hPF-MD and slip-spring dissipative particle dynamics, is compared. Zhenghao Wu and Simon Alberti contributed SS-hPF and SS-DPD results, respectively. A separation of this paper into two would have made no sense.

OPEN ACCESS
IOP Publishing
Journal of Physics: Condensed Matter
J. Phys.: Condens. Matter **33** (2021) 244001 (11pp)
https://doi.org/10.1088/1361-648X/abef25

Knotting behaviour of polymer chains in the melt state for soft-core models with and without slip-springs

Zhenghao Wu[1], Simon A N Alberti[1], Jurek Schneider and Florian Müller-Plathe[*]

Technical University of Darmstadt, Eduard-Zintl-Institute for Inorganic and Physical Chemistry and Profile Area Thermofluids and Interfaces, Alarich-Weiss-Strasse 8, D-64287 Darmstadt, Germany

E-mail: f.mueller-plathe@theo.chemie.tu-darmstadt.de

Received 13 November 2020, revised 9 January 2021
Accepted for publication 16 March 2021
Published 13 May 2021

Abstract

We analyse the knotting behaviour of linear polymer melts in two types of soft-core models, namely dissipative-particle dynamics and hybrid-particle-field models, as well as their variants with slip-springs which are added to recover entangled polymer dynamics. The probability to form knots is found drastically higher in the hybrid-particle-field model compared to its parent hard-core molecular dynamics model. By comparing the knottedness in dissipative-particle dynamics and hybrid-particle-field models with and without slip-springs, we find the impact of slip-springs on the knotting properties to be negligible. As a dynamic property, we measure the characteristic time of knot formation and destruction, and find it to be (i) of the same order as single-monomer motion and (ii) independent of the chain length in all soft-core models. Knots are therefore formed and destroyed predominantly by the unphysical chain crossing. This work demonstrates that the addition of slip-springs does not alter the knotting behaviour, and it provides a general understanding of knotted structures in these two soft-core models of polymer melts.

Keywords: polymer knotting, slip-spring, molecular modelling

Supplementary material for this article is available online

(Some figures may appear in colour only in the online journal)

1. Introduction

There has been a considerable activity in the development and use of soft-core polymer models, i.e., models where the non-bonded interactions between monomers do not approach a singularity at short intermonomer distances, but assume a finite value. The value is low enough, say of the order of 10 k_BT (k_B being Boltzmann's constant), so that it does not even present 'practical infinity' in a simulation. Such models are engineered to reproduce static structural and thermodynamic properties of hard-core excluded-volume models as well as possible, with little attention given so far to their ability or disability to capture the propensity for polymer chains to form knots. As a consequence of the soft interactions, however, monomers can (infrequently) pass through each other, which leads to a qualitatively incorrect polymer dynamics. Polymer chains do not entangle, regardless of their length, they are not forced to reptate around each other, and each one moves like a chain in a solvent, not like a chain in a polymer melt. We have employed two different classes of such soft-core models. The first is

[1] Z Wu and S A N Alberti contributed equally to this work.

[*] Author to whom any correspondence should be addressed.

dissipative-particle dynamics (DPD) [1], a very coarse-grained particle model with one bead representing a substantial fraction of a real polymer chain. The second is hybrid-particle-field molecular dynamics (hPF-MD) [2], whose base particle model can be of arbitrary resolution from atomistic to low-resolution coarse-grained. It treats, however, the nonbonded interactions not pairwise but mediated by a density field. This necessarily leads to them becoming effectively soft-core. Both methods are introduced in more detail below.

To re-introduce qualitatively correct polymer dynamics, we have augmented both DPD and hybrid-particle-field (hPF) by so-called slip-springs [3, 4]. These are temporary bonds between normally nonbonded beads, which migrate along polymer chains, disappear and reappear according to their own dynamics. We and others have shown that they can very effectively mimic the effects of excluded-volume interactions, chain-noncrossability and entanglements, and that they restore reptation dynamics to the soft-core models of polymer melts [5–10]. At the same time, it has been shown that the introduction of slip-springs does not alter the polymer structure. Descriptors on the monomer scale [radial distribution function (RDF)], the chain scale (radius of gyration) and bulk scale (density) are identical to within the error bars between soft-core models with and without slip-springs, for the case of polymer melts. (For polymers in solution, there is a small, predictable and well-understood contraction of the radius of gyration [11].) In contrast, there is a structural difference at the monomer scale, e.g. in the RDF, between a soft-core model and its parent hard-core model. (In the case of hPF, for example, both models are available.) Predictably, the field description allows a closer approach or even overlap of particles [12]. On larger scale structures, however, hPF and the hard-core model agree [13].

It is the purpose of the present contribution to compare our models in terms of their knot structure, which is yet another descriptor, whose scale is on the order of the chain size. In a melt of long-enough polymer chains, some will invariably contain knots [14]. The average number of knots and their topologies depend on chain length, chain stiffness [15] but also on chain-crossability, i.e. hard-core vs soft-core description [16]. In particular, it is possible that models, which produce otherwise identical polymer structures, differ in the number of knots. Similarly, there is the possibility for the models to differ in the speed of knot formation and destruction, as different mechanisms may prevail. We therefore investigate the knotting/unknotting dynamics via a correlation-function analysis.

We are in a position to compare the same polymer melts at different levels of modelling. For the hPF-series, we have the (i) parent hard-core MD model, the (ii) soft-core hPF description derived from it, and the (iii) hPF description with slip-springs added. We can therefore not only compare knotting differences between hard and soft core (i) and (ii). We can also study, whether the slip-spring emulation of entangled dynamics leads to a change of knottedness (compare (ii) and (iii)). The latter comparison can also be made for our DPD models without and with slip-springs (there is no parent hard-core model for DPD, since it is a top–down multiscale approach). We keep the analysis simple and restrict it to the simplest and most common knot topology, mathematically denoted as 3_1 knot, known to sailors as overhand knot [17]. This knot involves only a single polymer chain, i.e. it does not tie two chains together. We want to know the probabilities of our models to contain knots and, thus, supplement their structural characterization. We do not wish, however, to dive into a full analysis of more complicated knots. This is all the more justified, as there is little evidence for the knottedness of a polymer melt influencing its more practical properties, such as mechanical or rheological. This is probably associated with the synthetic challenge to experimentally prepare and characterize polymers with a defined knot structure.

2. Methods and model

2.1. Hybrid-particle-field molecular dynamics

The hPF-MD approach and its applications to atomistic and coarse-grained (bio)macromolecular systems have been extensively presented in previous publications [2, 12, 13, 18–25]. Here, we briefly recall the main ideas. In hPF-MD, the intramolecular interactions (bond, angle…) are the same as the standard molecular dynamics (MD) simulations, while pairwise interactions between nonbonded particles in standard MD simulations are transformed into an interaction of a particle with an external potential depending on the density field. For a system composed of two different types of particles, the potential energy in the density field is

$$W[\rho(r)] = \frac{1}{\rho_0}\int \mathrm{d}r \left(\frac{k_\mathrm{B}T}{2}\sum_{i,j}\chi_{ij}\rho_i(r)\rho_j(r) + \frac{1}{2\kappa}\left(\sum_i \rho_i(r) - \rho_0\right)^2 \right). \quad (1)$$

By applying the saddle point approximation, it is possible to obtain the mean-field external potential $V_i^{\mathrm{field}}(r)$ acting on an individual particle (type i) at position r from the functional derivative of the potential energy $W[\rho(r)]$ with respect to the local density:

$$V_i^{\mathrm{field}}(r) = \frac{\delta W[\rho(r)]}{\delta \rho_i(r)} = \frac{1}{\rho_0}\left(k_\mathrm{B}T\sum_j \chi_{ij}(r)\rho_j(r) + \frac{1}{\kappa}\left(\sum_i \rho_i(r) - \rho_0\right)\right). \quad (2)$$

Here, the Flory–Huggins parameter χ_{ij} represents the strength of the mean field interaction between particles of type i and j, ρ_0 is the average number density of the system, κ is the compressibility factor for the system, and ρ_i and ρ_j are number densities of particles of type i and j in the density field at position r, respectively. The forces acting on particles are computed by interpolating the gradients of the external potential on spatial grids. More details about the implementation of density fields and its force calculations in MD simulations can

Table 1. Simulation details of MD simulations with regular hard-core pairwise interactions, hPF simulations without slip-springs and with slip-springs (SSPF). N, M, l and N_{SS} are the number of monomers per chain, the number of chains in the system, the length of the cubic simulation box and the total number of slip-springs in SSPF simulations, respectively.

System code	N	M	l (nm)	N_{SS}
MD-100	100	300	17.48	
MD-200	200	150	17.48	
MD-400	400	75	17.48	
MD-600	600	50	17.48	
MD-750	750	40	17.48	
hPF-100	100	300	17.48	
hPF-200	200	150	17.48	
hPF-400	400	75	17.48	
hPF-600	600	50	17.48	
hPF-750	750	40	17.48	
hPF-1000	1000	30	17.48	
SSPF-100	100	300	17.48	86
SSPF-200	200	150	17.48	161
SSPF-400	400	75	17.48	199
SSPF-600	600	50	17.48	211
SSPF-750	750	40	17.48	216

be found in references [2, 22, 26]. Replacing hard-core nonbonded pair interaction by the interaction with a field on a lattice turns MD into an $O(N)$ algorithm, but also makes the nonbonded interactions necessarily soft-core. Polymer chains are thus able to cross each other and fail to show entangled dynamics such as reptation [27]. To remedy this shortcoming, we recently employed slip-springs in hPF-MD simulations of polymer melts, which successfully restored their entangled dynamics [7].

We study a model system of polystyrene melts, which has been introduced in previous publications [12, 13, 21]. The coarse-grained force field of polystyrene melts was originally developed by Qian and co-workers [28]. In this model, two different bead types (R and S) are defined to reproduce the tacticity of the polymer chain with the bead placed at the centre of mass of the repeating unit. Coarse-grained atactic polystyrene chains are created by randomly generating the sequence of R and S beads. Specifically, by using the iterative Boltzmann inversion method [29] to retain probability distribution functions of their all-atom counterparts, coarse-grained bond interactions, namely bonds, angles and dihedral angles, are derived. The coarse-grained nonbonded interactions are computed through the density-functional field, whose update time interval is $\Delta t_{\text{field}} = 1$ hPF-MD time step. In this density-functional field, the grid spacing is chosen as 0.55 nm, comparable to the average bond length between connected coarse-grained beads. The latter is $l \approx 0.52$ nm for both standard MD and hPF simulations. The Flory–Huggins parameter χ is 0 for a homogeneous polymer melt. To probe the effect of different incompressibility conditions, two incompressibility parameters $\kappa = 0.1$ and 0.05 mol $\times$ kJ^{-1} are employed. Their influence on the monomer diameter is derived from the potential of mean force (PMF) between monomers. Specifically, the PMF is computed by Boltzmann inversion of the intermolecular RDF, and the monomer diameter is identified as the length where it equals 0. This definition can be applied in the same way to both MD with pairwise interactions and to hPF. The resulting monomer diameters for MD and the two hPF models with $\kappa = 0.05$ and $\kappa = 0.1$ are 1.01 nm, 1.24 nm, and 1.27 nm, respectively. All details of the simulated systems such as the number of chains, chain length, box sizes and the total number of slip-springs in hPF simulations (if present at all) are listed in table 1.

All simulations are performed using GPU-accelerated large-scale molecular simulation toolkit (GALAMOST [26]) package with our version of the slip-spring model. The initial configurations are obtained from the reference MD simulations after their density is converged at a temperature of $T = 500$ K. The equilibration of the hPF systems is achieved by utilizing the fast equilibration procedure reported previously [12]. Specifically, we perform a pure hPF simulation to pre-equilibrate the system up to 4×10^8 steps, with the grid spacing slowly decreasing from $l_{\text{grid}} \approx 1$ nm to $l_{\text{grid}} \approx 0.55$ nm. The mean squared internal distance is tracked throughout the equilibration step to ensure a complete equilibration [30]. Data are then collected from production simulations continued from these equilibrated systems with $l_{\text{grid}} \approx 0.55$ nm. Both hPF simulations with and without slip-springs are run in an NVT ensemble using a Langevin thermostat with a frictional coefficient of 226 g $\times$ mol^{-1} $\times$ ps^{-1}.

Slip-springs are modelled by employing a soft Lennard-Jones potential with its parameters mapped to the corresponding hard-core MD systems. The slip-spring bond length follows a Gaussian distribution, whose mean value is close to half of the tube diameter of polystyrene melts $\langle l_{\text{ss}} \rangle = \frac{1}{2} d_{\text{T}} \approx 3.75$ nm [31]. It should be noted here that the slip-spring bond length in hPF models is longer than that employed in DPD models compared to the respective bead sizes. Slip-spring motion is governed by a Monte Carlo (MC) algorithm. In our example CG-PS systems, the MC motion of slip-springs is activated every $\Delta t_{\text{MC}} = 100$ hPF time steps (3 ps). This is close to the relaxation time of a single monomer, which we estimated as the transition time of the monomer's mean squared displacement $g_1(t)$ from ballistic ($g_1(t) \sim t^2$) to Rouse motion ($g_1(t) \sim t^{0.5}$). The mobility of slip-springs is controlled by a hopping frequency v_{hop}, which is a control parameter determined by matching corresponding experimental or MD simulation data. In the present model, comparison with MD diffusion coefficients yielded $v_{\text{hop}} = 1.25 \times 10^{-4}$ ps^{-1}. We note that this implementation of a hopping-frequency-controlled migration is slightly different from our original slip-spring model [5, 6], where MC blocks have a fixed amount of time steps. Nonetheless, both methods successfully restore entanglement dynamics. If a slip-spring reaches a chain end, it attempts a relocation move. Slip-springs are only allowed to relocate from one chain end to another: in a relocation attempt, a new slip-spring is created by connecting a randomly chosen chain end to any other bead within a distance closer than $0.95 \times d_{\text{T}} \approx 7.125$ nm. A Metropolis MC trial between the initial and the new slip-spring position determines whether the relocation is successful; the 'loosing' slip-spring is discarded.

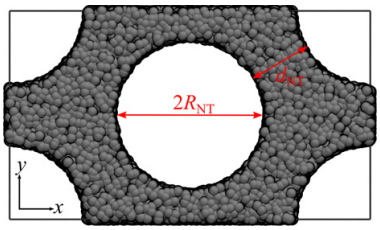

Figure 1. Simulation box of a polymer melt confined by an array of nanotubes. Nanotubes are placed on a hexagonal grid on the xy-plane and are infinite in z-direction. They are modelled by a purely repulsive potential which acts as a barrier of particles at a distance R_{NT} from the nanotube centre (see text). The hexagonal symmetry relates the box dimensions l_x, l_y and the nanotubes' radii and distances R_{NT}, d_{NT} as $l_y = l_x/\sqrt{3}$ and $d_{NT} = l_y - 2R_{NT}$.

More details about the implementation of slip-springs in the coarse-grained polystyrene (CG-PS) model can be found in reference [25].

2.2. Dissipative-particle dynamics

DPD [1, 32, 33] is a mesoscopic simulation method that describes particle interactions in terms of purely pairwise conservative, dissipative, and random contributions. The coarse-grained, soft-core conservative force allows for large integration steps at low computational costs, which makes DPD a popular technique for simulations of soft matter [34]. The coupled dissipative and random forces account for the system's friction and act as a thermostat. Here, we follow the methodology of Groot and Warren [1], where the conservative force between two beads i and j is linear and defined by a cutoff radius r_c and a repulsion parameter a_{ij} (equation (3)).

$$\vec{F}^{C}_{ij} = a_{ij}\left(1 - \frac{r_{ij}}{r_c}\right)\vec{e}_{ij}. \tag{3}$$

Polymer chains are modelled using a standard bead-spring model, where DPD beads are connected by a weak Hookean spring in addition to their nonbonded interactions. As a computationally inexpensive answer to the physical shortcomings of soft-core conservative interactions, slip-springs have been employed in DPD simulations of polymer melts [5, 6, 8] and solutions [35, 36] by different groups. In this study, we follow the work of Langeloth *et al* [5]: initially, a fixed number of slip-springs is distributed between pairs of nonbonded beads, following a similar distance criterion as in the slip-spring hPF model. During the simulation, slip-springs are allowed to migrate along the chains governed by a Metropolis MC criterion. If slip-springs reach the end of a chain, a relocation move to a different, randomly chosen chain end is attempted as described in the previous subsection. Slip-springs are frozen after a number of MC migration attempts and act as fixed bonds in the next set of DPD steps. By performing alternating blocks of MC and DPD steps, entanglement dynamics such as reptation and constraint release are restored. For further details, we refer to the initial work in reference [5].

In addition to unrestricted melts, we present simulations of systems confined by an array of nanotubes (figure 1). Nanotubes are modelled by a purely repulsive potential and placed on a hexagonal grid in the xy-plane. They are infinite in z-direction. The nanotubes are positioned in the centre and on the corners of the simulation box, so that one periodic image contains two tubes. They interact with DPD beads via the conservative potential: in a modified version of equation (3), a_{ij} and r_{ij} are replaced by the nanotubes' repulsion parameter $a_{NT,i}$ and the distance between a bead and their 'surface' $r_{NT,i}$. A nanotube's surface is defined by its radius R_{NT}, which is also used to evaluate its *effective* excluded volume $V_{NT} = \pi R^2_{NT} l_z$, where l_z is the box size in z-direction. The nanotubes' repulsion parameter $a_{NT,i}$ is chosen to be twice as repulsive as the regular a_{ij}. Notably, interactions between beads and nanotubes are still soft-core, which theoretically allows beads to penetrate the tubes. In this case, $r_{NT,i}$ becomes formally negative. However, we have not observed polymers crossing into the nanotubes, so the repulsion appears to be large enough to keep them out.

DPD simulation results are presented in reduced units: time, distance, mass, and energy are given in units of t_{DPD}, r_c, m_{DPD}, and $k_B T$, respectively. If need be, our simulations can be mapped onto a polystyrene model [36]. All DPD parameters are taken from reference [1] for a density of $\rho = 3\ r_c^{-3}$. The repulsion parameters for bead-bead and bead-nanotube interactions are $a_{ij} = 25\ k_B T \times r_c^{-1}$ and $a_{NT,i} = 50\ k_B T \times r_c^{-1}$. Bonds and slip-springs have a force constant of $k_B = k_{SS} = 2\ k_B T \times r_c^{-2}$. The integration step is $\Delta t = 0.06\ t_{DPD}$. The monomer radius is $1\ r_c$ by definition, and an average bond length of $l \approx 1.21\ r_c$ emerges from the sum of bonded and nonbonded interactions.

Our simulations feature chains of length $N = 25, 50, 75, 100$, and 150. For the unconfined melts, 1668, 834, 556, 417, and 278 of these chains are simulated in a cubic $(24\ r_c)^3$ box, respectively. Chains under confinement are investigated for different nanotube surface-to-surface distances d_{NT}. On a hexagonal grid, only two of the parameters d_{NT}, R_{NT}, l_x, and l_y can be chosen independently. Here, we fix the nanotube radius at $R_{NT} = 10\ r_c$ and the x-dimension as $l_x = 38, 42, 48$ and $56\ r_c$ with $l_x > l_y$. Consequently, $l_y = l_x/\sqrt{3} = 21.939$, 24.249, 27.713, 32.332 r_c and $d_{NT} = l_y - 2R_{NT} = 1.9, 4.2, 7.7, 12.3$ are determined. The z-length is $l_z = 21\ r_c$ for all systems. To match a density of $3\ r_c^{-3}$ in the accessible volume $V_{box} - 2V_{NT}$, the total number of beads in the $d_{NT} = 1.9, 4.2, 7.7$ and 12.3 systems is set to 12 900, 25 000, 45 000, and 74 500, respectively. Exceptions are the $(d_{NT} = 4.2, N = [75, 150])$ and $(d_{NT} = 12.3, N = [75, 150])$ systems where the total number of beads is 24 900 and 74 550, respectively, to allow an integer number of chains. Simulations are performed with and without slip-springs for every setup. If present, the number of slip-springs is always 10% of

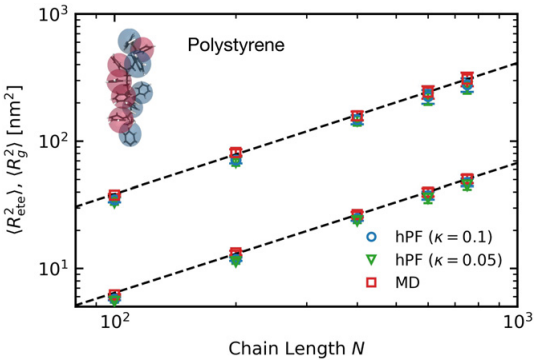

Figure 2. Mean squared end-to-end distance $\langle R^2_{ete} \rangle$ (upper set of symbols) and radius of gyration $\langle R^2_g \rangle$ (lower set of symbols) of polystyrene melts derived from MD and hPF simulations employing different compressibility parameters κ. The lines indicate a linear scaling with the number of monomers N.

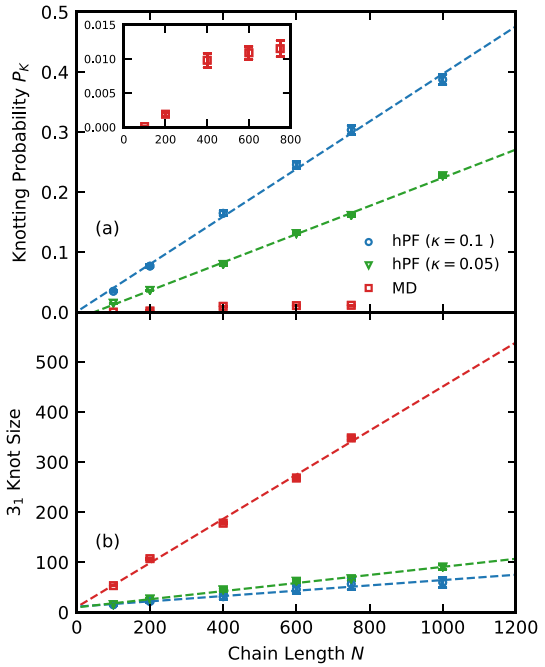

Figure 3. Knotting in polystyrene chains derived from hPF and MD simulations. (a) Shows the probability P_K to find at least one knot in a chain of length N. hPF simulations are performed with different compressibility parameters κ. Dashed lines are linear fits with slopes of 3.9×10^{-4} and 2.3×10^{-4} for $\kappa = 0.1$ and 0.05, respectively. The inset shows a close-up of the MD results. The average size of a 3_1 trefoil knot in numbers of monomers is shown in (b) as a function of the chain length N. Dashed lines are linear fits with slopes of 0.05, 0.08 and 0.44 for hPF simulations with $\kappa = 0.1$ and 0.05 and MD chains, respectively.

the total number of beads. Details of the slip-spring method can be found in reference [5]. Here, we use the same block sequence lengths of 500 DPD steps and 500 MC migration attempts, a pattern chosen to match the spatial correlation of slip-springs in both blocks [5]. The unconfined melts are equilibrated for 5×10^5 ($N = [25, 50, 75]$) and 1.5×10^6 ($N = [100, 150]$) time steps, which is longer than any chains' longest relaxation time. Production runs are performed for 3×10^6 time steps. All confined melts are equilibrated for 10^6 ($N = [25, 50, 75]$) and 2×10^6 ($N = 100, 150$) time steps, while data is extracted from 10^6 ($N = [25, 50, 75]$) and 5×10^6 ($N = [100, 150]$) time steps of production. If not denoted otherwise, errors are the standard deviation of the mean of all chains.

2.3. Knot analysis

In order to describe a knot in a chain mathematically, the chain is required to be closed. The Alexander polynomials [37] are then used as topological invariants to characterize the knots. In this work, we utilize the Kymoknot software [38] (version 1.0), which enables us to analyse knots in open and closed polymers. For the closure of open chains, the minimally-interfering closure scheme [38, 39] is applied. Within this closure scheme, two distinct ways of connecting the chain ends are compared—they are either connected by direct bridging, or via the closest points of the convex hull of the chain portion. The end-to-end distance of the chain is thus compared with the sum over the distances between the chain ends and their closest points on the convex hull. If the former is smaller, simple bridging is applied, otherwise the chain is closed via the convex hull. This closure scheme has shown to be robust and computationally efficient and leads to the least amount of additional entanglements [39].

The smallest region of the chain that has the same topology as the entire chain after closure is considered as the knotted region. Various search schemes can be used for determining knots in a polymer chain which may return different knotted regions [38]. We use a bottom-up approach, which starts from very short, unknotted portions of the chain. These portions are gradually increased until the physical knot of the chain portion equals the knotting type of the whole chain. The remainder of the chain is unknotted. The knot size is then defined as the number of beads within the knotted region.

The kinetics of the constant transition between the knotted and the unknotted state can be analysed as well. For a single chain i, we introduce a state function $h_i(t)$, which equals 1 if chain i contains at least one knot and is 0 otherwise. We then define a correlation function $C(t)$ for the knotting dynamics using this state function:

$$C(t) = \frac{1}{M} \sum_i \frac{\langle (h_i(t) - \langle h \rangle)(h_i(0) - \langle h \rangle) \rangle}{\langle (h_i(t) - \langle h \rangle)^2 \rangle}. \qquad (4)$$

Here, we average over all M chains in the system. The relaxation time of a knot τ_K is obtained as the integral of the

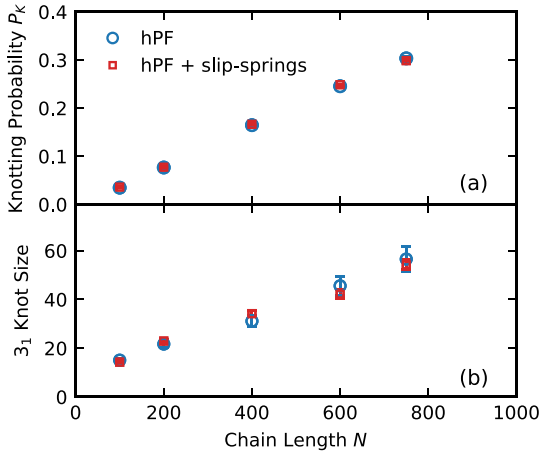

Figure 4. Probability P_K for a chain to carry at least one knot (a) and the average size of a 3_1 trefoil knot in numbers of monomers (b) as a function of the chain length N. Systems are hPF simulations with $\kappa = 0.1$, with and without slip-springs.

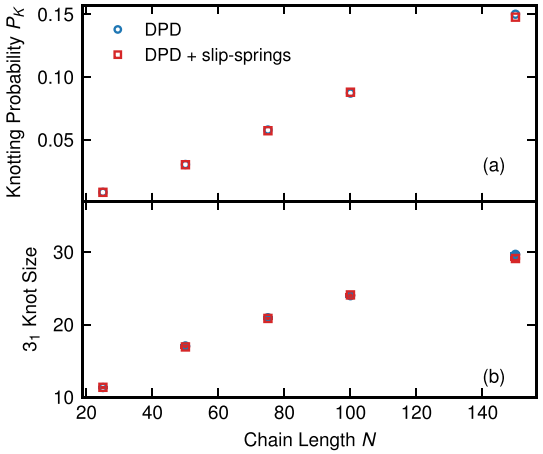

Figure 5. Probability P_K for a chain to carry at least one knot (a) and the average size of a 3_1 trefoil knot in numbers of beads (b) as a function of chain length N. Systems are DPD simulations with and without slip-springs. Error bars are within the symbol size.

correlation function $C(t)$

$$\tau_K = \int_0^\infty C(t)\mathrm{d}t. \tag{5}$$

3. Results

3.1. Comparison between hard-core molecular dynamics and soft-core hybrid-particle-field simulations

In this section, we discuss the differences in the knotting behaviour of our hard-core standard MD model and the soft-core hPF model derived from it. In the hPF model, the softness of nonbonded interactions can be controlled by tuning the compressibility parameter κ. Specifically, a smaller value of κ gives a less compressible system, in which less particle overlapping occurs. The chain dimensions of all polystyrene models are shown in figure 2. Among these models, the chain structures are found to be consistent, indicating that the soft-core and hard-core natures do not necessarily alter polymer structural properties on the chain scale. Both the ensemble-averaged squared end-to-end distance $\langle R_{ete}^2 \rangle$ and radius of gyration $\langle R_g^2 \rangle$ show the expected linear scaling with the number of monomer N (dashed lines in figure 2) [40]. It should be noted that the compressibility parameter κ must have an impact on the structural behaviour of polymer chains; here, the structural deviation for the employed range of κ is within 3%.

Next, we examine the knotting probability and knot size in both soft-core and hard-core models using the knotting analysis presented in subsection 2.3. As shown in figure 3(a), the knotting probability P_K of hPF models is profoundly higher than the MD models over the whole range from $N = 100$ to $N = 750$ monomers. Moreover, the knotting probability P_K of hPF models continuously increases with the polymer chain length N. A linear fit yields slopes of $k \approx 3.9 \times 10^{-4}$ and $k \approx 2.3 \times 10^{-4}$ for the hPF models with $\kappa = 0.1$ and $\kappa = 0.05$, respectively. This indicates that the knotting probability in hPF models with $\kappa = 0.1$ is almost 50% higher than that with $\kappa = 0.05$. It is noted that the linearity of the knotting probability with the chain lengths in hard-core MD simulations is not as evidently seen as that in the soft-core models. This probably comes from the rather small low statistical value of P_K in MD simulations. Nevertheless, the knotting probability in hard-core MD models is sufficiently low in comparison to the soft-core models, implying that the degree of overlapping plays an important role. We further investigate the knot size where we focus on the dominating simple trefoil (3_1) knot. As illustrated in figure 3(b), the average size detected in the MD model is significantly larger than that in hPF models. Linear fits reveal that approximately 44% of all monomers of any chain are involved in one trefoil 3_1 knot in the MD model. In contrast, only ~5% and ~8% of the monomers per chain form a 3_1 knot in the hPF models with $\kappa = 0.1$ and $\kappa = 0.05$, respectively. With the similar characteristic ratio of the polystyrene melt in hPF and MD models, the overestimated knotting probability and underestimated knot size are expected to be intimately related to the soft-core interactions, implying that the overlapping of particles facilitates the localization and occurrence of the formation of a trefoil 3_1 knot. Recently, Meyer *et al* [16] studied the knotting properties of generic polymer models with various characteristic ratios using MD simulations and compared their results with the random walk (RW) polymer model. The RW model is found to overestimate the knotting probability and underestimate the knot size in comparison with the simulation model with hard-core repulsive interactions, consistent with our observations in hPF and MD models.

3.2. Comparison between soft-core models with and without slip-springs

In this section, we study the influence of slip-springs, which are initially designed to mimic the chain entanglements for dynamical properties, on the knotting behaviour of soft-core hPF and DPD models. The typical reptation behaviour of polymer melts was recovered by the introduction of slip-springs to these soft-core models in prior studies [5, 7]. The effect of slip-springs on the conformational properties of polymer chains (e.g. the radius of gyration) in the melt state was found to be negligible. How slip-springs, as artificial ad hoc interactions, affect the self-entanglements (knottedness) of polymer chains is still unknown.

3.2.1. Hybrid-particle-field simulations. We analyse the knotting behaviour in terms of the probability P_K to carry at least one knot in hPF models of polystyrene melts with and without slip-springs at various chain lengths. As displayed in figure 4(a), P_K of the hPF chains with slip-springs is in good agreement with that without slip-springs at all investigated chain lengths. Figure 4(b) shows the average trefoil 3_1 knot size for chain lengths between $N = 100$ and 750 in hPF models with and without slip-springs. Consistent with previous observations for hPF, we find the 3_1 knot size in hPF simulations with slip-springs to increases with increasing chain length. No significant difference is observed between systems with and without slip-springs. Both of these analyses suggest that slip-springs indeed have a negligible effects on the self-entanglements (knottedness) of polymer chains in hPF simulations within the tested parameter space.

3.2.2. Dissipative-particle dynamics simulations of polymer melts. DPD simulations of polymer melts with and without slip-springs are investigated for their probability P_K to carry at least one knot per chain, as well as the size of the simple 3_1 trefoil knot. The results are shown as a function of the number of beads N in figures 5(a) and (b), respectively. They are comparable with those of the hPF model in terms of slip-springs, which show no significant impact on the knotting probability or the knot size. The knotting probability as well as the average knot size of the 3_1 trefoil knots both increase roughly linearly with the chain length.

3.2.3. Dissipative-particle dynamics simulations of confined polymer melts. We finally study the knottedness of DPD chains confined by a regular array of nanotubes for different distances d_{NT} between two nanotubes and thus different degrees of confinement. Generally, confinement increases the polymer's compactness. An example plot of the squared radius of gyration $\langle R_g^2 \rangle$ as a function of the chain length N is given as figure A1 in the supplementary information (https://stacks.iop.org/JPCM/33/244001/mmedia) for the strongest confinement ($d_{NT} = 1.9$) and the unconfined systems. $\langle R_g^2 \rangle$ shrinks by roughly 35–40% for $d_{NT} = 1.9$, however, the scaling of $\langle R_g^2 \rangle$ with $N - 1$ is barely affected. Further findings concerning the static and dynamic polymer properties will be reported elsewhere. The probability P_K of chains of length N to carry at least one knot is given in figure 6(a).

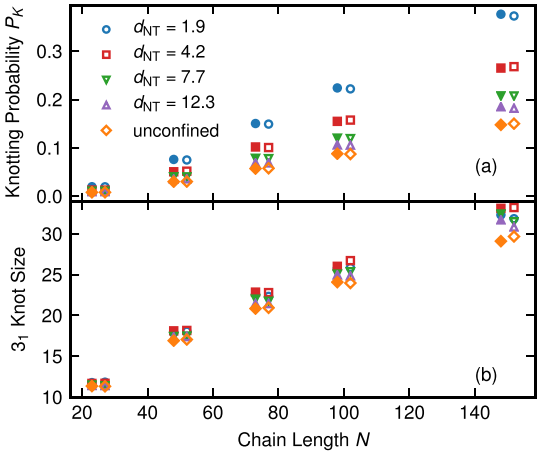

Figure 6. Probability P_K for a chain to carry at least one knot (a) and the average size of a 3_1 trefoil knot in numbers of beads (b) as a function of chain length N. Systems are DPD simulations with (full symbols) and without slip-springs (empty symbols). The melt is confined by a regular, hexagonal array of nanotubes with different inter-tube distances d_{NT}. For clarity, the symbols carry an offset of −2 (slip-springs), +2 (no slip-springs). Error bars are within the symbol size.

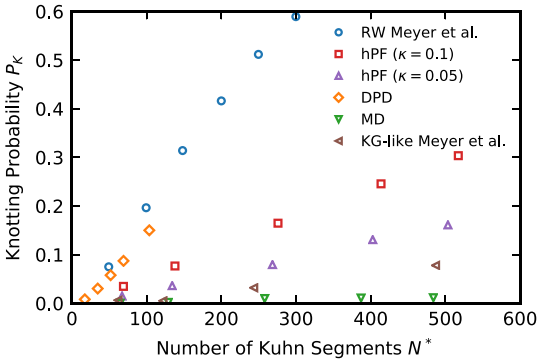

Figure 7. Comparison of the knotting probability P_K as a function of the number of Kuhn segments $N^* = N/C_\infty$ for different models. The characteristic ratio C_∞ is 1.55, 1.49, 1.45 and 1.45 for MD, (hPF, $\kappa = 0.1$ and 0.05), and DPD simulations, respectively. Probabilities for the fully flexible KG-like model and the RW are taken from reference [16].

Consistent with the observations made for unconfined melts, simulations with and without slip-springs are barely distinguishable. As the distance between the nanotubes d_{NT} decreases, the confined chains assume more compact structures, which is associated with a higher knottedness. For a chain length of $N = 150$, P_K is 18% in the pure melt, while it increases to 39% for a strongly confined system with a nanotube distance of $d_{NT} = 1.9$. For short chains ($N \leqslant 50$), the radius of gyration is of similar size as the range of the interstice region between three nanotubes. We do, however, still observe a distinct effect: for $N = 25$, we see an increase in P_K from

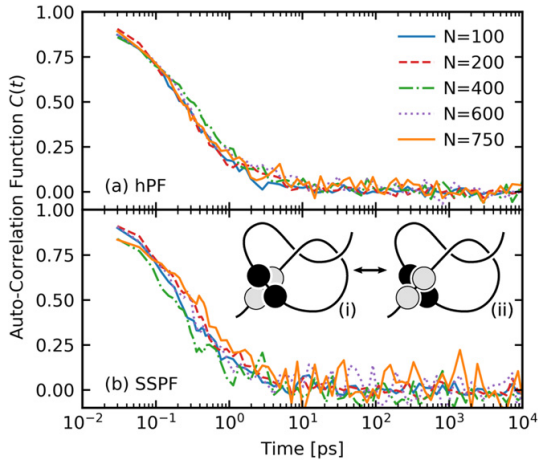

Figure 8. Autocorrelation function of the knotted-to-unknotted interconversion $C(t)$ in hPF simulations without (a) and with slip-springs (b) with a compressibility parameter of $\kappa = 0.1$ as a function of chain length N. The inset in (b) is a cartoon of the transition between knotted (i) and unknotted (ii) state via bond-crossing on the scale of single beads.

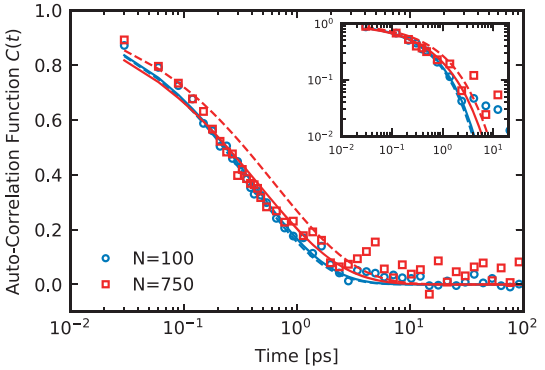

Figure 9. Stretched exponential fits to the knot formation ACFs of hPF simulations ($\kappa = 0.1$) with (solid lines) and without (dashed lines) slip-springs for polystyrene chains composed of 100 monomers (blue) and 750 monomers (red). The inset shows the same data in a double-logarithmic presentation.

0.8% (unconfined) to 2.0% ($d_{NT} = 1.9$), which is comparable to the increase detected for longer chains. We briefly study the knottedness of a chain as a function of its confinement: a plot of the knotting probability P_K against the squared radius of gyration $\langle R_g^2 \rangle$ for various chain lengths and degrees of confinement can be found in figure A2 (supplementary information). For a fixed confinement, P_K and $\langle R_g^2 \rangle$ show the expected linear relation, as they are both linked by the chain length ($P_K \propto N \propto \langle R_g^2 \rangle$). For a fixed chain length N, on the other hand, the knotting probability increases with decreasing $\langle R_g^2 \rangle$. However, we did not find a trivial relation between them, e.g. by a power law. This is likely due to the alignment of chains parallel to the nanotubes, and the therefore anisotropic nature of the confinement.

The average 3_1 knot size for all systems containing nanotubes (figure 6(b)) reveals a rather weak confinement effect. The influence of slip-springs is negligible, and the slight deviations for longer chains ($N \geqslant 100$) are likely of statistical nature. Interestingly, the decreasing nanotube distance appears to lead to an increase in the knot size, where a maximum is reached for $d_{NT} = 4.4$. By analysing the spatial components of the radius of gyration, we find that chains are elongated parallel to the nanotubes. Therefore, generally, chains tend to form larger knots when brought into confinement. However, the size of the interstice region between three nanotubes decreases with decreasing nanotube distance. The size of the radius of gyration of longer chains ($N \geqslant 50$) thus competes with the diameter of this interstice region, especially for short nanotube surface-to-surface distances. In the case of $d_{NT} = 1.9$, a larger fraction of chains are spread over multiple interstitial regions. In this case, knots might be formed in parts of the chain that are confined within the interstitial region, leading to smaller knot sizes.

3.3. Comparison with different models

We lastly compare the observed knottedness of our DPD and hPF chains with results reported for different limiting models. We focus on the knotting probabilities of systems without slip-springs. As discussed above, the same observations apply for the slip-spring systems. Recently, Meyer *et al* [16] investigated the knotting probabilities in self-avoiding model polymer chains with an adjustable bending potential and compared them to those of a RW. We follow their approach to compare the knotting probability of our models on the chains' Kuhn scale: by utilizing the ratio $N^* = N/C_\infty$, we normalize both the DPD and hPF chain lengths N to the number of Kuhn segments per chain. Here, C_∞ is the characteristic ratio and derived from the bond length l between two beads as $C_\infty = \langle R_{ete}^2 \rangle / \left(l^2 \times N\right)$. The results are shown in figure 7 along with the data reported in reference [16] for their fully flexible chain and the RW. The fully flexible chain consists of purely repulsive Lennard-Jones beads and a harmonic bond known to reproduce the same chain structures as finitely extensible (FENE) bonds. This, along with a reported characteristic ratio of $C_\infty = 2.1$, makes it very similar to the standard Kremer–Grest (KG) model ($C_{\infty,KG} = 1.7$) [41, 42]. We thus refer to it as a KG-like chain. Coarse-grained MD chains, hPF chains with $\kappa = 0.1$ and 0.05, and DPD chains have characteristic ratios of $C_\infty = 1.55$, $C_\infty = 1.49$, $C_\infty = 1.45$ and $C_\infty = 1.45$, respectively, which were derived from their bond lengths of 0.52 nm (hPF) and 1.21 r_c (DPD). We find the knotting probability of our hard-core MD simulations to be in the range of, but lower than, that of KG-like chains. The difference probably arises from the different number densities of these two models, as higher densities in polymer systems are known to favour higher knotting probabilities [16]. However, a comparison of both models' number densities is not straightforward and depends on the spatial quantity utilized for mapping. The knotting probability increases for the $\kappa = 0.05$ and $\kappa = 0.1$ hPF models and the DPD model, respectively, with those of the DPD chain being somewhat lower than for the

Table 2. Relaxation times of knot formation of hPF simulations ($\kappa = 0.1$) with and without slip-springs of polystyrene melts at chain length N ranging from 100 monomers to 750 monomers.

τ_{knot} (ps)/N	100	200	400	600	750
hPF	0.52	0.70	0.36	0.55	1.19
hPF + slip-springs	0.55	0.62	0.89	0.89	0.70

RW. We note that the Kuhn-scale-reduced DPD model should be taken with a grain of salt, as the mapping of DPD chains usually happens on even coarser scales; however, it serves well for the comparison between models. The P_{K} of the less compressible hPF model ($\kappa = 0.05$) lies between those of the more flexible hPF ($\kappa = 0.1$) and DPD chains and the hard-core MD model. These results are generally consistent with the findings of Meyer *et al*: comparing their fully-flexible KG-like chain and the RW, they identify the knotting behaviour to be closely connected to the models' bond–bond correlation functions: since the formation of a knot requires a negative correlation on the respective length scale, the bond–bond correlations as well as their fluctuations determine at which scale and how likely knots are formed [16]. For hard-core models, knots are thus rather rare. In the soft-core limit, RWs allow many and strongly localized knots. Meyer *et al* conclude that 'real' polymer chain melts, such as the KG-like chain, are rather poorly described by RWs on a local scale [16]. It becomes apparent from figure 7 that soft-core models, especially our DPD system, are much closer to the RW on *all* scales. Consequently, their knotting probability is much closer to a RW than to a KG-like chain. However, weak local repulsion still exists, and the full knotting probability of the RW is not yet reached. The deviations from a local random-walk behaviour become stronger with increasing excluded-volume effects when going from DPD to the $\kappa = 0.1$ and $\kappa = 0.05$ hPF models and the hard-core MD model, which all have bending potentials. This causes a decrease of the knotting probability. We note that, if need be, the local structure of hard-core MD or KG-like chains can at least in parts be restored to the hPF models by tuning the compressibility parameter κ.

3.4. Dynamics of knot formation and destruction

In addition to the static properties related to knotting, we investigate the dynamics of the knotted-to-unknotted transition in the hPF model. Figure 8 displays the autocorrelation function (ACF) of this transition in hPF simulations of polystyrene melts without (a) and with slip-springs (b). In both models, the ACFs exhibit no chain-length dependence. Moreover, we find that the ACFs decay to zero in about $\sim$10 ps. In order to quantitatively characterize the relaxation time of knot formation dynamics, we fit the ACF by a stretched exponential function

$$C(t) = \exp\left[-\left(\frac{t}{\tau^*}\right)^{\beta}\right]. \tag{6}$$

One example is shown in figure 9 for hPF simulations ($\kappa = 0.1$) of $N = 100$ and $N = 750$ with (solid lines) and without slip-springs (dashed lines). The relaxation time τ_{knot} is then calculated as

$$\tau_{\text{knot}} = \int_0^{\infty} C(t)\mathrm{d}t = \frac{\tau^*}{\beta}\Gamma\left(\frac{1}{\beta}\right), \tag{7}$$

where Γ represents the complete gamma function. The calculated relaxation times are summarized in table 2. The relaxation time τ_{knot} evidently does not depend on the chain length. The knot relaxation happens on a time scale comparable to the time which a monomer needs to diffuse its own diameter. The same results are observed for our DPD models (not shown). Indeed, these results of fast knotting dynamics are not surprising. In the soft-core hPF model, the nonbonded interactions are so soft that the bonds can cross each other. As illustrated in the inset of figure 8(b), the knotted-to-unknotted transition can easily take place at the monomer length and time scale. This transition is essentially insensitive to the chain length and effectively dictated by the monomer relaxation time. A similarly fast relaxation of knotted structures in soft-core models has qualitatively been observed by Meyer *et al*, who also reported a change in knotting probabilities on drastically shorter time scales than the structural chain relaxation. Moreover, slip-springs in our systems are expected to alter the polymer dynamics only above the entanglement length (N_{e}) and time (τ_{e}) scales. This is consistent with the observation in table 2 that the knot formation dynamic is genuinely unaffected by the addition of slip-springs.

4. Conclusion

For linear polymer chains in the melt, we have investigated the probability to form knots, the number of monomers involved in an average trefoil knot, as well as the dynamics of knot formation and destruction. The focus was on two series of soft-core polymer models, which we have developed and used in recent years. Firstly, there is the hPF model. For this model, we tested both the standard variant [2] and a variant with slip-springs for better reproduction of entangled dynamics [7]. The interesting aspect of the hPF series of models is that there is also a reference model from which they were derived. This is a veteran hard-core coarse-grained MD model of polystyrene [28]. Secondly, there are two DPD models, one without, the other with slip-springs [5]. No parent hard-core model is available here. We are, thus, able to not only characterize our models for their knotting behaviour, but also to compare, on the one hand, hard-core and soft-core models and, on the other hand, the effect of slip-springs on the knotting properties. It is obvious that the introduction of soft-core nonbonded repulsions leads to a massive increase in the probability for a chain to be knotted, cf e.g. figure 3(a). Throughout all polymer lengths, the increase is more than one order of magnitude (the precise ratio is hard to calculate, because of the very small number of knots of the hard-core model and the resulting noisy statistics). Within the knotting map of polymer models of different hardness or softness, our hard-core CG-PS is in the same class as the KG model as one of the standard hard-core polymer models (figure 7). However, the soft-core DPD model, but also

the hPF models, are much closer to the knotting pattern of the random walk, which is the ultimate soft-core model. The knottedness of the hPF model can be tuned, within limits, by manipulating its compressibility, which is linked to the softness of the nonbonded repulsion. The knot size, i.e. the number of monomers participating in a knot, is about 5 times larger for the hard-core models. It should be stressed that, in all other structural aspects, hard-core and soft-core models are identical, with the foreseeable and well-understood exception of the pair-correlation function at short distances [2].

The introduction of slip-springs to a soft-core model (hPF or DPD) influences dramatically the polymer dynamics: it restores successfully the proper reptation motion to the soft-core models [5–7]. However, slip-springs have next to no effect on the knotting probability (figures 4(a) and 5)(a), including for melts under heavy confinement (figure 6(a)). Soft-core models with slip-springs may lead to a marginally smaller knot size than the same models without slip-springs (figures 4(b), 5(b) and 6(b)). It is not clear, however, if this deviation is statistically significant, and it is only found for the longest chains studied.

The investigation of the dynamics of reversible knot formation and destruction sheds some light on the knot formation mechanism in soft-core models. It turns out that all knotting and unknotting happens on the time-scale of single-monomer mobility. In other words, soft-core polymers do not form knots by running one chain end through an existing loop, but by monomers or short chain-segments exchanging positions. This mechanism is not altered by the introduction of slip-springs, as slip-springs enforce a long-time entangled-like dynamics on the polymer chains without actually preventing chains from crossing one another. Therefore, they have no effect on the short-time motion of monomers. The question as to whether the reason for our hard-core model to have much fewer knots than either soft-core model is thermodynamic (hard-core and soft-core models do have different Hamiltonians) or kinetic (hard-core models are forced to physically tie the knot, rather than taking the short-cut of chain-crossing) cannot be answered in this contribution. The hard-core model has too few knotting and unknotting events to calculate a reliable relaxation time for the process.

Note added in the revised manuscript

After the initial submission of this article, a study of knots in soft-core polymer models was published by Zhang *et al* [43]. Their findings further confirm the importance of local chain properties on their knotting probability, and are generally in line with ours.

Acknowledgments

Fruitful discussions with Peter Virnau are gratefully acknowledged. This work has been funded by the Collaborative Research Centre Transregio 146 'Multiscale Simulation Methods for Soft Matter', project A8, of the Deutsche Forschungsgemeinschaft.

Data availability statement

The data that support the findings of this study are available upon reasonable request from the authors.

ORCID iDs

Zhenghao Wu https://orcid.org/0000-0003-2862-4432
Simon A N Alberti https://orcid.org/0000-0002-5361-4124
Jurek Schneider https://orcid.org/0000-0002-0286-1678
Florian Müller-Plathe https://orcid.org/0000-0002-9111-7786

References

[1] Groot R D and Warren P B 1997 *J. Chem. Phys.* **107** 4423
[2] Milano G and Kawakatsu T 2009 *J. Chem. Phys.* **130** 214106
[3] Likhtman A E 2005 *Macromolecules* **38** 6128–39
[4] Uneyama T and Masubuchi Y 2012 *J. Chem. Phys.* **137** 154902
[5] Langeloth M, Masubuchi Y, Böhm M C and Müller-Plathe F 2013 *J. Chem. Phys.* **138** 104907
[6] Langeloth M, Masubuchi Y, Böhm M C and Müller-Plathe F 2014 *J. Chem. Phys.* **141** 194904
[7] Wu Z, Kalogirou A, De Nicola A, Milano G and Müller-Plathe F 2021 *J. Comput. Chem.* **42** 6–18
[8] Chappa V C, Morse D C, Zippelius A and Müller M 2012 *Phys. Rev. Lett.* **109** 148302
[9] Ramírez-Hernández A, Detcheverry F A, Peters B L, Chappa V C, Schweizer K S, Müller M and de Pablo J J 2013 *Macromolecules* **46** 6287–99
[10] Vogiatzis G G, Megariotis G and Theodorou D N 2017 *Macromolecules* **50** 3004–29
[11] Schneider J, Panagiotopoulos A Z and Müller-Plathe F 2017 *J. Phys. Chem.* C **121** 27664–73
[12] de Nicola A, Kawakatsu T, Müller-Plathe F and Milano G 2016 *Eur. Phys. J. Spec. Top.* **225** 1817–41
[13] Munaò G, Pizzirusso A, Kalogirou A, de Nicola A, Kawakatsu T, Müller-Plathe F and Milano G 2018 *Nanoscale* **10** 21656–70
[14] Virnau P, Kantor Y and Kardar M 2005 *J. Am. Chem. Soc.* **127** 15102–6
[15] Poier P, Likos C N and Matthews R 2014 *Macromolecules* **47** 3394–400
[16] Meyer H, Horwath E and Virnau P 2018 *ACS Macro Lett.* **7** 757–61
[17] Ashley C W 1944 *The Ashley Book of Knots* (New York: Doubleday)
[18] Bore S L and Cascella M 2020 *J. Chem. Phys.* **153** 094106
[19] Bore S L, Kolli H B, Kawakatsu T, Milano G and Cascella M 2019 *J. Chem. Theor. Comput.* **15** 2033–41
[20] Kolli H B *et al* 2018 *J. Chem. Theor. Comput.* **14** 4928–37
[21] Munaò G, de Nicola A, Müller-Plathe F, Kawakatsu T, Kalogirou A and Milano G 2019 *Macromolecules* **52** 8826–39
[22] Zhao Y, de Nicola A, Kawakatsu T and Milano G 2012 *J. Comput. Chem.* **33** 868–80
[23] Zhao Y, Byshkin M, Cong Y, Kawakatsu T, Guadagno L, de Nicola A, Yu N, Milano G and Dong B 2016 *Nanoscale* **8** 15538–52
[24] Zhu Y-L, Lu Z-Y, Milano G, Shi A-C and Sun Z-Y 2016 *Phys. Chem. Chem. Phys.* **18** 9799–808
[25] Wu Z, Milano G and Müller-Plathe F 2021 *J. Chem. Theor. Comput.* **17** 474–87
[26] Zhu Y-L, Liu H, Li Z-W, Qian H-J, Milano G and Lu Z-Y 2013 *J. Comput. Chem.* **34** 2197–211

[27] de Gennes P G 1971 *J. Chem. Phys.* **55** 572–9
[28] Qian H-J, Carbone P, Chen X, Karimi-Varzaneh H A, Liew C C and Müller-Plathe F 2008 *Macromolecules* **41** 9919–29
[29] Reith D, Pütz M and Müller-Plathe F 2003 *J. Comput. Chem.* **24** 1624–36
[30] Auhl R, Everaers R, Grest G S, Kremer K and Plimpton S J 2003 *J. Chem. Phys.* **119** 12718–28
[31] Spyriouni T, Tzoumanekas C, Theodorou D, Müller-Plathe F and Milano G 2007 *Macromolecules* **40** 3876–85
[32] Hoogerbrugge P J and Koelman J M V A 1992 *Europhys. Lett.* **19** 155
[33] Español P and Warren P 1995 *Europhys. Lett.* **30** 191
[34] Kong Y, Manke C W, Madden W G and Schlijper A G 1994 *Int. J. Thermophys.* **15** 1093–101
[35] Masubuchi Y, Langeloth M, Böhm M C, Inoue T and Müller-Plathe F 2016 *Macromolecules* **49** 9186–91
[36] Schneider J, Süss L D and Müller-Plathe F 2020 *J. Chem. Eng. Data* **65** 1264–72
[37] Alexander J W 1928 *Trans. Am. Math. Soc.* **30** 275
[38] Tubiana L, Polles G, Orlandini E and Micheletti C 2018 *Eur. Phys. J.* E **41** 72
[39] Tubiana L, Orlandini E and Micheletti C 2011 *Prog. Theor. Phys. Suppl.* **191** 192–204
[40] de Gennes P G 1979 *Scaling Concepts in Polymer Physics* (Ithaca, NY: Cornell University Press)
[41] Kremer K and Grest G S 1990 *J. Chem. Phys.* **92** 5057–86
[42] Everaers R, Karimi-Varzaneh H A, Fleck F, Hojdis N and Svaneborg C 2020 *Macromolecules* **53** 1901–16
[43] Zhang J, Meyer H, Virnau P and Daoulas K C 2020 *Macromolecules* **53** 10475–86

Supplementary Information for: Knotting Behaviour of Polymer Chains in the Melt State for Soft-Core Models with and without Slip-Springs

Zhenghao Wu*, **Simon A N Alberti***, **Jurek Schneider**, **Florian Müller-Plathe**

Technical University of Darmstadt, Eduard-Zintl-Institut of Inorganic and Physical Chemistry and Profile Area Thermofluids and Interfaces, Alarich-Weiss-Strasse 8, D-64287 Darmstadt, Germany

* Z. Wu and S. A. N. Alberti contributed equally to this work.

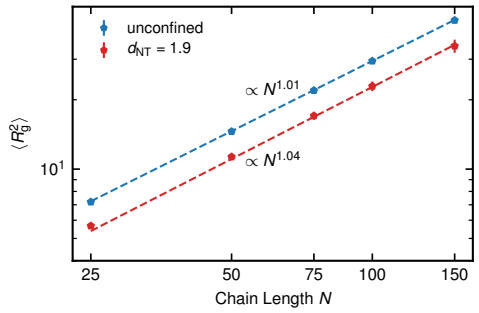

Figure A1: Squared radius of gyration $\langle R_g^2 \rangle$ plotted against the chain length N for the pure polymer melt and the most confined system with a nanotube distance of $d_{\mathrm{NT}} = 1.9$. The dashed lines are power-law fits as $\langle R_g^2 \rangle = A_0 N^{A_1}$, where A_0 and A_1 are fitting coefficients.

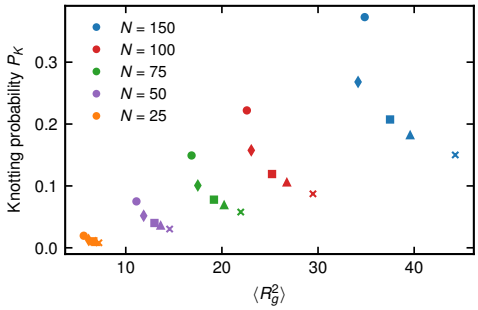

Figure A2: Knotting probability P_K plotted against the squared radius of gyration $\langle R_g^2 \rangle$ for various chain lengths and degrees of confinement. Orange, purple, green, red, and blue symbols show chains of lengths $N = 25, 50, 75, 100$, and 150, respectively. Circles, diamonds, squares, triangles, and crosses denote systems with nanotube distances of $d_{\mathrm{NT}} = 1.9, 4.2, 7.7, 12.3$, and unconfined melts.

4 Conclusion and Outlook

In this thesis, I have considered the polymer dynamics in hPF-MD simulations. Due to the soft-core nature of the density-functional-field interactions, the polymer chains in hPF-MD simulations are able to cross each other, leading to the loss of dynamical mechanisms such as entangled dynamics crucial for high-molecular-weight polymer melts or concentrated polymer solutions. The second technique, namely, multi-chain slip-spring models is thus proposed to reintroduce entangled dynamics of polymers in hPF-MD simulations. The integration of slip-springs into hPF-MD models results in a novel multi-scale simulation method (SS-hPF) which is capable of predicting structural and dynamical properties of realistic polymer systems with large system sizes and long simulated times. Therefore, the primary scientific achievement of this study lies in the development of new computational algorithms and models for polymers. These are demonstrated by the applications of SS-hPF on a range of polymer systems at various resolutions including the atomistic model of linear polyethylene melts (Section 3.1), CG models of linear (Section 3.2) and branch (Section 3.3) polystyrene melts.

During the development of SS-hPF, several other multi-scale modeling approaches have been proposed to predict dynamical and rheological properties of polymeric materials. For instance, Behbahani *et al.*[57] employed a systematic hierarchical simulation methodology by combining three levels of modeling: atomistic, monomer-level (moderately) coarse-grained, and Kuhn-segment-level (highly) coarse-grained multi-chain slip-spring simulations to predict diffusion and viscosity properties of cis-1,4-polybutadiene. Their quantitative predictions are also in good agreement with selected experimental measurements. Another similar hierarchical approach can be found in a recent work by Becerra et al.[56], which involves atomistic and single-chain slip-link simulations. Compared with these methods, the SS-hPF is a consistent and efficient modeling technique with flexible control on the model resolution. For example, the SS-hPF can accelerate the simulation compared to standard MD using polymer models with the same resolution. Moreover, due to its capability of describing the chemistry that dictates the system properties, the SS-hPF can be easily extended to various polymer chemistries such as polyamides and polyesters which bear polar groups. Additionally, the multi-chain nature of SS-hPF allows us to simulate large-scale multi-phase systems without much effort, although the density-functional-field interactions must be systematically parameterized. Recently, Caputo et al.[38] developed an efficient coarse-grained hPF models of polyethylene-filler systems. These polymer nanocomposite systems consist of a very high density of polymer/filler interfaces. The density-functional-field interactions have proven successful in capturing the details of polymer/filler interface and interphase. Unfortunately, their work using the pure hPF simulations can not reproduce reasonable dynamics and rheology of the polymer/filler systems with high-molecular-weight polymers. With the development of SS-hPF, it is now promising to predict these important properties for the polymer industry.

Since the SS-hPF is fairly new, and there are still many possibilities to explore. Firstly, the range of applicability of SS-hPF approach can be broadened extensively. Besides the aforementioned polymer-polymer, polymer-solid interface and interphase systems, the polymer-air interface is also of interest to be investigated. A prominent example of polymer systems is solvent evaporation, which, e.g., occurs during thermal annealing of spin-coated block copolymer films and can affect polymer microstructure

in particular. Recently, Sevink *et al.*[63] proposed an improved hPF-MD method to model systems with phase coexistence via incorporating other equation-of-states such as Carnahan–Starling[64]. In addition, it is unclear how the distribution of slip-spring changes through the different kinds of interfaces, and this requires further investigation. This direction will benefit the theoretical development of slip-spring models as well. Furthermore, the electrostatic interactions play a significant role in determining structural and dynamical behaviors of polyelectrolytes[65] and ionomers[66]. The standard MD usually suffers from the high computational expense in calculating electrostatic interactions. In hPF-MD simulations, a novel charge-density-functional-field has been proposed by Zhu *et al.*[36] and Kolli *et al.*[67] to efficiently compute the electrostatic interactions. It will be of great interest to study how complex electrostatics affects the dynamical and conformational behaviors in large-scale systems using the SS-hPF method.

On the other hand, the SS-hPF itself has experienced several limitations during its development. As a result, I believe that the following research directions can extend the capabilities of the SS-hPF method to make it more efficient and accurate. Firstly, when developing new models in SS-hPF simulations, especially, complex systems with multiple components, it is often challenging to choose the density-functional-field interaction parameter χ matrix for coarse-grained beads. Currently, two main approaches have been employed to determine the χ matrix: 1. Flory-Huggins polymer theory to derive the χ matrix analytically[33] and 2. simple optimization methods to match certain properties of reference systems numerically[58]. It is usually difficult to apply the former method to a specific CG bead such as a polyelectrolyte segment with electrostatics. Nevertheless, it is promising to couple certain advanced numerical optimization algorithm, e.g., genetic algorithm[68], with the latter method to obtain the χ matrix for complex systems focusing less on physics and interpretation but more on constructing a systematic and automatic procedure. Recently, Ledum *et al.*[69] proposed an automatic Bayesian optimisation strategy to determine the χ matrix for coarse-grained models of lipid membranes in hPF-MD simulations. Next, the interaction energy in the current hPF-MD simulation technique is calculated using the simple Flory-Huggins interaction energy form. This form implements a mixing term for different types of beads and an isotropic repulsive term between all beads responsible for the incompressibility of the liquid. It will be insufficient for, e.g., complex CG systems with different bead sizes. The current implementation of the mixing term may still be fine, but the repulsive term must differ between beads of different sizes. This requires us to further improve the interaction energy form of SS-hPF simulations. If we go one step further, we can even use a purely numerical form to represent the density-functional-field interaction energy. For instance, a spline representation of the density functional can be constructed and optimized globally via a neural network or a genetic algorithm from a reference fine-grained simulation model in order to calculate more accurate potential energies derived from the numerical density-functional. Moreover, the SS-hPF method currently supports only a constant number of slip springs in the system, which is physical for polymer melts under equilibrium conditions. The slip springs can be considered as explicit entanglements. In non-equilibrium simulations, the entanglements, which are characterized as topological kinks, vary greatly[70]. Therefore, we need to extend the current slip-spring model to capture the varying number of slip springs (entanglements) in the simulation. Two methods have been proposed in previous simulation studies using highly CG models. On the one hand, the number of slip-springs can be controlled by a grand canonical ensemble[53]; on the other hand, the number of slip-springs can be coupled to the local polymer bead densities[71].

With tremendous advances in machine learning (ML) and high-performance computing (HPC) technologies, computational materials design using molecular simulations is at its best. The SS-hPF method developed in this work has opened a way to construct efficient chemistry-specific models for predicting polymer dynamics at large spatial-temporal scales. Although it is fairly new and still has many limitations, the combination of ML, SS-hPF and HPC offers a promising strategy for high-throughput material discovery[72] in a more efficient and accurate manner.

Literatur

(1) Müller-Plathe, F. Coarse-Graining in Polymer Simulation: From the Atomistic to the Mesoscopic Scale and Back. *ChemPhysChem* **2002**, *3*, 754–769.

(2) Praprotnik, M.; Site, L. D.; Kremer, K. Multiscale Simulation of Soft Matter: From Scale Bridging to Adaptive Resolution. *Annu. Rev. Phys. Chem.* **2008**, *59*, 545–571.

(3) Padding, J. T.; Briels, W. J. Systematic coarse-graining of the dynamics of entangled polymer melts: the road from chemistry to rheology. *J. Phys.: Condens. Matter* **2011**, *23*, 233101.

(4) Van der Giessen, E. u. a. Roadmap on multiscale materials modeling. *Model. Simul. Mater. Sci. Eng.* **2020**, *28*, 043001.

(5) Fish, J.; Wagner, G. J.; Keten, S. Mesoscopic and multiscale modelling in materials. *Nat. Mater.* **2021**, *20*, 774–786.

(6) Friesner, R. A. Ab initio quantum chemistry: Methodology and applications. *Proc. Natl. Acad. Sci. U.S.A.* **2005**, *102*, 6648–6653.

(7) French, M.; Becker, A.; Lorenzen, W.; Nettelmann, N.; Bethkenhagen, M.; Wicht, J.; Redmer, R. AB INITIO SIMULATIONS FOR MATERIAL PROPERTIES ALONG THE JUPITER ADIABAT. *ApJS* **2012**, *202*, 5.

(8) Chen, M.; Ko, H.-Y.; Remsing, R. C.; Calegari Andrade, M. F.; Santra, B.; Sun, Z.; Selloni, A.; Car, R.; Klein, M. L.; Perdew, J. P.; Wu, X. Ab initio theory and modeling of water. *Proc. Natl. Acad. Sci. U.S.A.* **2017**, *114*, 10846–10851.

(9) Frisch, M. J. u. a. Gaussian∼16 Revision C.01, Gaussian Inc. Wallingford CT, 2016.

(10) Hafner, J. *Ab-initio* simulations of materials using VASP: Density-functional theory and beyond. *J. Comput. Chem.* **2008**, *29*, 2044–2078.

(11) Voelz, V. A.; Bowman, G. R.; Beauchamp, K.; Pande, V. S. Molecular Simulation of *ab Initio* Protein Folding for a Millisecond Folder NTL9(139). *J. Am. Chem. Soc.* **2010**, *132*, 1526–1528.

(12) Timko, J.; Bucher, D.; Kuyucak, S. Dissociation of NaCl in water from *ab initio* molecular dynamics simulations. *J. Chem. Phys.* **2010**, *132*, 114510.

(13) Morales, M. A.; Pierleoni, C.; Schwegler, E.; Ceperley, D. M. Evidence for a first-order liquid-liquid transition in high-pressure hydrogen from ab initio simulations. *Proc. Natl. Acad. Sci. U.S.A.* **2010**, *107*, 12799–12803.

(14) Soldera, A.; Metatla, N. Glass transition of polymers: Atomistic simulation versus experiments. *Phys. Rev. E* **2006**, *74*, 061803.

(15) Serapian, S. A.; Marchetti, F.; Triveri, A.; Morra, G.; Meli, M.; Moroni, E.; Sautto, G. A.; Rasola, A.; Colombo, G. The Answer Lies in the Energy: How Simple Atomistic Molecular Dynamics Simulations May Hold the Key to Epitope Prediction on the Fully Glycosylated SARS-CoV-2 Spike Protein. *J. Phys. Chem. Lett.* **2020**, *11*, 8084–8093.

(16) Kremer, K.; Grest, G. S. Dynamics of entangled linear polymer melts: A molecular-dynamics simulation. *J. Chem. Phys.* **1990**, *92*, 5057–5086.

(17) Reith, D.; Pütz, M.; Müller-Plathe, F. Deriving effective mesoscale potentials from atomistic simulations: Mesoscale Potentials from Atomistic Simulations. *J. Comput. Chem.* **2003**, *24*, 1624–1636.

(18) Izvekov, S.; Voth, G. A. A Multiscale Coarse-Graining Method for Biomolecular Systems. *J. Phys. Chem. B* **2005**, *109*, 2469–2473.

(19) Brini, E.; Marcon, V.; van der Vegt, N. F. A. Conditional reversible work method for molecular coarse graining applications. *Phys. Chem. Chem. Phys.* **2011**, *13*, 10468.

(20) Wang, J.; Olsson, S.; Wehmeyer, C.; Pérez, A.; Charron, N. E.; de Fabritiis, G.; Noé, F.; Clementi, C. Machine Learning of Coarse-Grained Molecular Dynamics Force Fields. *ACS Cent. Sci.* **2019**, *5*, 755–767.

(21) Noé, F.; Tkatchenko, A.; Müller, K.-R.; Clementi, C. Machine Learning for Molecular Simulation. *Annu. Rev. Phys. Chem.* **2020**, *71*, 361–390.

(22) Zhang, L.; Han, J.; Wang, H.; Car, R.; E, W. DeePCG: Constructing coarse-grained models via deep neural networks. *J. Chem. Phys.* **2018**, *149*, 034101.

(23) Husic, B. E.; Charron, N. E.; Lemm, D.; Wang, J.; Pérez, A.; Majewski, M.; Krämer, A.; Chen, Y.; Olsson, S.; de Fabritiis, G.; Noé, F.; Clementi, C. Coarse graining molecular dynamics with graph neural networks. *J. Chem. Phys.* **2020**, *153*, 194101.

(24) Ruza, J.; Wang, W.; Schwalbe-Koda, D.; Axelrod, S.; Harris, W. H.; Gómez-Bombarelli, R. Temperature-transferable coarse-graining of ionic liquids with dual graph convolutional neural networks. *J. Chem. Phys.* **2020**, *153*, 164501.

(25) Groot, R. D.; Warren, P. B. Dissipative particle dynamics: Bridging the gap between atomistic and mesoscopic simulation. *J. Chem. Phys.* **1997**, *107*, 4423–4435.

(26) Murat, M.; Kremer, K. From many monomers to many polymers: Soft ellipsoid model for polymer melts and mixtures. *J. Chem. Phys.* **1998**, *108*, 4340–4348.

(27) McCarty, J.; Lyubimov, I. Y.; Guenza, M. G. Multiscale Modeling of Coarse-Grained Macromolecular Liquids. *J. Phys. Chem. B* **2009**, *113*, 11876–11886.

(28) Ma, S.; Hu, Y.; Wang, R. Self-Assembly of Polymer Tethered Molecular Nanoparticle Shape Amphiphiles in Selective Solvents. *Macromolecules* **2015**, *48*, 3112–3120.

(29) Aydin, F.; Chu, X.; Uppaladadium, G.; Devore, D.; Goyal, R.; Murthy, N. S.; Zhang, Z.; Kohn, J.; Dutt, M. Self-Assembly and Critical Aggregation Concentration Measurements of ABA Triblock Copolymers with Varying B Block Types: Model Development, Prediction, and Validation. *J. Phys. Chem. B* **2016**, *120*, 3666–3676.

(30) Daoulas, K. C.; Müller, M. Single chain in mean field simulations: Quasi-instantaneous field approximation and quantitative comparison with Monte Carlo simulations. *J. Chem. Phys.* **2006**, *125*, 184904.

(31) Schneider, L. Y.; Müller, M. Engineering Scale Simulation of Nonequilibrium Network Phases for Battery Electrolytes. *Macromolecules* **2019**, *52*, 2050–2062.

(32) Milano, G.; Kawakatsu, T. Hybrid particle-field molecular dynamics simulations for dense polymer systems. *J. Chem. Phys.* **2009**, *130*, 214106.

(33) De Nicola, A.; Zhao, Y.; Kawakatsu, T.; Roccatano, D.; Milano, G. Hybrid Particle-Field Coarse-Grained Models for Biological Phospholipids. *J. Chem. Theory Comput.* **2011**, *7*, 2947–2962.

(34) Pizzirusso, A.; De Nicola, A.; Sevink, G. J. A.; Correa, A.; Cascella, M.; Kawakatsu, T.; Rocco, M.; Zhao, Y.; Celino, M.; Milano, G. Biomembrane solubilization mechanism by Triton X-100: a computational study of the three stage model. *Phys. Chem. Chem. Phys.* **2017**, *19*, 29780–29794.

(35) Bore, S. L.; Milano, G.; Cascella, M. Hybrid Particle-Field Model for Conformational Dynamics of Peptide Chains. *J. Chem. Theory Comput.* **2018**, *14*, 1120–1130.

(36) Zhu, Y.-L.; Lu, Z.-Y.; Milano, G.; Shi, A.-C.; Sun, Z.-Y. Hybrid particle–field molecular dynamics simulation for polyelectrolyte systems. *Phys. Chem. Chem. Phys.* **2016**, *18*, 9799–9808.

(37) Munaò, G.; Pizzirusso, A.; Kalogirou, A.; De Nicola, A.; Kawakatsu, T.; Müller-Plathe, F.; Milano, G. Molecular structure and multi-body potential of mean force in silica-polystyrene nanocomposites. *Nanoscale* **2018**, *10*, 21656–21670.

(38) Caputo, S.; Hristov, V.; Nicola, A. D.; Herbst, H.; Pizzirusso, A.; Donati, G.; Munaò, G.; Albunia, A. R.; Milano, G. Efficient Hybrid Particle-Field Coarse-Grained Model of Polymer Filler Interactions: Multiscale Hierarchical Structure of Carbon Black Particles in Contact with Polyethylene. *J. Chem. Theory Comput.* **2021**, acs.jctc.0c01095.

(39) Padding, J. T.; Briels, W. J. Time and length scales of polymer melts studied by coarse-grained molecular dynamics simulations. *J. Chem. Phys.* **2002**, *117*, 925–943.

(40) Iwaoka, N.; Hagita, K.; Takano, H. Multipoint segmental repulsive potential for entangled polymer simulations with dissipative particle dynamics. *J. Chem. Phys.* **2018**, *149*, 114901.

(41) Doi, M.; Edwards, S. F. Dynamics of concentrated polymer systems. Part 1.—Brownian motion in the equilibrium state. *J. Chem. Soc. Faraday Trans.* **1978**, *74*, 1789–1801.

(42) Doi, M.; Edwards, S. F. Dynamics of concentrated polymer systems. Part 2.—Molecular motion under flow. *J. Chem. Soc. Faraday Trans.* **1978**, *74*, 1802–1817.

(43) McLeish, T. C. B. Tube theory of entangled polymer dynamics. *Adv. Phys.* **2002**, *51*, 1379–1527.

(44) Hua, C. C.; Schieber, J. D. Segment connectivity, chain-length breathing, segmental stretch, and constraint release in reptation models. I. Theory and single-step strain predictions. *J. Chem. Phys.* **1998**, *109*, 10018–10027.

(45) Khaliullin, R. N.; Schieber, J. D. Analytic Expressions for the Statistics of the Primitive-Path Length in Entangled Polymers. *Phys. Rev. Lett.* **2008**, *100*, 188302.

(46) Schieber, J. D.; Andreev, M. Entangled Polymer Dynamics in Equilibrium and Flow Modeled Through Slip Links. *Annu. Rev. Chem. Biomol. Eng.* **2014**, *5*, 367–381.

(47) Andreev, M.; Schieber, J. D. Accessible and Quantitative Entangled Polymer Rheology Predictions, Suitable for Complex Flow Calculations. *Macromolecules* **2015**, *48*, 1606–1613.

(48) Masubuchi, Y.; Takimoto, J.-I.; Koyama, K.; Ianniruberto, G.; Marrucci, G.; Greco, F. Brownian simulations of a network of reptating primitive chains. *J. Chem. Phys.* **2001**, *115*, 4387–4394.

(49) Likhtman, A. E. Single-Chain Slip-Link Model of Entangled Polymers: Simultaneous Description of Neutron SpinEcho, Rheology, and Diffusion. *Macromolecules* **2005**, *38*, 6128–6139.

(50) Uneyama, T.; Masubuchi, Y. Multi-chain slip-spring model for entangled polymer dynamics. *J. Chem. Phys.* **2012**, *137*, 154902.

(51) Chappa, V. C.; Morse, D. C.; Zippelius, A.; Müller, M. Translationally Invariant Slip-Spring Model for Entangled Polymer Dynamics. *Phys. Rev. Lett.* **2012**, *109*, 148302.

(52) Langeloth, M.; Masubuchi, Y.; Böhm, M. C.; Müller-Plathe, F. Recovering the reptation dynamics of polymer melts in dissipative particle dynamics simulations via slip-springs. *J. Chem. Phys.* **2013**, *138*, 104907.

(53) Ramírez-Hernández, A.; Peters, B. L.; Schneider, L.; Andreev, M.; Schieber, J. D.; Müller, M.; de Pablo, J. J. A multi-chain polymer slip-spring model with fluctuating number of entanglements: Density fluctuations, confinement, and phase separation. *J. Chem. Phys.* **2017**, *146*, 014903.

(54) Vogiatzis, G. G.; Megariotis, G.; Theodorou, D. N. Equation of State Based Slip Spring Model for Entangled Polymer Dynamics. *Macromolecules* **2017**, *50*, 3004–3029.

(55) Sgouros, A. P.; Megariotis, G.; Theodorou, D. N. Slip-Spring Model for the Linear and Nonlinear Viscoelastic Properties of Molten Polyethylene Derived from Atomistic Simulations. *Macromolecules* **2017**, *50*, 4524–4541.

(56) Becerra, D.; Córdoba, A.; Katzarova, M.; Andreev, M.; Venerus, D. C.; Schieber, J. D. Polymer rheology predictions from first principles using the slip-link model. *J. Rheol.* **2020**, *64*, 1035–1043.

(57) Behbahani, A. F.; Schneider, L.; Rissanou, A.; Chazirakis, A.; Bačová, P.; Jana, P. K.; Li, W.; Doxastakis, M.; Polińska, P.; Burkhart, C.; Müller, M.; Harmandaris, V. A. Dynamics and Rheology of Polymer Melts via Hierarchical Atomistic, Coarse-Grained, and Slip-Spring Simulations. *Macromolecules* **2021**, *54*, 2740–2762.

(58) De Nicola, A.; Kawakatsu, T.; Müller-Plathe, F.; Milano, G. Fast relaxation of coarse-grained models of polymer interphases by hybrid particle-field molecular dynamics: Polystyrene-silica nanocomposites as an example. *Eur. Phys. J. Spec. Top.* **2016**, *225*, 1817–1841.

(59) Sevink, G. J. A.; Schmid, F.; Kawakatsu, T.; Milano, G. Combining cell-based hydrodynamics with hybrid particle-field simulations: efficient and realistic simulation of structuring dynamics. *Soft Matter* **2017**, *13*, 1594–1623.

(60) Allen, M. P.; Tildesley, D. J., *Computer simulation of liquids*, Second edition; Oxford University Press: Oxford, United Kingdom, 2017.

(61) Rapaport, D. C., *The Art of Molecular Dynamics Simulation*, OCLC: 776967671; Cambridge University Press: Cambridge, 2004.

(62) Farah, K.; Karimi-Varzaneh, H. A.; Müller-Plathe, F.; Böhm, M. C. Reactive Molecular Dynamics with Material-Specific Coarse-Grained Potentials: Growth of Polystyrene Chains from Styrene Monomers. *J. Phys. Chem. B* **2010**, *114*, 13656–13666.

(63) Sevink, G. J. A.; Blokhuis, E. M.; Li, X.; Milano, G. Efficient and realistic simulation of phase coexistence. *J. Chem. Phys.* **2020**, *153*, 244121.

(64) Carnahan, N. F.; Starling, K. E. Equation of State for Nonattracting Rigid Spheres. *J. Chem. Phys.* **1969**, *51*, 635–636.

(65) Rumyantsev, A. M.; Jackson, N. E.; de Pablo, J. J. Polyelectrolyte Complex Coacervates: Recent Developments and New Frontiers. *Annu. Rev. Condens. Matter Phys.* **2021**, *12*, 155–176.

(66) Potaufeux, J.-E.; Odent, J.; Notta-Cuvier, D.; Lauro, F.; Raquez, J.-M. A comprehensive review of the structures and properties of ionic polymeric materials. *Polym. Chem.* **2020**, *11*, 5914–5936.

(67) Kolli, H. B.; de Nicola, A.; Bore, S. L.; Schäfer, K.; Diezemann, G.; Gauss, J.; Kawakatsu, T.; Lu, Z.-Y.; Zhu, Y.-L.; Milano, G.; Cascella, M. Hybrid Particle-Field Molecular Dynamics Simulations of Charged Amphiphiles in an Aqueous Environment. *J. Chem. Theory Comput.* **2018**, *14*, 4928–4937.

(68) Mondal, A.; Young, J. M.; Barckholtz, T. A.; Kiss, G.; Koziol, L.; Panagiotopoulos, A. Z. Genetic Algorithm Driven Force Field Parameterization for Molten Alkali-Metal Carbonate and Hydroxide Salts. *J. Chem. Theory Comput.* **2020**, 11.

(69) Ledum, M.; Løland Bore, S.; Cascella, M. Automated determination of hybrid particle-field parameters by machine learning. *Mol. Phys.* **2020**, *118*, e1785571.

(70) Baig, C.; Mavrantzas, V. G.; Kröger, M. Flow Effects on Melt Structure and Entanglement Network of Linear Polymers: Results from a Nonequilibrium Molecular Dynamics Simulation Study of a Polyethylene Melt in Steady Shear. *Macromolecules* **2010**, *43*, 6886–6902.

(71) Masubuchi, Y.; Langeloth, M.; Böhm, M. C.; Inoue, T.; Müller-Plathe, F. A Multichain Slip-Spring Dissipative Particle Dynamics Simulation Method for Entangled Polymer Solutions. *Macromolecules* **2016**, *49*, 9186–9191.

(72) Jackson, N. E.; Webb, M. A.; Pablo, J. J. d. Recent advances in machine learning towards multiscale soft materials design. *Curr. Opin. Chem. Eng.* **2019**, *23*, 106–114.

Erklärung zum Eigenanteil an den Veröffentlichungen

Im Folgenden ist aufgelistet, mit welchem Anteil ich an den Veröffentlichungen beteiligt war.

Mein Anteil an der folgenden Veröffentlichung beträgt 60%

[1] Wu, Z.; Kalogirou, A.; De Nicola, A.; Milano, G.; Müller - Plathe, F. Atomistic Hybrid Particle - field Molecular Dynamics Combined with: Restoring Entangled Dynamics to Simulations of Polymer Melts. J Comput Chem 2021, 42 (1), 6 – 18.

Mein Anteil an der folgenden Veröffentlichung beträgt 85%

[2] Wu, Z.; Milano, G.; Müller-Plathe, F. Combination of Hybrid Particle-Field Molecular Dynamics and Slip-Springs for the Efficient Simulation of Coarse-Grained Polymer Models: Static and Dynamic Properties of Polystyrene Melts. J. Chem. Theory Comput. 2021 *17* (1), 474-487

Mein Anteil an der folgenden Veröffentlichung beträgt 40%

[3] Wu, Z.; Alberti, S. A. N.; Schneider, J.; Mueller-Plathe, F. Knotting Behaviour of Polymer Chains in the Melt State for Soft-Core Models with and without Slip-Springs. J. Phys.: Condens. Matter 2021, 33, 244001.

Mein Anteil an der folgenden Veröffentlichung beträgt 90%
(Eingereicht zur Begutachtung am 28/7/2021).

[4] Wu, Z.; Mueller-Plathe, F. Slip-Spring Hybrid Particle-Field Molecular Dynamics for Coarse-Graining Branched Polymer Melts: Polystyrene Melts as an Example. Submitted to Macromolecules.

Datum: 31.08.2021

Unterschrift: Zhenghao Wu

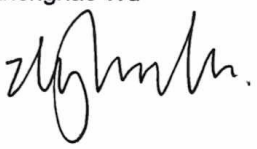

Erklärung zur Begutachtung der Veröffentlichungen

F. Müller-Plathe
Referent*in

N. van der Vegt
Korreferent*in

31.8.2021
Datum:

Weder Referent*in (Prof. Dr. Florian Müller-Plathe) noch Koreferent*in (Prof. Dr. Nico van der Vegt) der vorliegenden kkumulativen Doktorarbeit waren an der Begutachtung nachstehender Veröffentlichungen beteiligt:

[1] Atomistic hybrid particle-field molecular dynamics combined with slip-springs: Restoring entangled dynamics to simulations of polymer melts
[2] Combination of Hybrid Particle-Field Molecular Dynamics and Slip-Springs for the Efficient Simulation of Coarse-Grained Polymer Models: Static and Dynamic Properties of Polystyrene Melts
[3] Knotting behaviour of polymer chains in the melt state for soft-core models with and without slip-springs
[4] Slip-Spring Hybrid Particle-Field Molecular Dynamics for Coarse-Graining Branched Polymer Melts: Polystyrene Melts as an Example

Datum: 31.8.2021

Referent*in
Prof. Dr. Florian Müller-Plathe

Korreferent*in
Prof. Dr. Nico van der Vegt